Volcanology of the Lake Wanaka diatreme in the Alpine Dike Swarm, New Zealand

Samuel P. Maloney

a thesis submitted for the degree of

Master of Science

at the University of Otago, Dunedin,

New Zealand

December 11, 2015

Frontispiece: Lake Wanaka, northwest Otago, New Zealand

Abstract

The Lake Wanaka diatreme represents an eroded Oligocene maar-diatreme volcano situated within the Alpine Dike Swarm, northwest Otago, New Zealand. Current levels of exposure display lithofacies that are characteristic of lower diatreme and root zone deposits.

There are four main lithofacies exposed within the Lake Wanaka diatreme; (1) country-rock breccia, (2) lapilli tuff and tuff breccia, (3) schist megablocks, and (4) coherent lamprophyre. The country-rock breccia is monomict and composed of randomly orientated schist clasts millimetre to a metre in size with no juvenile material present. Lapilli tuff and tuff breccias are unbedded, poorly mixed, and clast-supported by juvenile pyroclasts. They contain common composite loaded pyroclasts with dispersed schist lithics within. The schist megablocks are large blocks of schist country-rock up to 4 m in size that protrude from cliffs of the coherent lamprophyre. The coherent lamprophyre is the most prominent rock within the diatreme, is typically columnar jointed, and contains xenoliths of schist and peridotite, plus amphibole megacrysts.

The country-rock breccia represents the deposit of rock fall into an open cavity, sourced from weakened and unstable wall rock. The open cavity was created by explosions, probably thermohydraulic, within the root zone that drove volcanic material upwards, leaving behind a temporarily evacuated volume. Further volcanic activity produced shaking that led to the clasts of the country-rock breccia becoming tightly packed in places and caused brittle fragmentation at clast contacts. The large schist megablocks were slabbed off the vent wall, and accumulated on a ledge before becoming enveloped by the lamprophyre. Lapilli tuff and tuff breccia were primarily deposited as spatter. Local agglutination textures can be seen at the point contacts of some juvenile pyroclasts, implying they were above the minimum glass transition temperature. Fragmentation of the magma was driven by bubble bursts or more intensive lava fountaining inferred to have been driven by vapour explosions generated by magma-water interactions at depth. Abundant composite loaded juvenile pyroclasts formed when wall rock lithics were shed into the magma prior to, and during fragmentation. Void space that remained between clasts in the lapilli tuff deposit was later cemented by ankerite. Isotopic signatures of the ankerite suggest it was sourced from mixing between meteoric

waters and atmospheric CO_2. The columnar jointed coherent lamprophyre is interpreted to have been a late stage intrusive sill that entrained schist xenoliths of various sizes as it intruded the diatreme.

Paleomagnetic determination of emplacement temperatures suggests that the lapilli tuff was deposited hot, above 580 °C and the same deposit was later reheated to 295–349 °C. A schist xenolith in the coherent lamprophyre was heated to a minimum of 630 °C. These results indicate high temperatures in the diatreme soon after lapilli tuff deposition, and later heating when a nearby lamprophyre sill was intruded.

Acknowledgments

Thanks to my supervisor, James White. Firstly for giving me the opportunity to study under your supervision here in New Zealand, but also for your help and guidance along the way with this thesis. You have helped me expand my knowledge and skills in a new field of volcanology.

Thanks also goes to Christian for your advice on paleomagnetic work and reviewing my results. Claudio, you were of great assistance in the paleomagnetic lab for showing me how to use the various equipment (and not break it). Thanks Brent for preparing my thin sections and helping out with other work in the lapidary. Other people who have been of great help during the year include James Scott for geochemical advice, Gemma for the XRD, Luke for various advice with illustration and word processing, Kat on the SEM and Katrin for the isotopic analyses.

Thanks to all the other staff and students who have made the Geology Department at the University of Otago a friendly place to study at.

Lastly, thanks Sarah for leaving everything back home to move to Dunedin with me for the year and your support throughout it.

Table of Contents

List of Figures

List of Tables

Chapter 1

Introduction

1.1 Aim of Thesis

This thesis aims to contribute to the understanding of intraplate maar-diatreme volcanism during the Cenozoic era on the South Island of New Zealand. It presents the Lake Wanaka diatreme (LWD), a lesser known product of intraplate diatreme volcanism within the Alpine Dike Swarm (ADS), northwest Otago. Maar-diatreme volcanoes are characterised by explosions that cut deeply into the country rock, with most of the activity taking place beneath the land surface (White and Ross 2011). This style of volcano is of research interest due to economic benefits from diamond bearing kimberlites, volcanic hazards created by the pyroclastic eruptions, paleoclimate data from preserved maar-crater lake sediments, and mantle xenoliths providing information about the lower lithosphere. The origin of explosions that facilitate the growth of diatremes is still very much debated, but research to date suggests that diatremes can involve both phreatomagmatic and magmatic eruptions. The classical model of a maar-diatreme volcano consists of the maar ejecta ring, diatreme deposits, and the root zone. Various features that can be observed within these three sites are indicative of the eruption processes that took place to create the maar-diatreme volcano.

The primary aims of this thesis are; (1) to determine the structural level of the Lake Wanaka diatreme where it is now exposed by erosion, (2) explain what the different pyroclastic and related lithofacies indicate about the eruptive history of the diatreme, (3) present a thermal history of some of the deposits within the diatreme, and (4) evaluate the Lake Wanaka diatreme in the context of other intraplate volcanoes on the South Island of New Zealand.

1.2 Thesis Structure

The current chapter (Chapter 1) briefly introduces the geological construction of the Zealandia continent from the Cretaceous period to the present day. A brief history of the widespread Cenozoic South Island intraplate volcanism is also presented with the timing and style of the

major volcanic episodes discussed. Chapter 2 takes a more in-depth look at the geology of the Alpine Dike Swarm and previous work that has been done in the area.

Volcanology of the Lake Wanaka diatreme is the focus of Chapter 3. This chapter contains the bulk of the findings that were compiled from fieldwork and subsequent research at the University of Otago during the thesis year. The first part of the chapter presents the geological features of the Lake Wanaka diatreme, primarily from observations gathered in the field. The final part of the chapter presents an interpretation based on these observations and considers how the interpretation relates to other diatremes globally and to other diatremes on the South Island of New Zealand.

Chapter 4 introduces the paleomagnetic method of determining emplacement temperatures of a pyroclastic deposit through progressive thermal demagnetisation. The chapter presents the results and interpretation for samples that were collected in the field at the Lake Wanaka diatreme and later analysed at the University of Otago Paleomagnetic Research Facility. In paleomagnetic studies, there is much emphasis on determining the magnetic mineralogy of the samples being investigated, which can be determined through the magnetic behaviour of the rock. The first part of the results presented in Chapter 4 is focused on this, with the second half of the results presenting the progressive thermal demagnetisation data that allows estimation of emplacement temperatures. The last part of the chapter presents an interpretation of the results in a thermal context of diatreme volcanoes, and it also refers to concepts of the volcanology discussed in Chapter 3, along with geochemistry data in Chapter 5 that supports some of the thermal findings.

Chapter 5 presents some geochemistry data, primarily from x-ray diffraction and carbon and oxygen stable isotope analyses. Both of these analyses were performed at the University of Otago, however, the Zeiss Sigma SEM was inoperable for much of the thesis year, and unfortunately no substantial energy-dispersive x-ray spectroscopy data could be collected. The results that are presented in this chapter provide support to some of the interpretations that are given in Chapters 3 and 4.

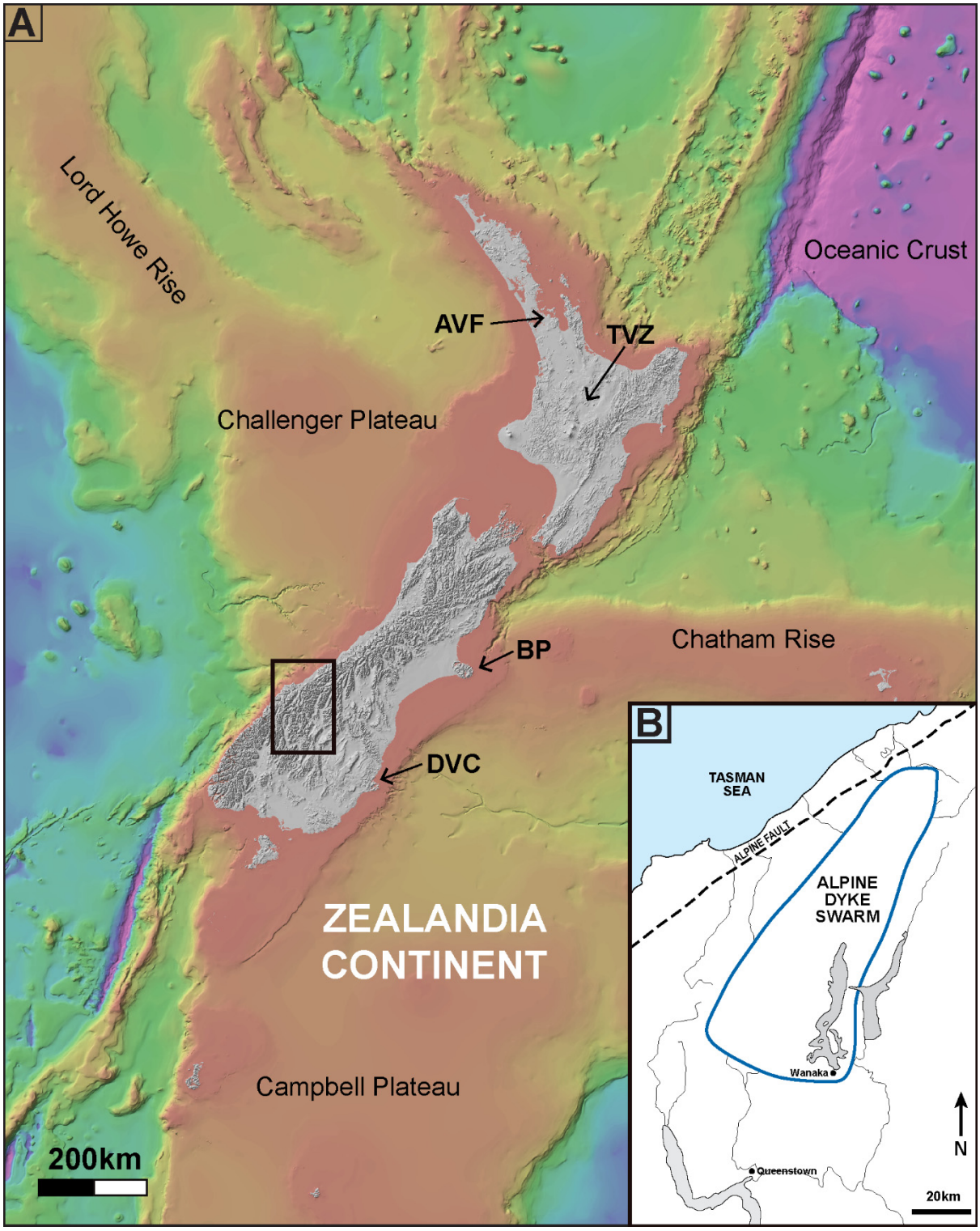

Figure 1.1: **(a)** Regional bathymetry of the predominantly submerged Zealandia continent (yellow to red colours) and present day New Zealand. Purple = ocean depths >5000 m, whereas red colours = depths <500 m. Major volcanic centres and continental features are shown. **(b)** Zoom-in of the rectangle in (a), displaying the approximate zone in which the Alpine Dike Swarm occurs. The Lake Wanaka diatreme, and other diatremes of the ADS only occur in the southern part of the zone, to the west of Lake Wanaka. AVF = Auckland Volcanic Field, TVZ = Taupo Volcanic Zone, BP = Banks Peninsula, DVC = Dunedin Volcanic Complex.

1.3 Geology of New Zealand

Present day New Zealand represents a fragment of Gondwana that was once part of eastern Australia and Antarctica, before sea floor spreading in the late Cretaceous (Fig. 1.2) shifted it to its current position (Mortimer 2004). The North and South Islands of New Zealand represent ~10% of the continent of Zealandia that is present above sea level. Zealandia, roughly a third the size of Australia, lies close to 2000 m below sea level (Fig. 1.1) and besides New Zealand, it is emergent in islands such as Lord Howe Island, Auckland Islands and the Chatham Islands. New Zealand straddles the tectonic boundary between the Australian and Pacific plates, with the Alpine Fault crossing through the South Island, the on-land expression of this boundary.

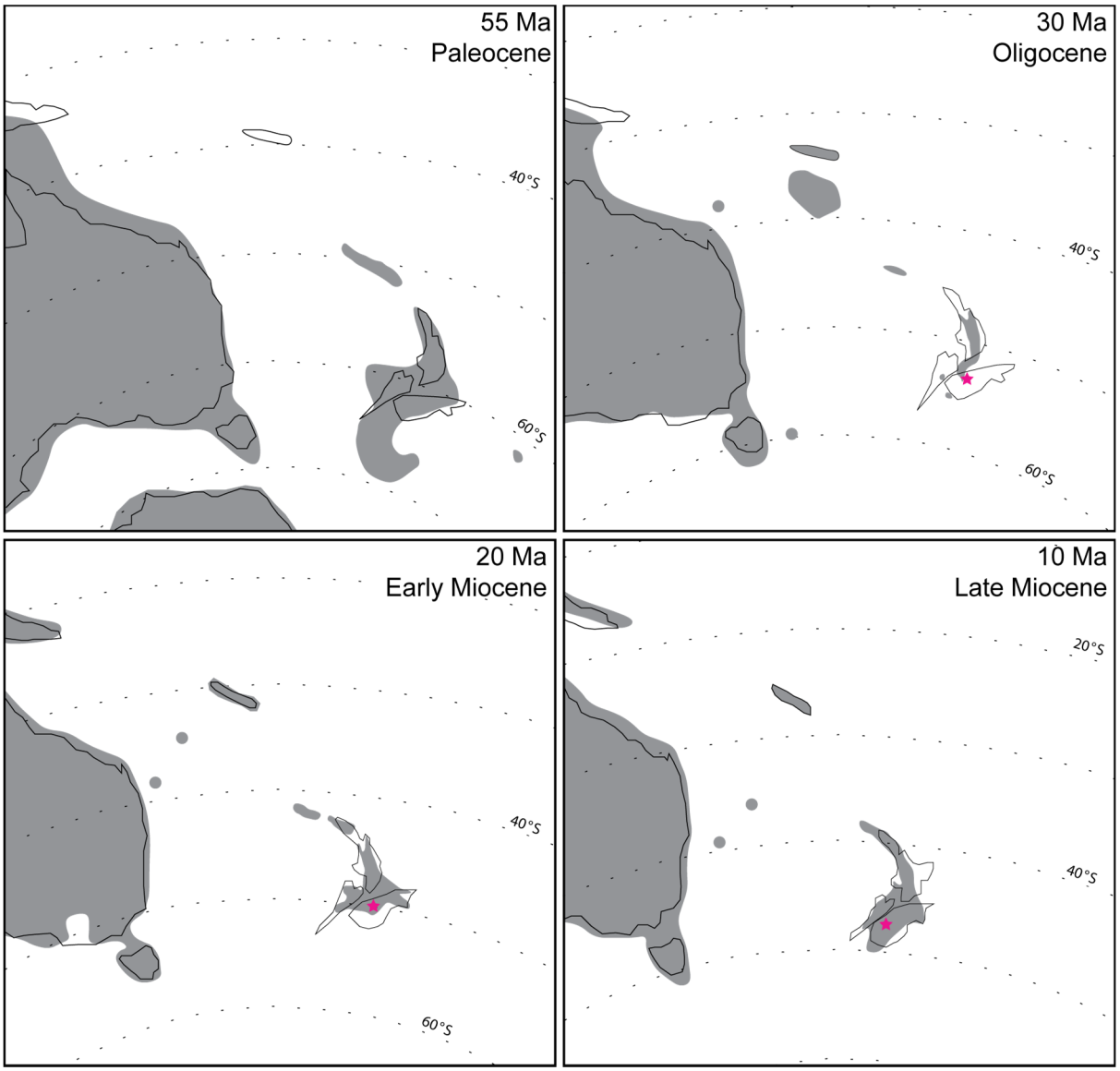

Figure 1.2: Evolution of New Zealand from 55 Ma to 10 Ma; grey shading indicates certain to probable landmasses. Outlines of Australia and the main crustal blocks of New Zealand and New Caledonia are shown, modified after Lee

et al. (2001). The star represents the approximate position of the Lake Wanaka diatreme on the Pacific plate block of the South Island.

No Precambrian basement rocks are exposed in New Zealand, and the Cambrian to early Cretaceous basement can be described in terms of nine major volcano-sedimentary terranes (e.g. Rakai Terrane), three composite regional batholiths, and three regional metamorphic-tectonic belts that overprint the terranes and batholiths (e.g. Haast Schist) (Mortimer 2004). These volcano-sedimentary and regional batholith terranes are divided into an eastern province and a western province, and these two provinces are now referred to as the Austral Superprovince (Mortimer et al. 2014). The westernmost volcano-sedimentary terrane probably represents rock that was deposited close to the continental Gondwana margin, whereas the easternmost terranes were likely trench deposits (Mortimer 2004). From west to east, the terranes represent different tectonic positions with respect to the subduction zone with the proto-Pacific plate that was pulling Zealandia away from Gondwana. Most of the volcano-sedimentary terranes were tectonically overprinted at around 120 Ma when they existed as an accretionary prism during ongoing subduction (Kear and Mortimer 2003). From around 100 Ma, the basement rocks of the eastern and western provinces were progressively buried beneath a series of sedimentary rocks during marine transgression and regression (Mortimer 2004). The level of marine transgression in New Zealand during the Cenozoic is still contentious, however, most of the land was probably submerged during the late Oligocene (Campbell and Landis 2001; Waters and Craw 2006). Throughout much of the South Island, large amounts of the post-100 Ma cover sequence have been eroded along the Waipounamu erosion surface. This surface represents the marine transgression beginning in the late Cretaceous that continued until earliest Miocene time, revealing much of the harder eastern and western province basement below (Landis et al. 2008). Both the North and South Islands have seen widespread volcanism (South Island discussed below), with recent examples on the North Island including the intraplate Auckland Volcanic Field and the subduction driven Taupo Volcanic Zone (Fig. 1.1).

Today, the Australia-Pacific plate boundary crosses through the South Island of New Zealand as the Alpine Fault (Fig. 1.3a). The Alpine Fault is an oblique transform fault system that developed during the mid-Tertiary and is responsible for the creation of the Southern Alps (Cooper et al. 1987). The fault converts into a subduction zone off the east coast of the North

Island, where the Pacific Plate is subducting under the Australian plate (Cole and Lewis 1981), while to the south of the South Island, the Australian plate is subducting under the Pacific plate (Fig. 1.3a).

1.4 Intraplate Volcanism on the South Island of New Zealand

Both the North and South Islands of New Zealand have seen widespread intraplate volcanism. The larger South Island in particular has experienced various styles of volcanism during the Cenozoic (Hoernle et al. 2006). These styles include small monogenetic volcanoes of the Waipiata Volcanic Field, low volume dikes found in the Alpine Dike Swarm, voluminous shield volcanoes such as Banks Peninsula and the Dunedin Volcano, and Surtseyan-style volcanoes found in the Waiareka-Deborah volcanic field (Fig 1.3b). Three distinct periods of Cenozoic volcanism have been recognised in the Otago region (Coombs et al. 1986). An offshore drill hole near Oamaru records the onset of known Cenozoic intraplate volcanism in the Otago region, with basaltic tuffs intersected in the drill hole producing a Paleocene age of around 65 to 54 Ma (Hoskins 1982).

The second period of regional volcanism occurred during the late Eocene to early Oligocene (40–34 Ma), when the Waiareka-Deborah volcanics formed as a series of submarine to emergent Surtseyan style volcanoes (Coombs et al. 1986; Cas et al. 1989; Moorhouse et al. 2015). Volcanism may have been intermittently continuous throughout this whole period, however, Otago-region volcanism in the early Oligocene appears to have been less voluminous (Coombs et al. 1986).

During the third period of volcanism in this region, the Dunedin Volcanic Group was formed, which includes volcanism from the Alpine Dike Swarm, Waipiata Volcanic Field and the Dunedin Volcanic Complex (Németh and White 2003). Volcanism in the Alpine Dike Swarm, located in NW Otago, formed lamprophyre dikes and sills, as well as minor now-eroded diatremes in the southern end of the swarm. Ages of Alpine Dike Swarm volcanism have been constrained to late Oligocene to early Miocene (32–20 Ma) and the younger end probably coincides with the eruption of the Waipiata Volcanic Field (Cooper et al. 1987; Adams and Cooper 1996). Volcanoes from the Waipiata Volcanic Field are characterised by remnants of scoria cones, tuff rings, maars, fissure vents and lava flows of various volumes, with 55

volcanoes being identified within an area of 5000 km^2 in central Otago (Németh and White 2003). The age of volcanism within the WVF has been constrained to 25–11 Ma (Hoernle et al. 2006). The Dunedin Volcano was a shield volcano active from 16 to10 Ma (Hoernle et al. 2006) and it erupted subaerially for much of its life, however, it was likely to have been submarine at the very beginning (Coombs et al. 1986; Martin and White 2001).

All volcanism in the Otago region stopped at approximately the late Miocene (c. 10 Ma), however, intraplate volcanism elsewhere on the South Island continued, with the Banks Peninsula volcanoes still experiencing episodes of activity up until 5.8 Ma along with the Timaru-Geraldine basalts which have been dated at 2.6 Ma (Stipp and McDougall 1968; Hoernle et al. 2006).

Explanations for the occurrence and cessation of this Cenozoic intraplate volcanism have been contentious and sometimes contradictory (Hoernle et al. 2006). Until recently, much of the volcanism in Otago was commonly explained by lithospheric extension related to the opening of the Tasman Sea and the separation of New Zealand from Gondwana (Adams 1981). Cessation of the volcanism was therefore linked to a change in compressional tectonics (King 2000). Cenozoic volcanism on the South Island of New Zealand displays long-lived episodes of volcanism, sporadic distribution, a lack of age progression in the direction of plate motion, and no geochemical variations with respect to the age or site of volcanism (Hoernle et al. 2006; Timm et al. 2010). The lack of any correlation between these factors suggests the intraplate volcanism is not a product of a mantle hotspot nor is it related to any changes in tectonic stresses. More recent work suggests that the intraplate volcanism can be attributed to upwelling of the asthenosphere due to removal of the lithospheric keel during the Cenozoic (Hoernle et al. 2006). Timm et al. (2010) support this argument, and go on to suggest that the large scale seismic anomaly that runs from Antarctica to New Zealand at a depth of 600 km represents a geochemical reservoir that has been supplying the upper mantle beneath Zealandia with HIMU-type plume material throughout the Cenozoic.

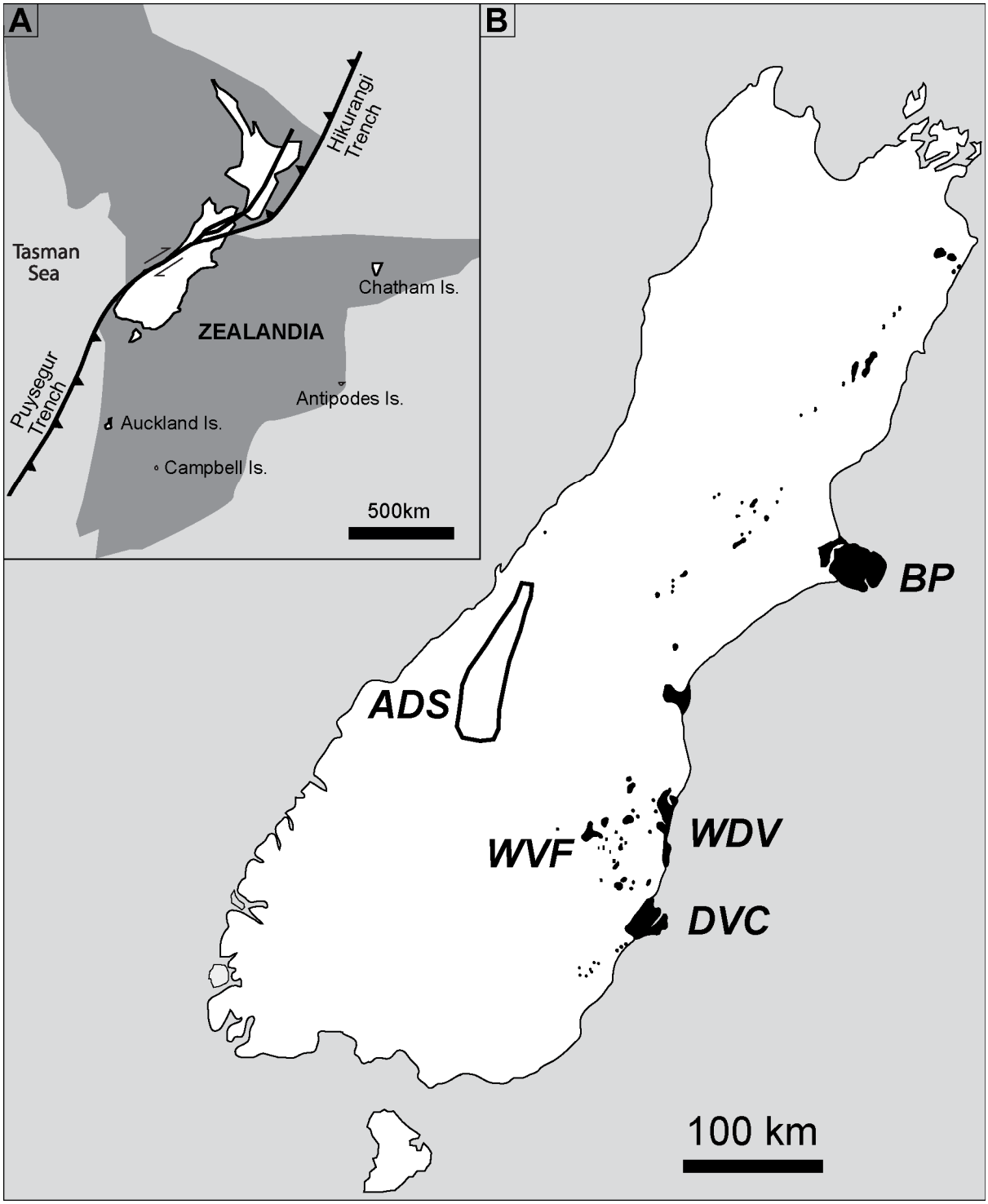

Figure 1.3: (a) Present day New Zealand showing the extent of the predominantly submerged Zealandia continent (dark grey) and the Australian-Pacific plate boundary that intersects the South Island of New Zealand as the Alpine Fault, after Scott et al. (2014b) **(b)** Intraplate volcanic occurrences on the South Island of New Zealand (black or black outlines) modified from Németh (2001) and Coombs et al. (1986). Alpine Dike Swarm (ADS), Banks Peninsula (BP), Waiareka-Deborah Volcanics (WDV), Waipiata Volcanic Field (WVF), Dunedin Volcanic Complex (DVC).

1.5 Fieldwork

The township of Wanaka is a three and a half hour drive northwest from the University of Otago. Gaining access to the Lake Wanaka diatreme then requires a 40 minute boat ride from the Wanaka township to approximately half way along the lake on the western shore. The diatreme occurs on land owned by Minaret Station. The fieldwork involved four days camping on the lakeshore beach, with the diatreme outcrop about a 10 minute walk from camp. The diatreme is only exposed along a steep and rocky cliff face, with the cliff face exposure varying in height up to 5–15 m. Whilst the cliff face provides adequate exposure, surface alteration is pervasive, making volcanic features and contacts difficult to quantify in some areas. Below the lamprophyre cliff face, a very steep hill leads down to the lakeshore, however the hill is covered in scree and vegetation. At the southern end of diatreme near the lakeshore, another cliff face exposes a schist country-rock breccia. The majority of mapping occurred along these two cliff faces. Steep areas around the cliff face made some areas inaccessible. The surrounding areas of the diatreme were also investigated to determine the extent of the diatreme. A number of samples were collected by hand and brought back to the University of Otago for various research analyses.

Chapter 2

Geology of the Alpine Dike Swarm

2.1 Introduction

This chapter summarises the geology of the Alpine Dike Swarm and the surrounding areas of northwest Otago. Chapter 3 presents an in-depth analysis of the geology of the Lake Wanaka diatreme, which is one of a handful of lamprophyre diatremes that occur in the southern part of the swarm. The Lake Wanaka diatreme was originally referred to as the "Minaret Diatreme" in an undergraduate report (Cook 1984), because the diatreme is located on land owned by Minaret Station. A new diatreme was subsequently discovered to the northwest on the slopes of Minaret Peaks (Cooper 1986), which is now referred to as the Minaret Peaks diatreme. Reports that discuss the Lake Wanaka diatreme typically refer to it as the diatreme on the shoreline of Lake Wanaka, and therefore for this study, it is simply called the Lake Wanaka diatreme (LWD).

2.2 Previous Work

Four Alpine Dike Swarm diatremes have been investigated to date at various levels since the early 1980s. Field projects from University of Otago students initially studied the Mt Alta diatreme (Gamble 1984), the Niger Peak diatreme (Cox 1984) and the Lake Wanaka diatreme (Cook 1984). The Minaret Peaks diatreme was studied along with the other diatremes in a comprehensive review of the Alpine Dike Swarm by Cooper (1986). The four diatremes of Mt. Alta, Niger Peak, Minaret Peaks and Lake Wanaka were explored by BP Oil New Zealand in 1987 for precious metals, base metals, and rare earth elements (REE) (Clough 1988). No significant mineralisation was discovered from rock sample assays, with most elements of interest below detection.

2.3 Geology

The Alpine Dike Swarm is a zone of predominantly lamprophyre dikes and sills that intrude the Haast Schist within the Southern Alps, northwest Otago (Fig. 2.1). The intrusions occur throughout a ~100 km zone extending north-east from Wanaka to just north of the Haast

River (Fig. 2.1). Cooper (1986) was the first worker to comprehensively document the dike swarm, determining that they intruded during the late Oligocene–early Miocene. The dikes have a predominantly east–west orientation which is interpreted to indicate the dikes intruded into Riedel shears that developed due to transtensional stress from the Alpine Fault (Cooper et al. 1987). Dikes are commonly <1 m wide, and at the northern end of the swarm around the Haast River, they are more abundant (Fig. 2.1). The northern dikes are also geochemically more diverse, with common carbonatitic dikes also occurring (Cooper 1986). Towards the southern end of the swarm near Lake Wanaka, dikes occurring within the diatremes and elsewhere as individual dikes or sills are predominantly lamprophyric in composition. All of the diatremes within the ADS occur within 20 km of each other to the west of Lake Wanaka, towards the Matukituki River (Fig. 2.1).

The Mt Alta diatreme (Fig. 2.2) is a nearly circular structure approximately 200 m in diameter. It contains schist country-rock breccias that are cross-cut by zones of finer grained schist micro-breccia (Cooper 1986). At the Minaret Peaks diatreme (Fig. 2.2), the major rock type is schist country-rock breccia, with clasts ranging from angular to sub-angular and millimetre to centimetre in size. The main body is 80 m × 40 m with a thin 1–2 m wide skin consisting of carbonate altered schist and lamprophyre breccia that separates the country rock from the massive lamprophyre core (Cooper 1986). The Niger Peak diatreme is inferred to be a long but narrow structure, almost 1000 m in length and 80 m across at its widest point (Cox 1984; Cooper 1986). The diatreme contains mainly carbonate-altered schist country-rock breccia with occasional coherent lamprophyre towards the centre of the diatreme.

Ages of the Alpine Dike Swarm intrusions have been constrained to 20 to 32 Ma, with the coherent lamprophyre from the Lake Wanaka diatreme of this study having a whole-rock K-Ar age of 26.7±0.6 Ma (Cooper et al. 1987; Adams and Cooper 1996). A lamprophyre from the Niger Peak diatreme had a K-Ar age of 26.3±0.4 Ma, similar to the LWD lamprophyre (Adams and Cooper 1996). Ages determined from dikes towards the northern end of the swarm around the Haast River (Fig. 2.1) appear to be slightly younger, with a reported age of 24.1±1.2 Ma (Cooper et al. 1987). A basanite at Nevis Bluff (off map), which is regarded as a southern outlier of the ADS, produced an age of 20 Ma, which puts it within the Waipiata Volcanic Field range, suggesting volcanism in the ADS and WVF may have been contemporaneous during the early Miocene. (Hoernle et al. 2006).

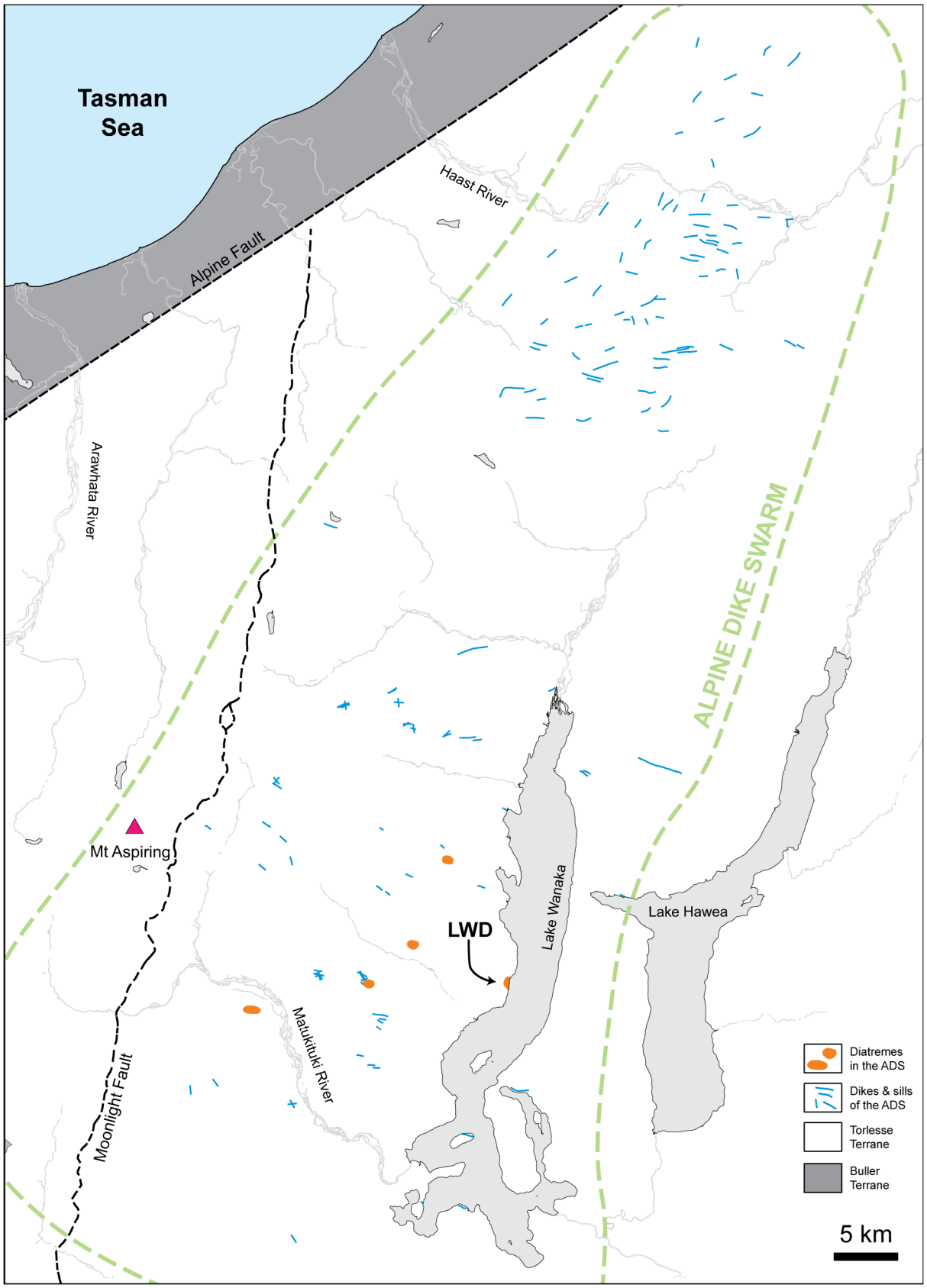

Figure 2.1: Geological map of the Alpine Dike Swarm, northwest Otago. Numerous dikes and sills are shown intruding into the Haast Schist of the Torlesse Composite Terrane. Eroded diatremes in the southern end of the swarm are shown with the Lake Wanaka diatreme (LWD) highlighted.

Recent work by Liu et al. (2015) and Scott et al. (2014b) on peridotite xenoliths from the Lake Wanaka diatreme have shown rhenium depletion model ages ranging from 0.5 to 2.7 Ga. Given that the age of the country rock surrounding the Lake Wanaka diatreme is around 300 Ma, this creates an age difference of ~2.4 Ga, the largest known on Earth (Liu et al. 2015). This age dichotomy is explained by the mixing of ancient Archean peridotitic mantle that has cycled through the asthenosphere over a billion year timescale with more fertile convecting mantle, and subsequently erupted onto young continents. Liu et al. (2015) suggest the range in depletion ages provides little evidence for an ancient mantle keel beneath the Zealandia continent.

Dikes and sills from the Alpine Dike Swarm intrude into country rock of the Rakaia Terrane, which is part of the Torlesse Composite Terrane/Supergroup (Mortimer et al. 2014). These rocks were tectonically overprinted to form the Haast Schist, and this name is used throughout the current study to refer to the country rocks within the area of the Lake Wanaka diatreme, and much of the country rock within the extent of the ADS. Rakaia Terrane rocks comprise New Zealand's largest terrane by area, and are predominantly composed of turbiditic quartzofeldspathic sandstones and mudstones of Permian to late Triassic age (Mortimer 2004). A Gondwana source for the Rakaia detritus is inferred, likely from an area that was originally northeast of Australia (Mortimer 2004). Workers generally agree that the rocks were tectonically overprinted to form the Haast Schist during accretionary wedge development at around 120 Ma (Kear and Mortimer 2003; Mortimer and Cooper 2004).

2.4 Paleodepth

Crustal thinning due to Zealandia's breakup from Gondwana helped drive marine transgression from the Cretaceous to the Oligocene. Maximum transgression probably occurred during the late Oligocene to early Miocene (25–22 Ma), however it is still contentious as to whether the whole of Zealandia was drowned e.g. Campbell and Landis (2001); Landis et al. (2008), or whether significant remnants of land survived the drowning (Fleming 1962; King 1999; Scott et al. 2014a). The Otago area, including the ADS, is historically regarded as having persisted as dry land from Gondwana break-up until the present day (Landis et al. 2008). Evidence often cited to support this persistence of land is the lack of Cenozoic marine strata, existence of subaerially eroded peneplain surfaces, and the need for a persistent Oligocene landmass to support New Zealand's Gondwana related biota (e.g. Bellamy et al. 1990). Refuting

these arguments, Landis et al. (2008) maintained that the erosional peneplain surfaces were in fact created by marine processes, that Cenozoic marine strata did occur throughout the central Otago area but have been largely stripped away by Neogene terrestrial erosion, and finally, that there is no biological need for a continuously present "land ark" to preserve the Gondwana biota. At present, there is still no consensus on whether all of the Zealandia continent was below sea level sometime during the Oligocene and/or earliest Miocene. In a review of the most recent research, Mildenhall et al. (2014) suggest a short period of complete submergence cannot yet be ruled out.

No Oligocene marine sediments are mapped in the Lake Wanaka area, with slivers of Oligocene sediment on the Moonlight Fault further south towards Lake Wakatipu being the closest documented occurrences (Cooper 1986). Given the lack of conclusive evidence, it cannot be said whether the Haast Schist in the Lake Wanaka region was overlain by marine sediments at the time of diatreme emplacement.

Crustal thickening due to development of the modern Australian and Pacific plate boundary (Cooper et al. 1987) led to marine regression during the Miocene and the re-emergence of the Otago region. Only limited research has focussed on the extent of erosion in the Lake Wanaka region since the Miocene. Craw (1995) used a combination of schistosity, metavolcanic horizons, preserved Miocene erosion surfaces, and inferred diatreme exposure depths to determine the original Miocene erosion surface around the Mt. Aspiring–Lake Wanaka area (Figs. 2.2, 2.3). This study area coincides with the southern end of the Alpine Dike Swarm (Fig. 2.2), the area of interest in this thesis.

Craw (1995) infers that the Miocene erosion surface lay close the present level at the site of the Lake Wanaka diatreme (i.e. there has been negligible erosion since the late Oligocene). This inference rests on Cooper (1986) suggestion that the current level of exposure in the diatreme is relatively near the eruptive surface. This interpretation is not supported in the current study, and the current level of exposure is discussed in the subsequent chapters. Figure 2.3 shows a modified erosion surface, reflecting the findings in this study. Around the Mt. Aspiring area at the southern end of the Southern Alps, Craw (1995) estimates erosion levels of <4 km since the Miocene at the valley floors, and even less along the ridge lines. The amount of material eroded from the Mt. Alta and Niger Peak diatremes since the Miocene is estimated to be 1 km and 3 km respectively. In the northern area of the ADS, uplift is estimated to have

been 12 km from Miocene to recent times (Kamp et al. 1989), whereas Craw (1995) suggests that the southern area of the ADS has undergone only minor regional tilting, with little disruption to pre-existing metamorphic structures.

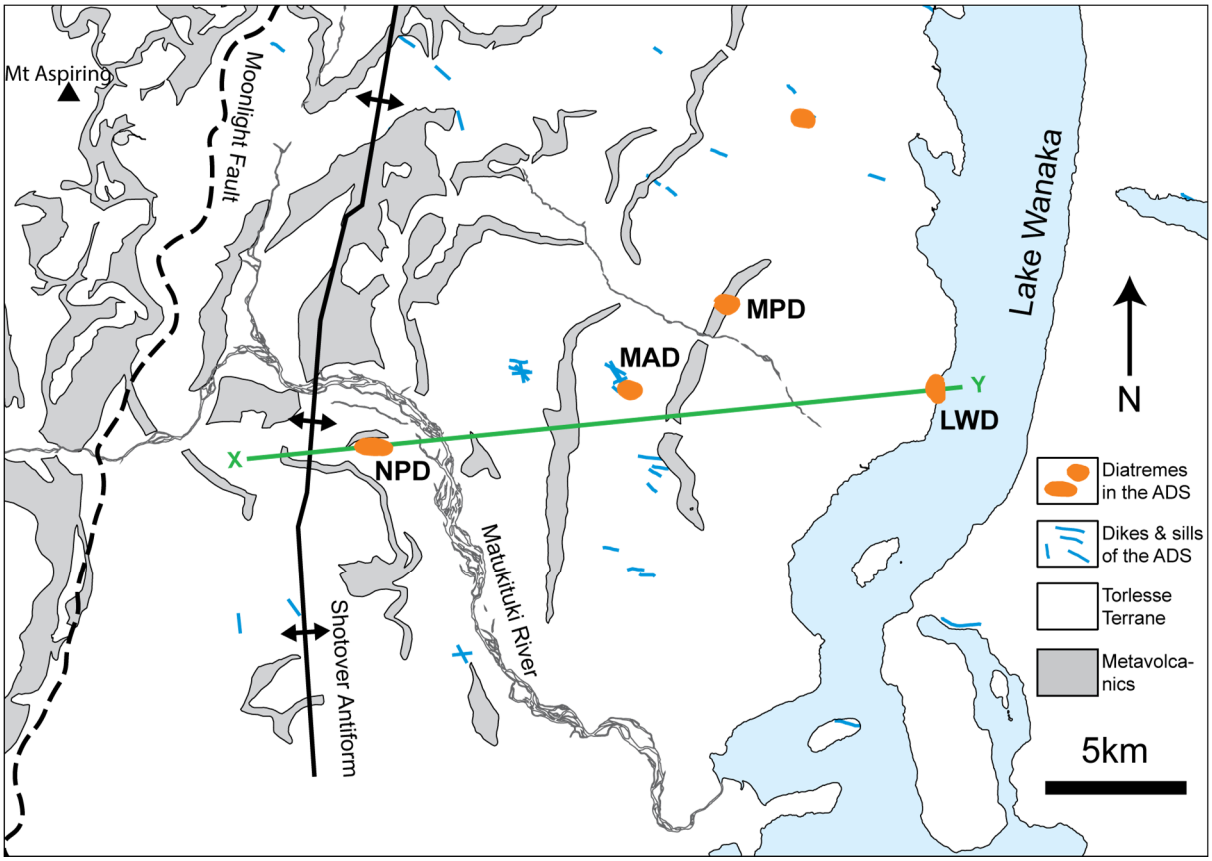

Figure 2.2: A detailed geological map of the southern end of the Alpine Dike Swarm where the lamprophyre diatremes are located. An approximate east–west cross-section (green X-Y) is displayed below in Fig. 2.3. NPD = Niger Peak diatreme, MAD = Mt. Alta diatreme, MPD = Minaret Peaks diatreme, LWD = Lake Wanaka diatreme.

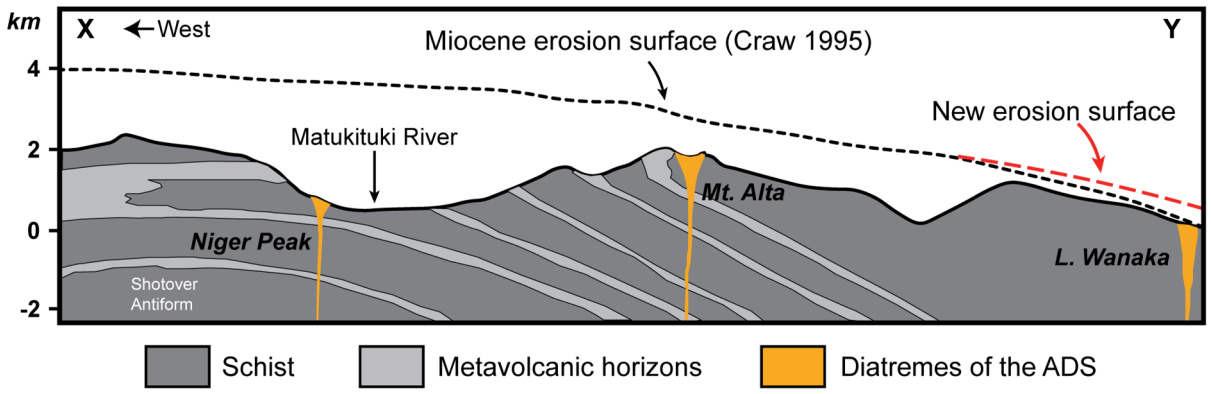

Figure 2.3: An approximately E-W cross-section through the Lake Wanaka, Mt. Alta and Niger Peak diatremes (see Fig. 2.2), modified from Craw (1995). The cross section shows the interpreted Miocene erosional surface, which has been modified near the Lake Wanaka diatreme to represent the findings in this study (red dashed line).

Chapter 3

The Lake Wanaka Diatreme

3.1 Introduction

Maar-diatreme volcanoes can be distinguished from other types of small volcanoes as they are formed by eruptions that excavate into the sub-surface. Most of the volcanic activity from maar-diatreme volcanoes takes place below the land surface as the diatreme is formed by excavation. This excavation forms a cone shaped conduit into which the majority of the pyroclastic material is deposited. Maar-diatreme volcanoes across a wide variety of magma compositions show similar characteristics, however, the method by which maar-diatremes self-excavate themselves is still contentious (White and Ross 2011). The two main camps interpret diatreme excavation as taking place by phreatomagmatic eruptions (Lorenz 1973, 1975; Lorenz 1986; Lorenz and Kurszlaukis 2007) or as driven by magmatic volatiles (Skinner and Marsh 2004; Porritt et al. 2008; Scott Smith 2008; Skinner 2008).

The internal architecture of a maar-diatreme volcano can be classified into three different structural levels, (1) the upper diatreme, (2) the lower diatreme and (3) the root zone (White and Ross 2011). Deposits in the upper diatreme structure may include post-eruptive maar lake sediments, with well-defined pyroclastic beds in the conduit comprising upper diatreme deposits. Lower diatreme deposits are typically unbedded with weak layering and steeply dipping contacts. Rafts and blocks of country rock are commonly mixed throughout the diatreme at this level. The root zone includes the feeder dike along with shattered country rock and contact breccias.

Exposures of complete maar-diatreme volcanoes from the root zone to the maar ejecta ring are rare, with most diatreme exposures only providing a snapshot into a particular level within the diatreme structure. The Lake Wanaka diatreme represents one of these snapshots into an eroded diatreme, and the following chapter will present the characteristics of the diatreme that were documented in this study.

3.2 Diatreme Geometry

The diatreme is situated along the shore of Lake Wanaka (Fig. 3.1, 3.2). The inferred shape of the diatreme is a rough ellipsoid trending approximately 200 m north-south, and ~100 m wide east-west. The vertical exposure of the diatreme is approximately 50 m from the lake shore waterline (Fig. 3.1b). The top of the diatreme has a hummocky surface (Fig. 3.1a) that is covered in vegetation with no reliable outcrop present. The western contact is inferred to occur between where the hummocky terrain ends and starts to rise into the schist country rock. The eastern margin likely continues into the lake towards the southern end, however, *in situ* schist country rock outcrops to the immediate north and south suggesting it is close to the diatreme margin (Fig. 3.2a). The northern and southern margins of the diatreme are inferred to be within <10 m of where the columnar jointed lamprophyre ends (Fig. 3.1b).

Three major lithofacies were identified within the diatreme, (1) country-rock (lithic) breccias, (2) lapilli tuffs and tuff breccias and (3) coherent lamprophyre, which accounts for up to 70% of the exposed diatreme.

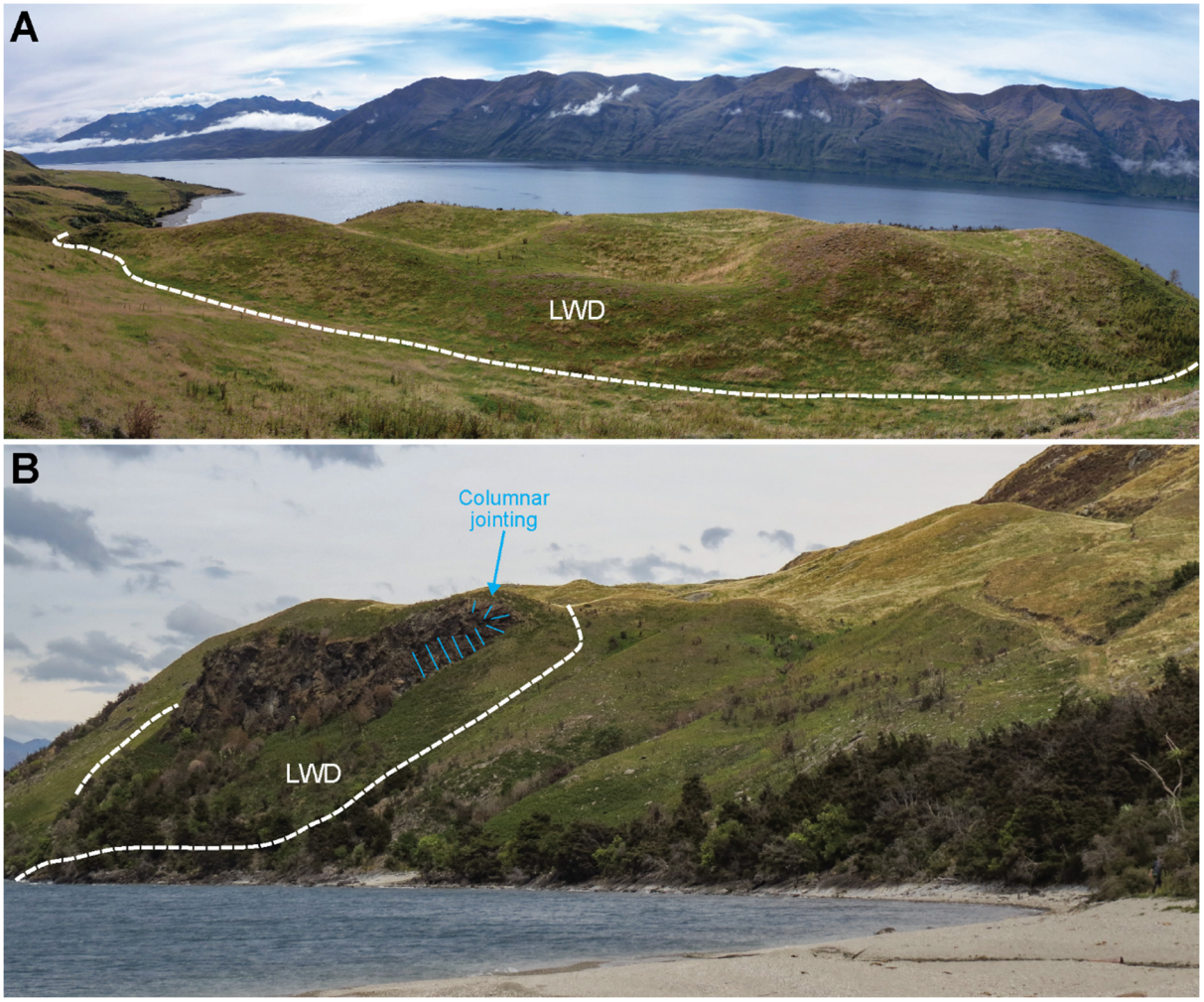

Figure 3.1: Photographs of the Lake Wanaka diatreme outcrop extent from two different perspectives (see Fig. 3.2a for photo locations). **(a)** Hummocky terrain at the top of the LWD, looking east. **(b)** View from the shore of Lake Wanaka looking southwest; the distinctive columnar jointed coherent lamprophyre can be observed. Inferred contacts between the diatreme and country rock is dashed in white.

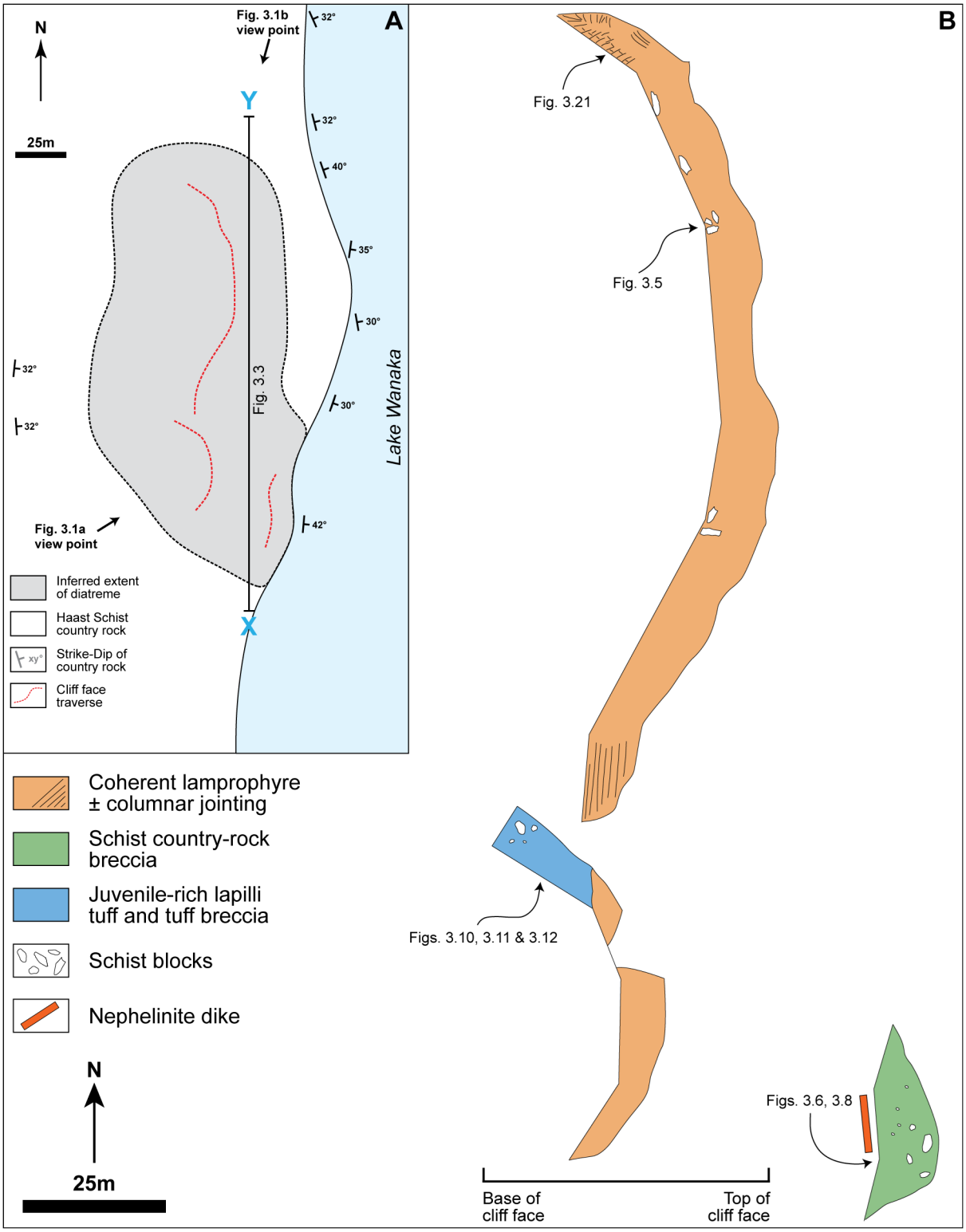

Figure 3.2: Plan view map of the Lake Wanaka diatreme. **(a)** Inferred outline of the Lake Wanaka diatreme, amongst the Haast Schist country rock. Structural measurements represent the strike and dip of the dominant foliation in the schist country rock. Cliff face traverse/outcrops used in this study are shown in red. **(b)** Geology of the cliff face exposures projected onto plan view – these represent the red traverse lines displayed in (a). The top of the cliff face is to the right of the map. The location of various figures referred to throughout this chapter are also displayed.

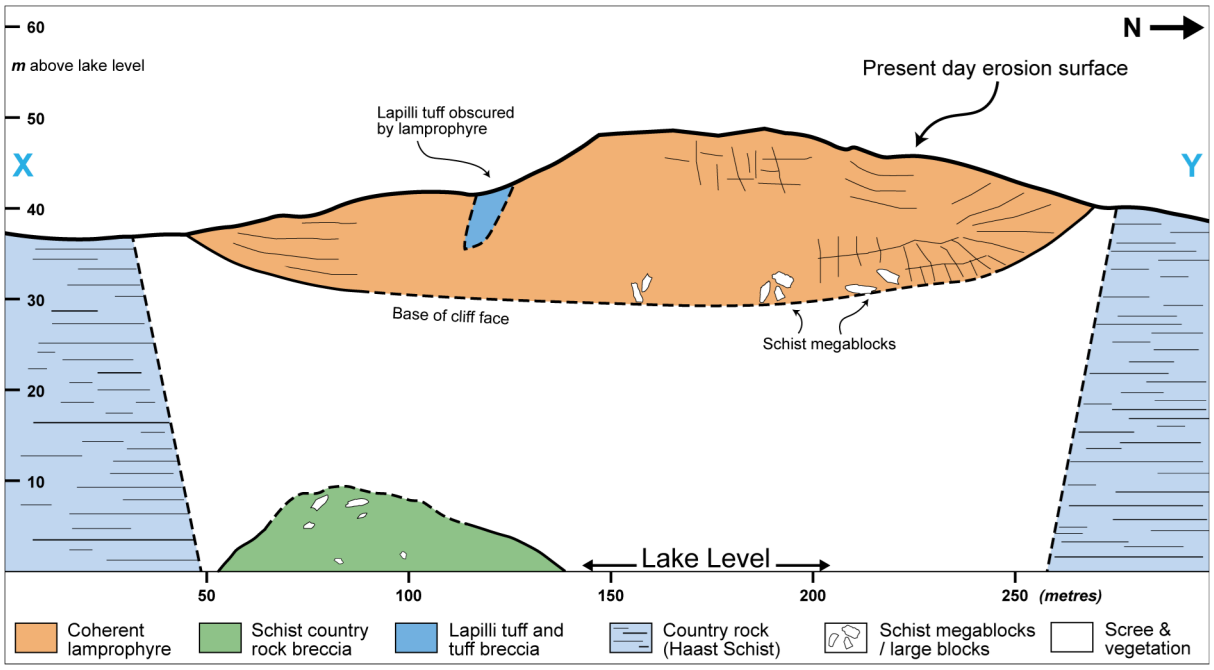

Figure 3.3: North–south cross-section of the Lake Wanaka diatreme (section line X–Y in Fig. 3.2a). The coloured units represent those which are in outcrop, whereas the white indicates where the diatreme is obscured by vegetation and scree. Solid black lines indicate mappable contacts, whereas dashed black lines indicate inferred contacts. Also shown is the general schist fabric dipping 30–40° east (toward the viewer) and striking N–S. The vertical scale is exaggerated by a factor of 2, and the horizontal extent of the section is 300 m.

3.3 Country-rock breccia deposits

Country-rock breccias are a common feature in the Lake Wanaka diatreme, accounting for over half of all clastic facies in outcrop. Country rock in the diatreme is entirely derived from the surrounding unstratified Haast Schist, making it impossible to correlate country rock fragments within the diatreme to a particular stratigraphic level. The country rock deposits are subdivided into two facies; (1) large blocks of schist (megablocks) up to 4 metres in size (Fig. 3.4) and (2), breccias with a large proportion of smaller <20 cm size schist clasts in a carbonate cement with no juvenile material (Figs. 3.2b. 3.3).

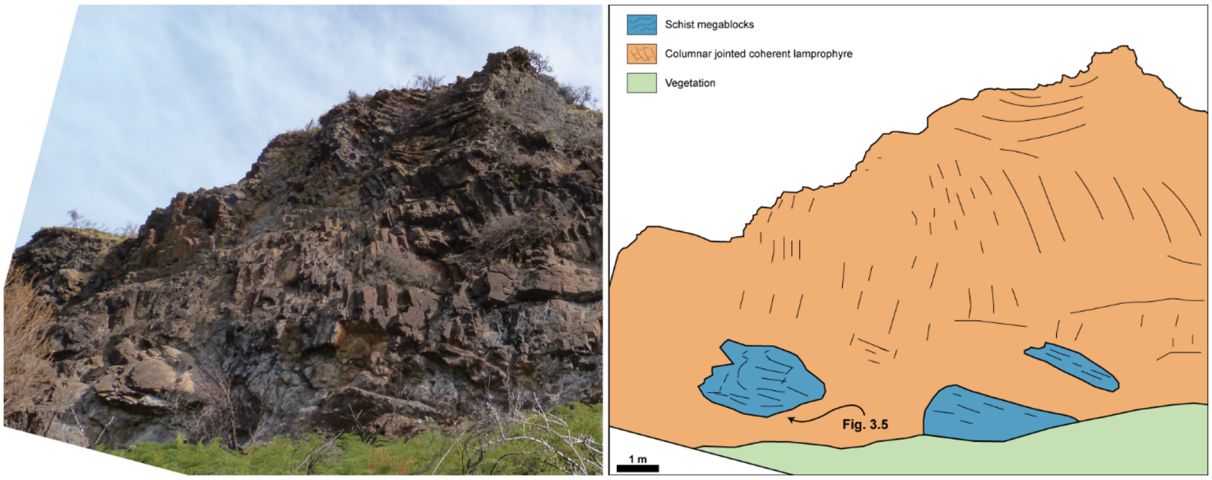

Figure 3.4: Schist megablocks protruding from the coherent columnar jointed lamprophyre. A closer image is shown below in Figure 3.5.

3.3.1 Schist megablocks and megablock breccia

Schist megablocks occur in places throughout the coherent lamprophyre within the LWD; however, they are most abundant towards the northern end (Figs. 3.4, 3.5). The blocks of schist are up to 4 m in size, angular to sub-angular in shape and randomly orientated (Fig. 3.4). No schist blocks occur within the coherent lamprophyre at heights more than 4 metres above the base of the cliff face (inferred base of the coherent lamprophyre). Blocks can occur alone, but also in groups of 3 or more large and randomly orientated blocks to form a megablock breccia.

Towards the northern end of the diatreme, a schist megablock breccia sits within the base of the coherent lamprophyre (Fig. 3.5a). These blocks are up to a few metres in size, and are situated on top of each other with blocky coherent lamprophyre filling most of the space between the large blocks.

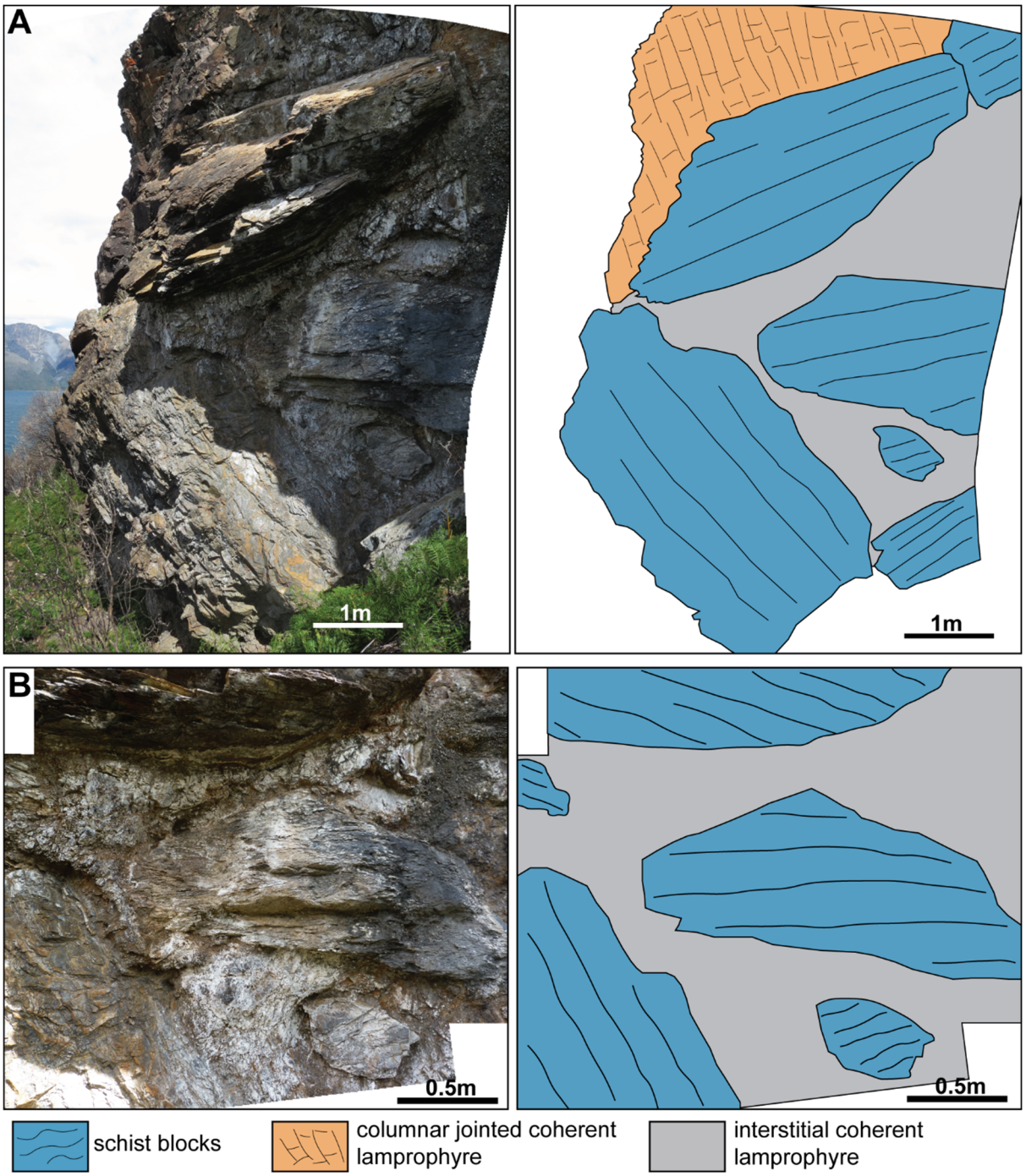

Figure 3.5: Photographs of the schist megablocks towards the northern end of the diatreme. **(a)** Randomly orientated metre sized blocks of schist protruding from the lamprophyre but also in contact with surrounding blocks. **(b)** Another image of (a) but from a closer perspective; blocky coherent lamprophyre is the interstitial material between the individual megablocks.

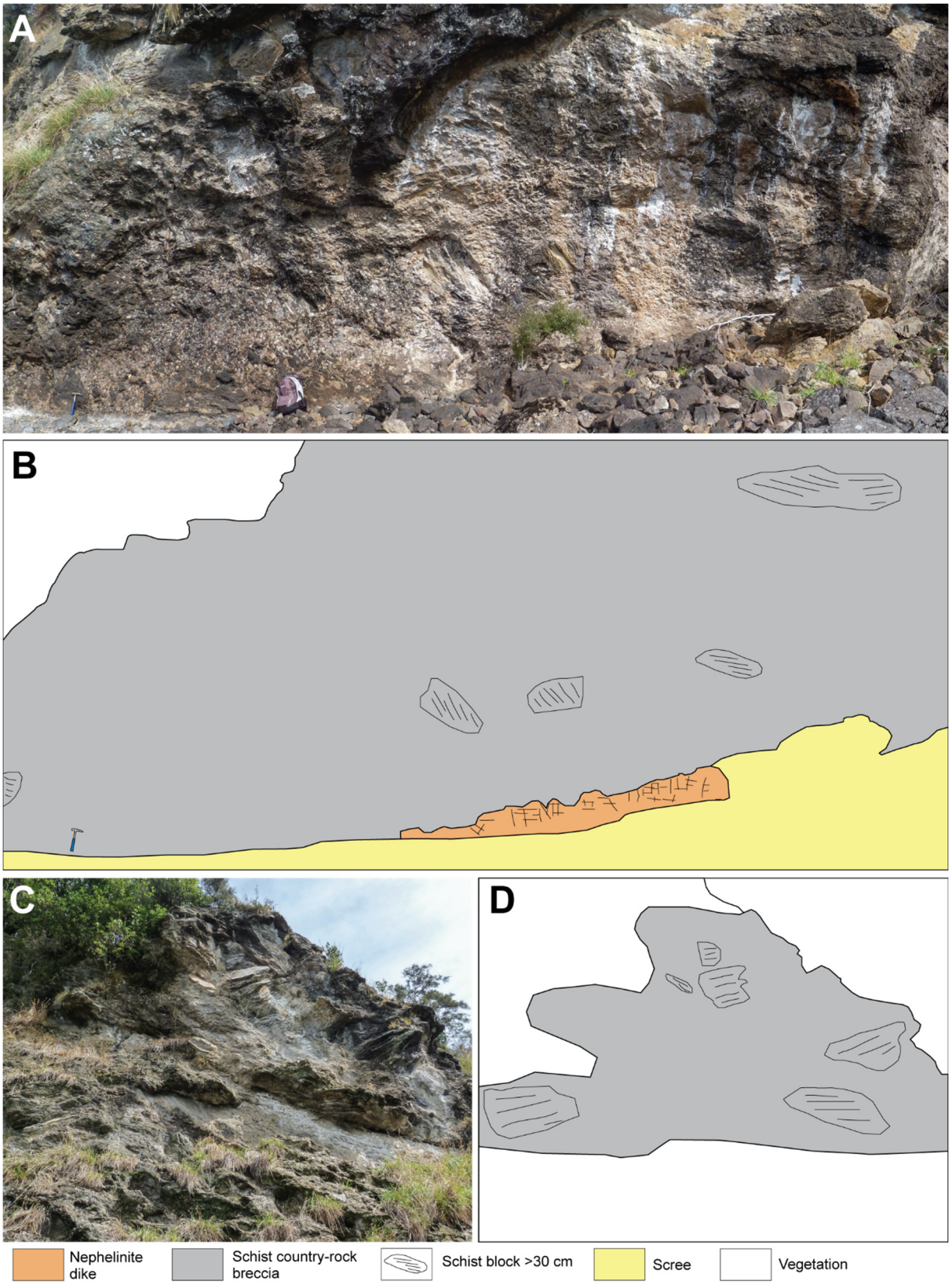

Figure 3.6: Photographs and diagrams of the schist country-rock breccia. **(a)** Weathered outcrop of the schist country-rock breccia near the lake shore towards the southern end of the diatreme; a small 1 m-wide dike is exposed at the base of the cliff face. **(b)** Sketch of the outcrop, schist blocks larger than 30 cm are highlighted. **(c, d)** Photo and diagram of large metre-sized schist blocks in the outcrop that sits above (a) and (b).

Unlike the smaller schist xenoliths that are common within the lamprophyre, the schist megablocks are never completely enveloped within the lamprophyre, and typically half of each megablock protrudes from the coherent lamprophyre. Schist megablocks are significantly weathered, and they do not show any obvious signs of partial melting from being in contact with the lamprophyre. The blocks do not display any "tails" of broken schist pieces, nor is there any chilled lamprophyre occurring away from the blocks other than that which is in direct contact. This unit of country-rock deposit is differentiated from the second subdivision of country-rock breccia by its close proximity to the coherent lamprophyre, and the consistent large size of the schist blocks.

3.3.2 Country rock schist breccia

The second type of country rock breccia only outcrops near the lake shore towards the southern end of the diatreme where a 20 m horizontal face of the unit is exposed (Figs. 3.2b, 3.3, 3.6, 3.8). This unit represents the lowest exposure visible within the diatreme, approximately 20-30 m below the level of the lapilli tuff/tuff breccia and coherent lamprophyre.

The country rock breccia consists of monomict, poorly sorted, unbedded, angular to sub-angular schist clasts, <1 mm to 20 cm in size. Rare blocks up to 1 metre size are also present (Fig. 3.6c, d). The breccia is completely composed of schist clasts with no juvenile material present. Schist clasts range from being tightly packed together with limited void space between them, to more commonly loosely packed, with carbonate having infilled the void space (Fig. 3.7a-d). No jigsaw-fit textures are observed. The schist clasts vary from dominantly micaceous to more quartzose, and often both types are present within the same clast. The schist clasts cannot be attributed to a particular stratigraphic level within the Haast Schist.

Matrix volume is typically 5 %, and it consists of smaller schist fragments (<5 mm) cemented in carbonate (Figs. 3.7, 3.9e, f). The carbonate cement is pervasive throughout the breccia, infilling voids and fractures within the breccia and fragments (Fig. 3.9e-f). The carbonate is a brown iron stained colour in weathered samples (Figs. 3.7a–c, 3.8a, b) and an off white/cream colour in fresh samples (Fig. 3.7d).

Some of the polished slabs display a weakly preferred orientation to the schist clasts (Fig. 3.7a–c). This preferred orientation was not visible in outcrop, but the weathering of the lake shore

exposure may have obscured any clear evidence of clast alignment. A less-weathered sample (Fig. 3.7d) displays minimal carbonate cement between the clasts of the breccia, with carbonate cement comprising <5 % of the rock. In comparison, the weathered slab samples contain 10-15 % carbonate cement between clasts. In thin section, brittle fragmentation textures between the schist clasts can occasionally be observed (Fig. 3.9a, b). The harder quartzose schist clasts appear to have fragmented in a brittle manner to produce a tightly-packed, but not jigsaw-fit, clast arrangement (Fig. 3.9a). Other examples show schist fragments more loosely packed in carbonate cement (Fig. 3.9e, f)

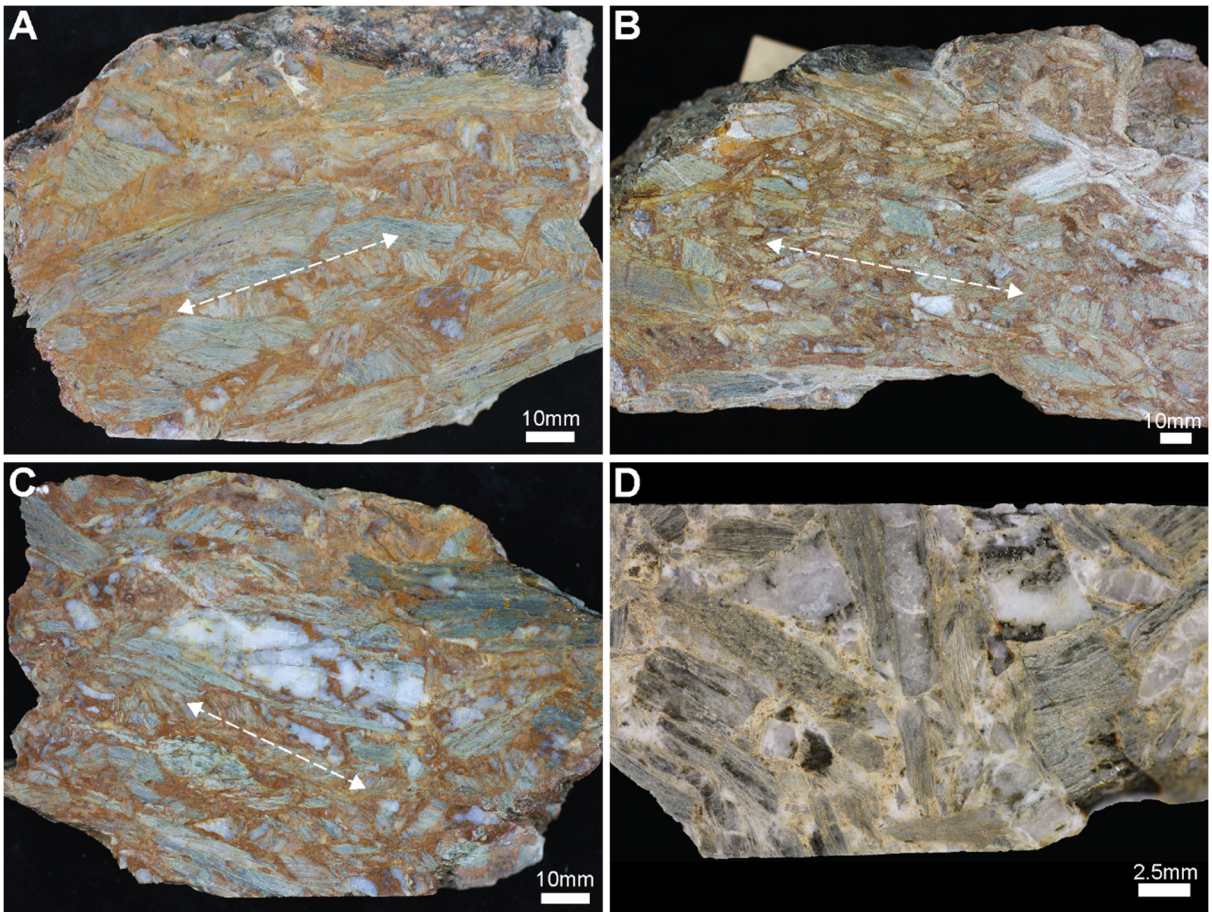

Figure 3.7: Hand specimen photographs of the schist country-rock breccia. **(a, b, c,)** Polished slab photographs of the schist country-rock breccia, these samples are altered, but a weak clast alignment can still be observed (white arrows). **(d)** Photograph of a sample of minimally altered schist country-rock breccia.

Further up the cliff face from the lake shore outcrop (Fig. 3.6a, b), large schist blocks metres in size appear to become common (Fig. 3.6c, d). These large blocks were inaccessible, but they

are inferred to represent a vertical continuation of the same breccia in Figure 3.6a, albeit with an increased amount of large schist blocks.

A 1 metre-wide coherent, aphanitic nephelinite dike is exposed at the base of the country rock breccia outcrop (Fig. 3.8d). It cuts in from the lake and has a sharp contact with the schist breccia before disappearing beneath scree.

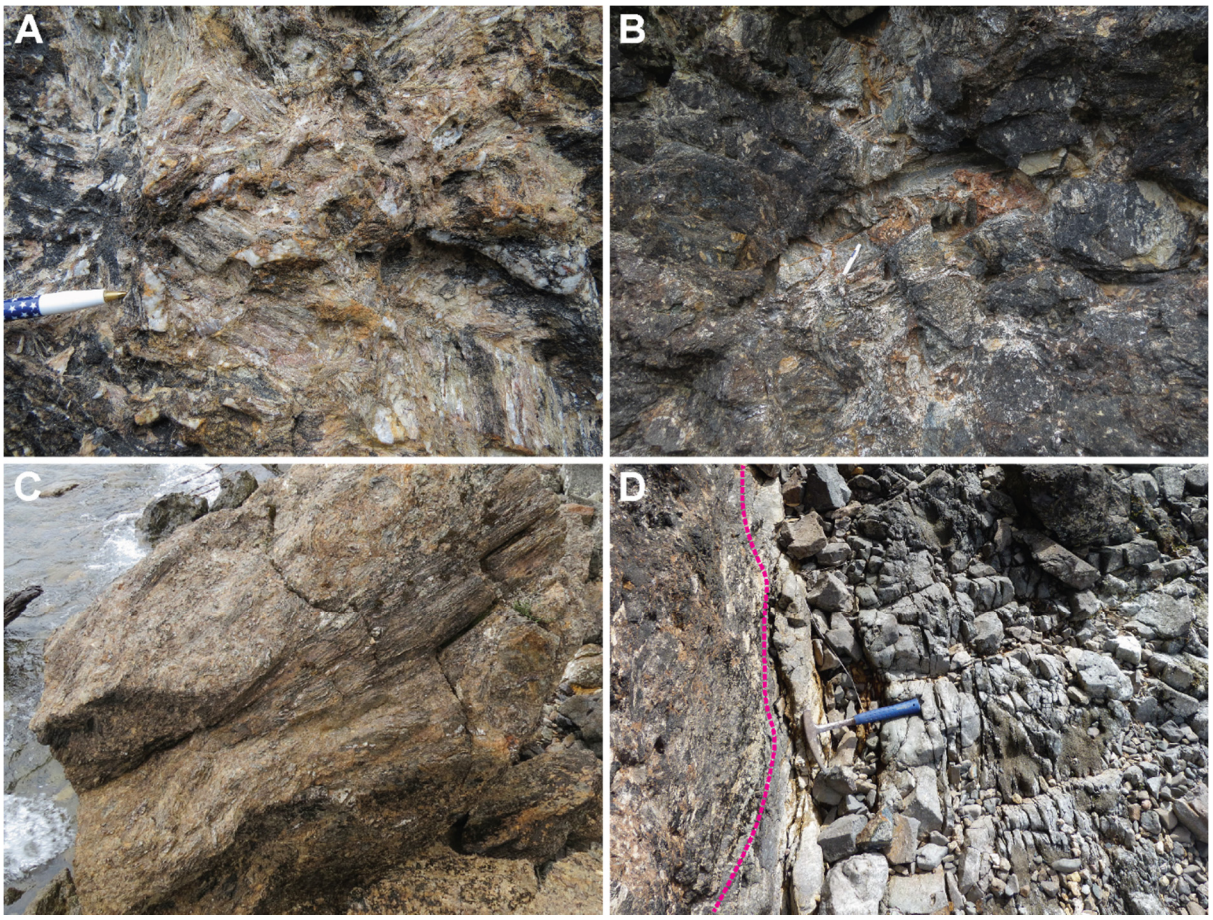

Figure 3.8: Photographs of the schist country-rock breccia. **(a)** Typical sub-angular and randomly orientated schist clasts. The white quartzose schist fragments are distinct from the mica rich type. **(b)** Schist country-rock breccia (pen for scale). **(c)** Broken block of schist country-rock breccia sitting on the lake shore, note the larger ~30 cm clast surrounded by much smaller fragments. **(d)** Coherent, fine grained nephelinite dike in sharp contact with the schist breccia. Contact shown in pink.

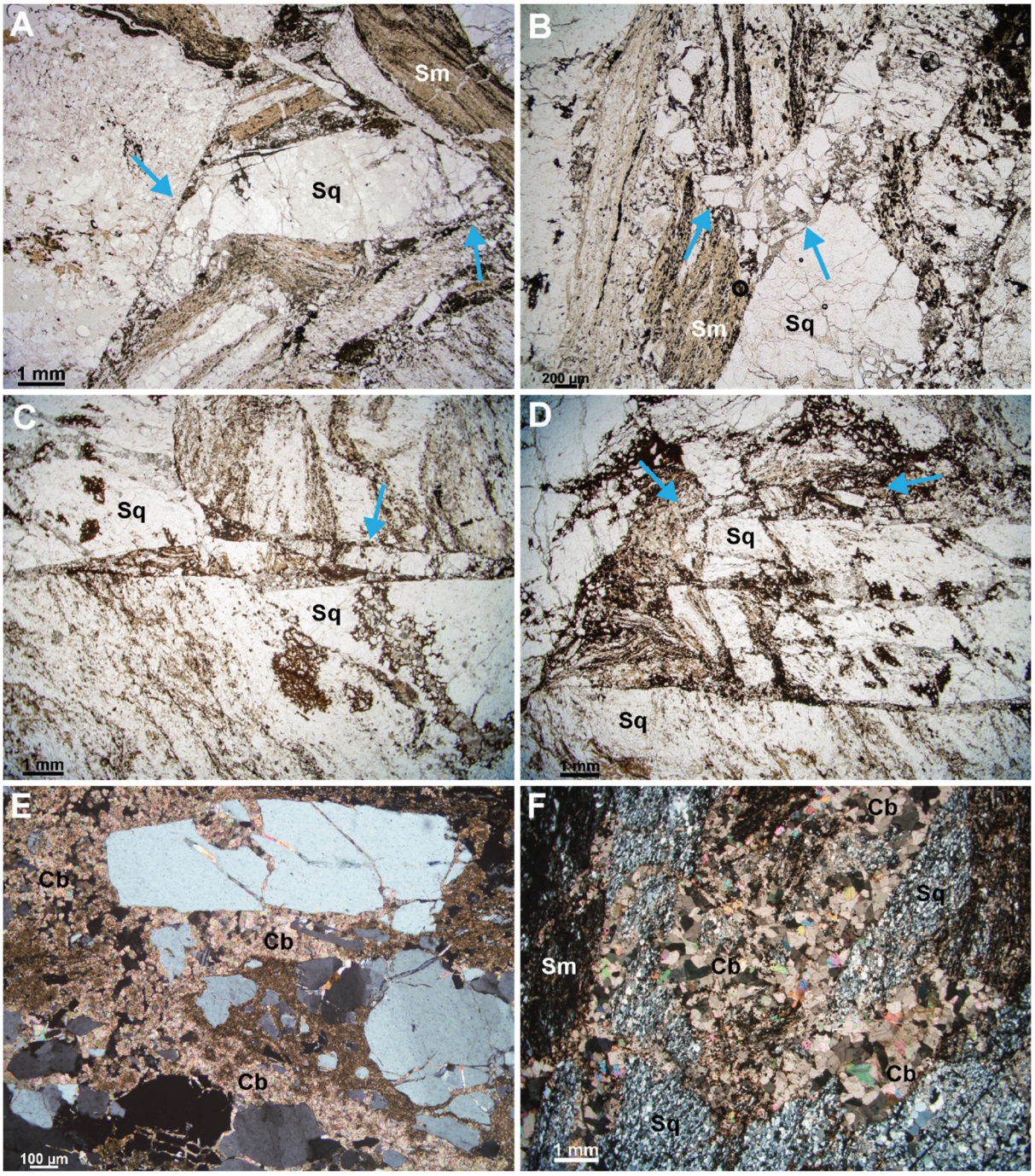

Figure 3.9: Photomicrographs of the schist country-rock breccia. **(a)** Arrows point to where the quartz has fragmented in order to lock into place and form a tightly packed, but not jigsaw-fit, breccia. **(b)** Another example where the schist has fragmented into smaller pieces. **(c)** Schist breccia; arrow points to small (<1 mm) quartz fragments forming the matrix. **(d)** An example of small quartz fragments forming a matrix with a carbonate cement. **(e)** Quartz fragments from the schist breccia surrounded by carbonate cement. The carbonate is pervasive; it has infilled crystal fractures and partially replaced the micaceous parts of the schist (crossed nicols). **(f)** Coarsely crystalline carbonate infilling a small void within the schist country-rock breccia (crossed nicols). Sq = quartzose schist, Sm = micaceous schist, Cb = carbonate.

Determining the lateral extent of the schist country-rock breccia within the diatreme is difficult because the unit is only exposed in cliff faces. However, the country rock breccia exposed at the lake shore is inferred to be within 10 m of the eastern margin of the diatreme because there is in-place schist country rock situated to the immediate north and south of the cliff face outcrop. The unit is inferred to represent a substantial and voluminous infill of the eastern side of the diatreme.

3.4 Lapilli tuff and tuff breccia deposits

A juvenile rich lapilli tuff and tuff breccia deposit outcrops towards the southern end of the diatreme along a steep section that cuts into the cliff face (Figs. 3.2b, 3.3). This is the only location where juvenile bearing deposits were documented within the diatreme. They occur in close proximity to the columnar jointed coherent lamprophyre. The deposit is poorly sorted with no bedding or layering present.

The lapilli tuff and tuff breccias are subdivided into 3 units; matrix-rich lapilli tuff and tuff breccia (unit A1), weakly welded juvenile-rich lapilli tuff and tuff breccia (unit A2) and country rock-rich tuff breccia (unit A3). Table 3.1 presents a list of component classes for volcaniclastic deposits to aid in the following descriptions.

Table 3.1: Component classes for primary volcaniclastic rocks, taken from White and Houghton (2006).

Component	Key criteria	Example
Juvenile	Primary juvenile: derived directly from erupting magma. Recycled juvenile: juvenile clast recycled during the eruption that formed it.	Dense to inflated fragments of chilled magma (pumice, scoria, dense juvenile).
Lithic	Clast formed by fragmentation of pre-existing rock or incorporated from unconsolidated sediment.	Fragments derived from wall rock (e.g., sandstone lithic).
Composite	Clast formed by mingling of magma with a clastic host, or incorporation of lithic debris into magma.	Fragments of peperite (composite clasts). Bomb with lithic core (cored bomb).

3.4.1 Unit A1: Matrix rich lapilli tuff and tuff breccia

Unit A1 (Figs. 3.10a–c, 3.13b–d) consists of primary juvenile pyroclasts of lamprophyre, composite pyroclasts, and lithics of schist country-rock supported within a matrix of smaller pyroclasts and lithics held together by a carbonate cement. Primary juvenile pyroclasts and composite pyroclasts comprise up to 70% of the unit, with matrix up to 20%, and the remainder schist lithics. Surface alteration of the outcrop face falsely suggests there is a high amount of matrix present in the deposit (Fig. 3.10a). Polished slabs, however, reveal that much of this matrix is finer lapilli fragments in carbonate cement (Fig. 3.13b–d). Juvenile and composite pyroclasts are sub-angular to sub-rounded in shape, with some pyroclasts having evident fluidal textures (Fig.3.15a). No welding textures, however, are observed. Composite loaded pyroclasts with dispersed schist lithics throughout are the dominant type of composite pyroclast. The schist lithics within the composite loaded pyroclasts are commonly millimetre sized to a few centimetres. The primary juvenile pyroclasts and composite loaded pyroclasts are both derived from the same juvenile material, and they are only distinguished on the basis of containing schist lithics. Composite loaded pyroclasts, which are loaded with recycled juvenile pyroclasts are rare, but present within this unit, and best observed in thin section (Fig. 3.15d). The recycled pyroclasts that were incorporated into the composite loaded pyroclasts are a microlitic-textured juvenile pyroclast type (Figs 3.15f, 3.17e, f). This second type of composite loaded pyroclast comprises <1 % of all pyroclasts within the unit. The composite loaded pyroclasts containing schist lithics account for >50 % of all pyroclasts, and the primary juvenile pyroclasts account for <50 %. The groundmass in the juvenile and composite loaded pyroclasts is composed of a dark brown tachylite which is rarely vesicular. Where vesicles are seen in 2 dimensions they are sub-round to very round, with no evidence of stretching (Fig. 3.16a, b).

Schist lithics occur freely in the matrix but are most abundant within the composite loaded pyroclasts (Fig. 3.13b–d). Single schist lithics are commonly sub-angular to sub-rounded and rarely larger than lapilli size. The matrix consists of ash-sized fragments of lamprophyre and schist lithics within a carbonate cement (Fig. 3.15a, f).

Unit A1 is unbedded and poorly sorted and is the most voluminous lapilli tuff and tuff breccia unit present in the diatreme.

3.4.2 Unit A2: Weakly welded juvenile rich lapilli tuff

Unit A2 (Figs. 3.10d–f, 3.13a, 3.14) is similar to unit A1, and consists of primary juvenile pyroclasts, composite loaded pyroclasts and schist country-rock lithics. Compared to unit A1, the primary juvenile and composite pyroclast content is higher, up to 80 %, with less than 5 % matrix and the remainder schist lithics. Both primary juvenile and composite loaded pyroclasts display fluidal textures, and weak agglutination textures are also occasionally observed between pyroclasts (Fig. 3.14). Primary juvenile and composite loaded pyroclasts clasts are rarely vesicular, and in those that are, the vesicles are sub-round to round with some rare examples of vesicle stretching (Figs. 3.16c, d, 3.17c, d). Primary juvenile and composite loaded pyroclasts typically have an opaque dark brown, tachylite groundmass similar to the pyroclasts from unit A1.

Schist lithics in the composite loaded pyroclasts are typically sub-angular to sub-rounded in shape (Fig. 3.15b) and they display no obvious signs of partial melting. Over 80 % of the schist material within unit A2 occurs within the composite loaded pyroclasts, with only a small amount of schist lithics occurring freely within the lapilli tuff (Fig. 3.14b). These freely occurring schist lithics range in size up to several centimetres (Fig. 3.10–f), and the lithics on the smaller end of the size range show evidence they were broken away from composite loaded pyroclasts (Fig. 3.15e).

The unit is exposed close to the coherent lamprophyre (Fig. 3.11), with an inter-fingering sub vertical contact. The unit also has a sub-horizontal contact with unit A3 (Fig. 3.11).

3.4.3 Unit A3: Country rock-rich tuff breccia

Unit A3 (Figs. 3.10g, h, 3.11, 3.12) is primarily distinguished from units A1 and A2 by the increased abundance of schist country-rock lithics. Schist lithics comprise up to 60 % of the unit, with juvenile pyroclasts up to 30%, and the remainder comprising matrix. The schist lithics are angular to sub-rounded and vary in size up to 20 cm with rare large blocks greater than 1 m (Fig. 3.12). Juvenile pyroclasts are typically lapilli sized and the composite loaded pyroclasts common in units A1 and A2 are more obscure here The unit is unbedded, poorly sorted and has a steep and planar contact with unit A1 (Fig. 3.12c). A lamprophyre is situated at the western end of the unit A3 exposure (Fig. 3.12a, b), but the contact is not exposed.

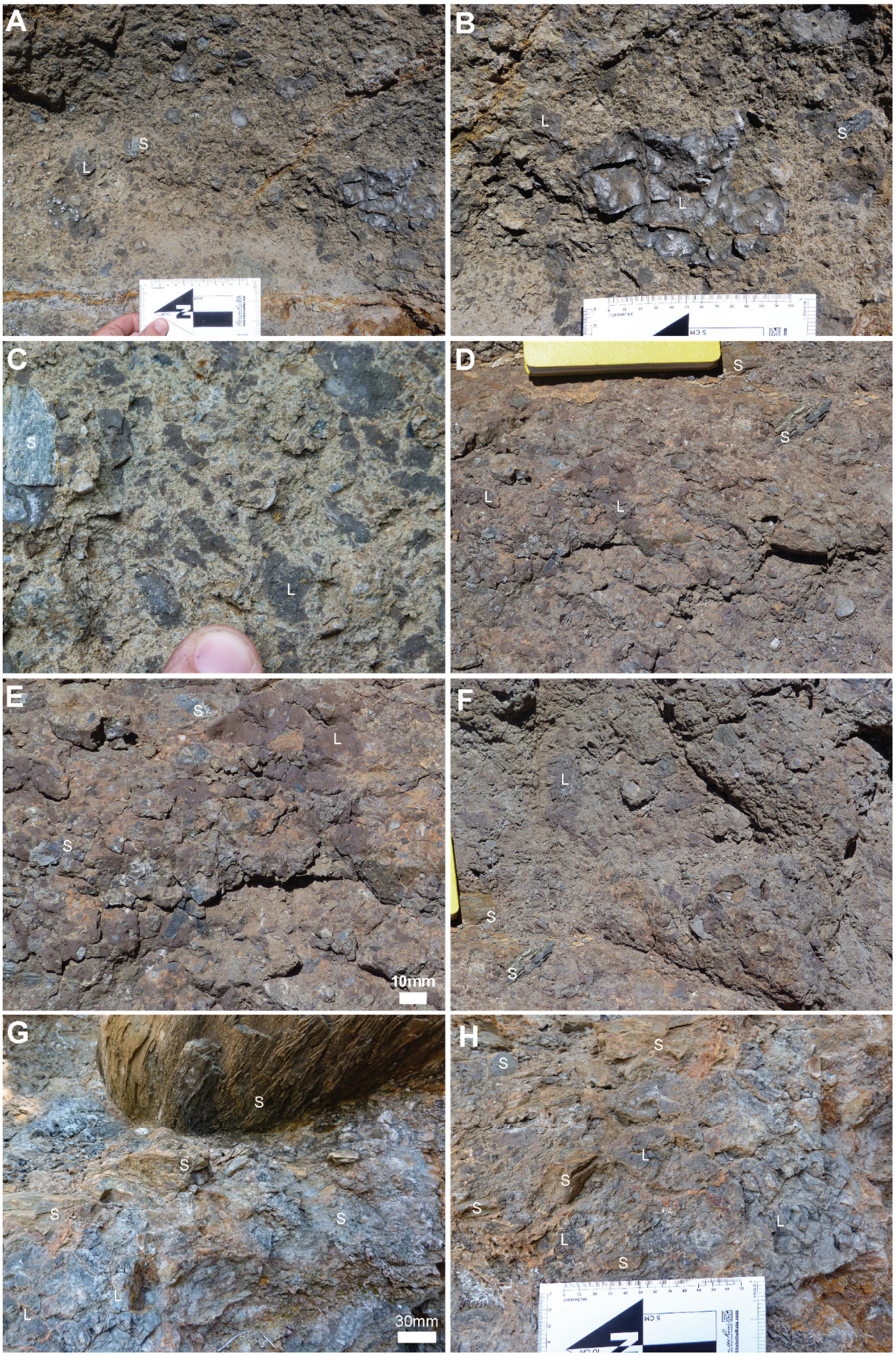
A
S
L
B
L
S
L
C
S
L
D
S
S
L
L
E
S
L
S
10mm
F
L
S
S
G
S
S
S
S
L
L
30mm
H
S
S
S
L
S
S
L
L
S

Figure 3.10: Photographs showing examples of typical unbedded and poorly sorted lapilli tuff and tuff breccia deposits. **(a)** Lapilli tuff deposit consisting of lapilli to bomb sized juvenile lamprophyre pyroclasts and schist country-rock lithics supported in a matrix of finer pyroclastic material and carbonate cement (unit A1). **(b)** Closer image of the previous photo showing a bomb sized juvenile pyroclast (unit A1). **(c)** Juvenile lapilli pyroclasts that exhibit sub-angular and fluidal shapes, light grey schist lithics can also be seen (unit A1). **(d)** Clast supported juvenile rich lapilli tuff and tuff breccia with common composite loaded pyroclasts and fluidal textures (unit A2). **(e)** Zoom of previous photo displaying a composite loaded bomb sized juvenile pyroclast and other loaded pyroclasts (unit A2). **(f)** Another photo of the deposit from (d) and (e) showing rare cm sized schist lithics (unit A2). **(g)** Schist rich tuff breccia with a large sub-rounded raft of schist (unit A3). **(h)** Schist rich tuff breccia with lapilli sized juvenile pyroclasts in the centre (unit A3). S = schist lithic, L = lamprophyric juvenile pyroclast.

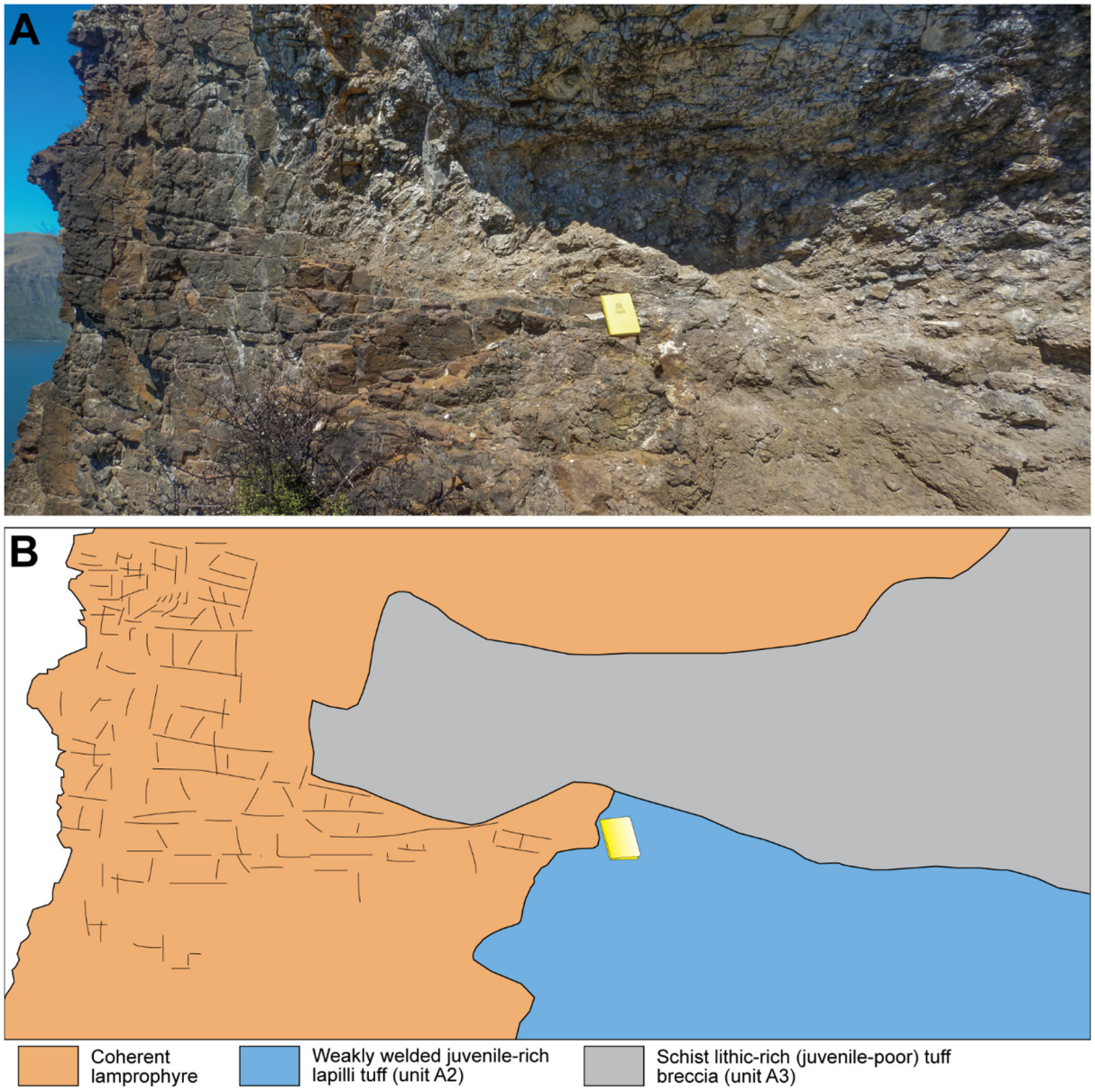

Figure 3.11: **(a)** Photo of the coherent lamprophyre, juvenile-rich lapilli tuff (unit A2) and country rock rich tuff breccia (unit A3). Sketch **(b)** shows the extent and the contacts between the 3 facies (yellow notebook for scale).

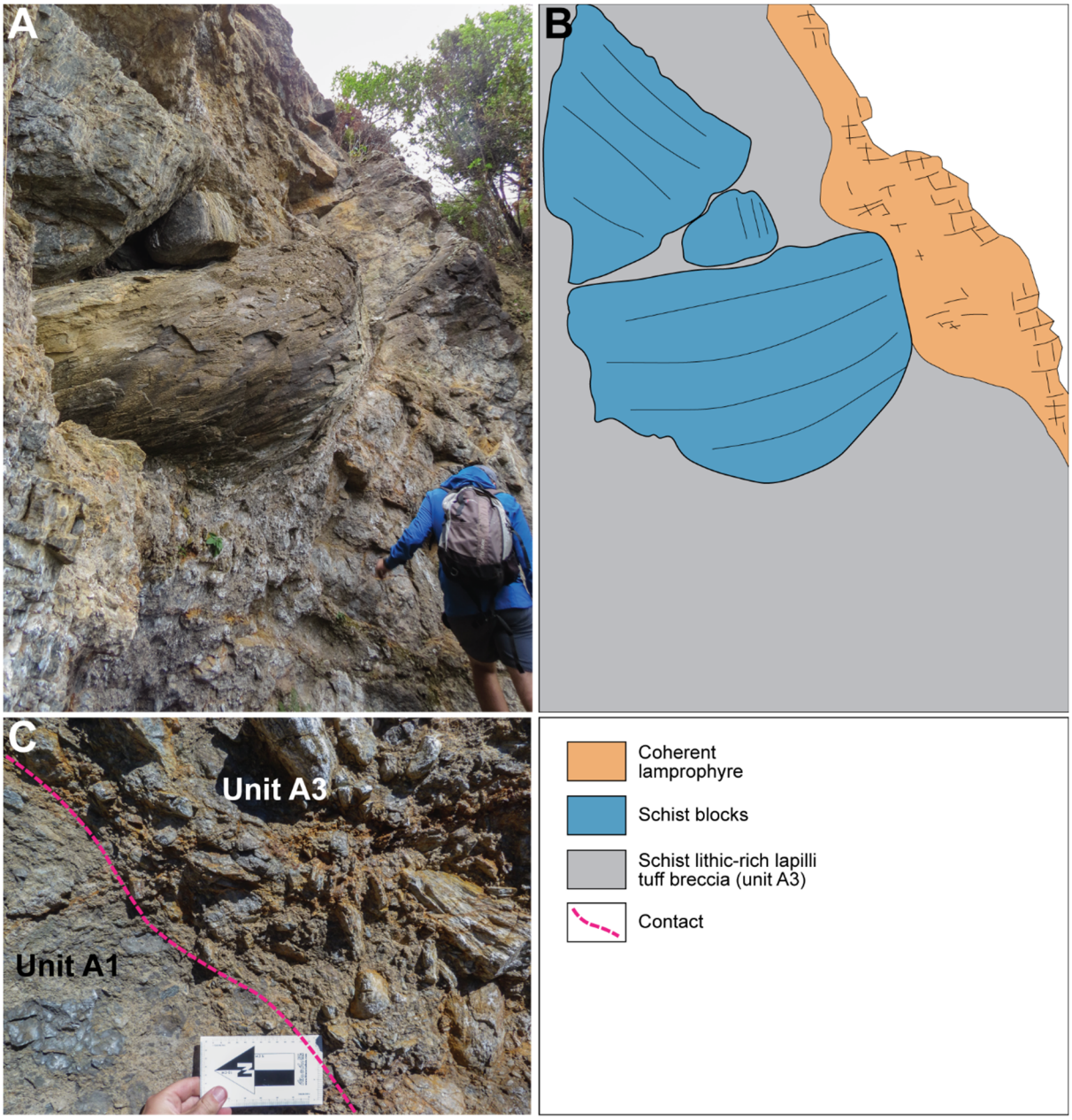

Figure 3.12: Photographs and a diagram of the schist lithic-rich lapilli tuff breccia (unit A3). **(a, b)** Large schist blocks, some over 1 m in size, within the country rock-rich tuff breccia (unit A3); the coherent lamprophyre can be seen towards the edge of the outcrop. **(c)** Contact between juvenile lapilli tuff (unit A1) on the left and the country rock rich tuff breccia (unit A3) on the right. The contact between the two units is sub-vertical with a generally planar orientation.

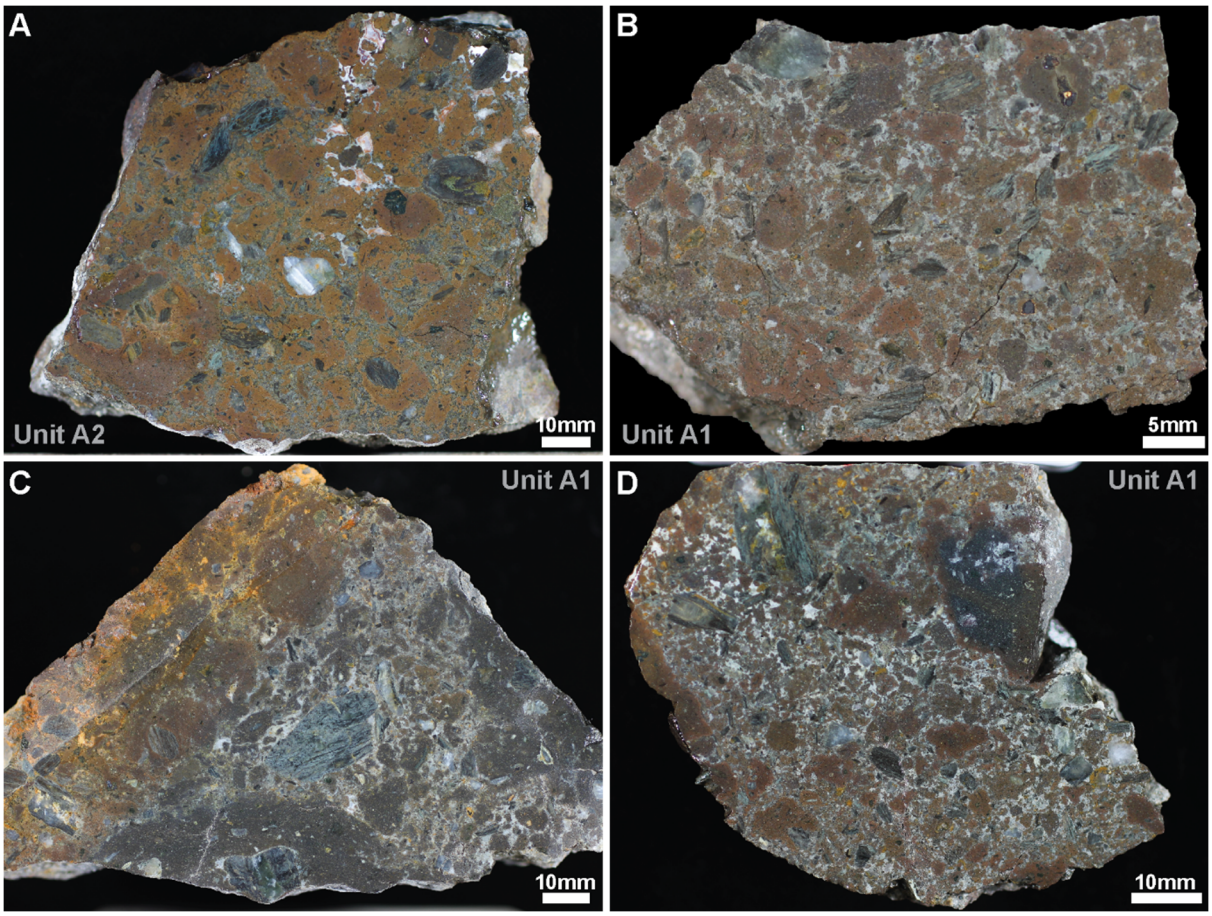

Figure 3.13: Polished slab photographs of lapilli tuff samples. **(a)** Juvenile rich/matrix poor lapilli tuff (unit A2) with composite loaded pyroclasts containing dispersed schist lithics, minor carbonate cement is visible. **(b)** Juvenile rich lapilli tuff with common primary juvenile and composite loaded pyroclasts with occasional schist lithics (unit A1). **(c)** Juvenile lapilli tuff/tuff breccia with common schist lithics and composite loaded lapilli sized pyroclasts (unit A1), note the composite loaded bomb-sized pyroclast towards the bottom of the photo. **(d)** Juvenile lapilli tuff with common schist lithics, and lapilli-sized primary juvenile and composite loaded pyroclasts in a white carbonate cement.

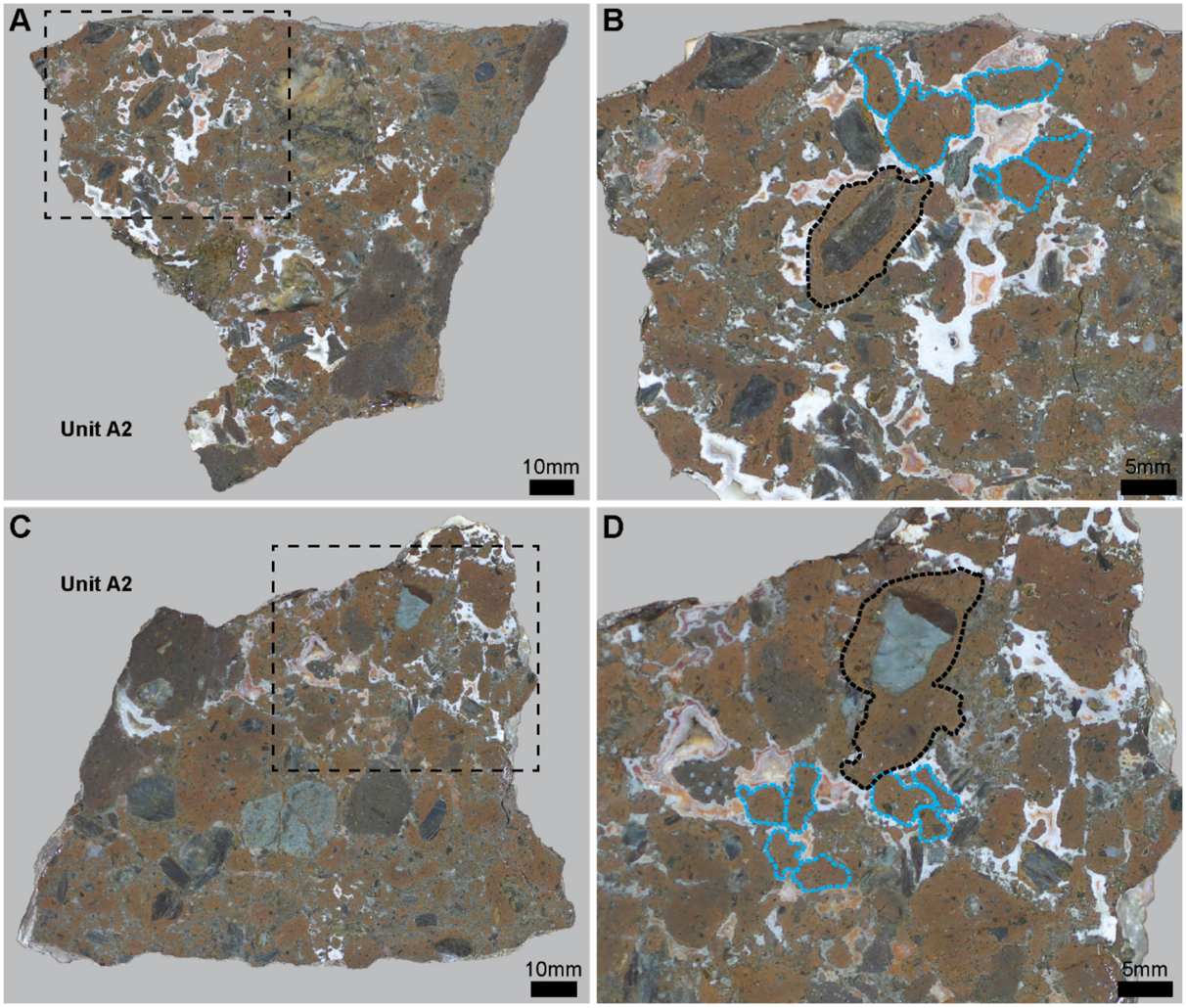

Figure 3.14: Polished slab photographs of lapilli tuff samples from unit A2. **(a)** Juvenile rich lapilli tuff with the box highlighting; **(b)** subtle welding textures (highlighted in blue) and composite loaded pyroclasts with dispersed fragments of schist within (black outline). **(c)** Juvenile lapilli tuff with the box highlighting; **(d)** subtle welding textures (blue) and fluidal composite loaded pyroclast (black). Also note the white carbonate that has infilled the voids in both examples.

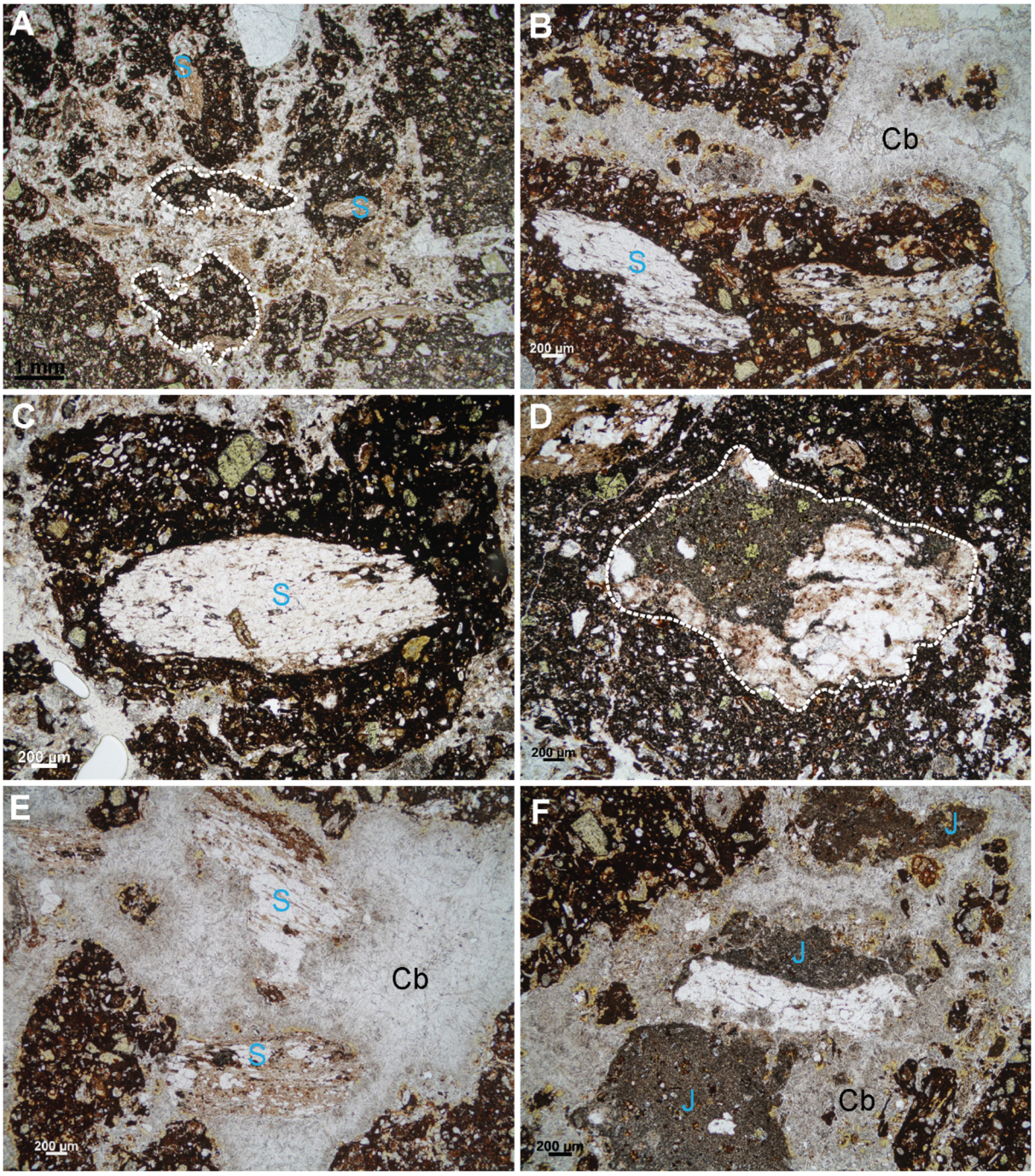

Figure 3.15: Photomicrographs of pyroclast textures. **(a)** Schist lithics occurring in composite loaded juvenile pyroclasts and as accidental lithics within carbonate cement, fluidal textures outlined (unit A1). **(b)** Composite loaded juvenile pyroclasts containing schist lithics (unit A2). **(c)** Composite loaded juvenile pyroclast with a sub-rounded schist lithic core (unit A1). **(d)** Composite loaded pyroclast containing a pyroclast that itself is composite loaded (outlined in white). The outlined pyroclast is the microlitic type pyroclast, and the schist has an irregular and deformed margin suggesting partial melting (unit A1). **(e)** Schist lithics within carbonate cement – lithics have brown juvenile material on their rims suggesting they were fragmented from previous loaded pyroclasts (unit A2). **(f)** Microlitic type juvenile pyroclasts (J) in a carbonate cement (unit A2). The middle pyroclast is composite loaded with a schist lithic comprising half of the clast. S = schist lithic, Cb = carbonate cement.

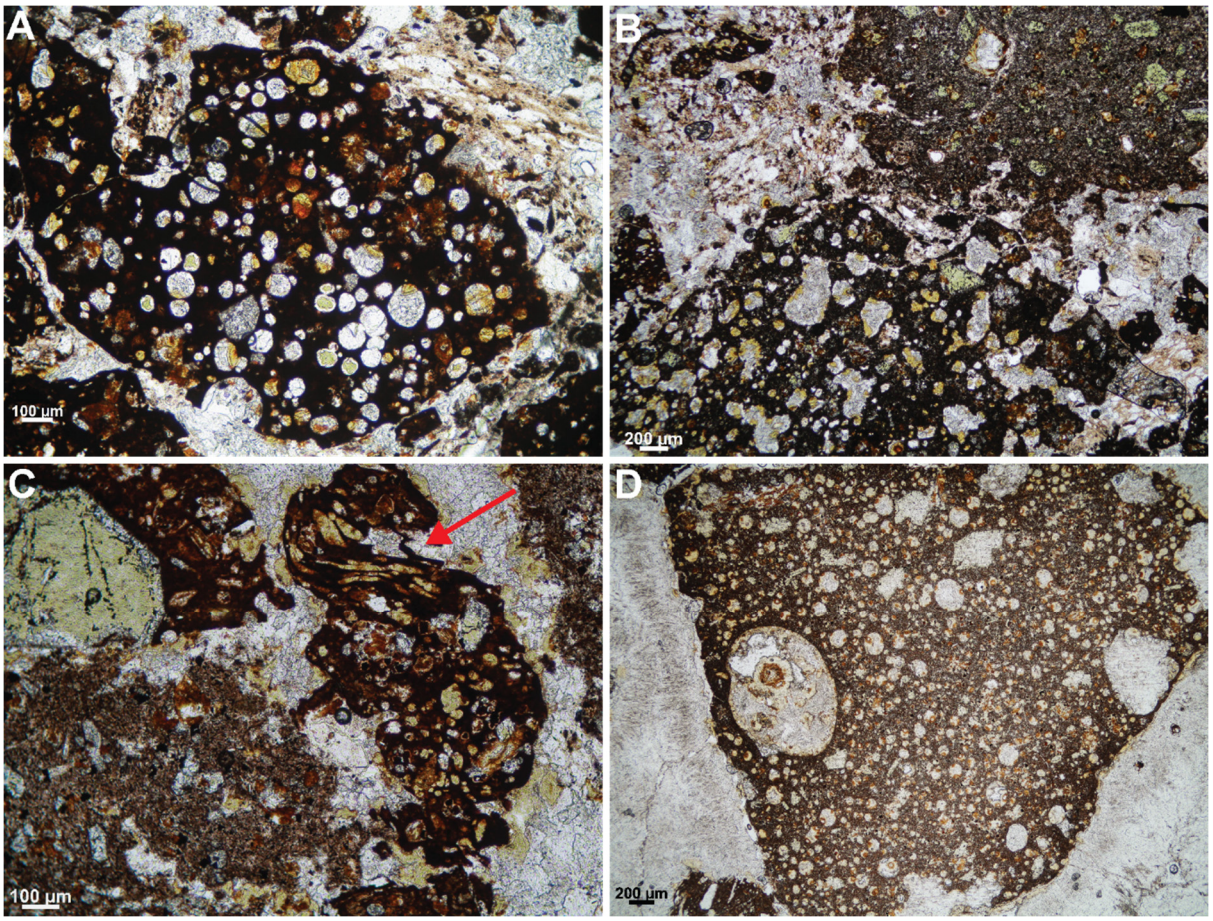

Figure 3.16: Photomicrographs of vesicular juvenile pyroclasts from units A1 and A2. **(a)** Round vesicles in a poorly vesicular (20-40 % vesicles) juvenile pyroclast (unit A1). **(b)** Sub-angular to sub-round vesicles in a poorly vesicular juvenile pyroclast (bottom, unit A1). A non-vesicular microlitic type juvenile pyroclast is visible at the top of the photomicrograph. **(c)** A poorly vesicular fluidal-shaped juvenile pyroclast (right, unit A2). The red arrow points to vesicles that are elongated. A non-vesicular microlitic type juvenile pyroclasts is present to the bottom left of the photomicrograph. **(d)** A moderately vesicular (40-60 % vesicles) juvenile pyroclast with sub-round to round vesicles (unit A2). Vesicularity classifications taken from Houghton and Wilson (1989).

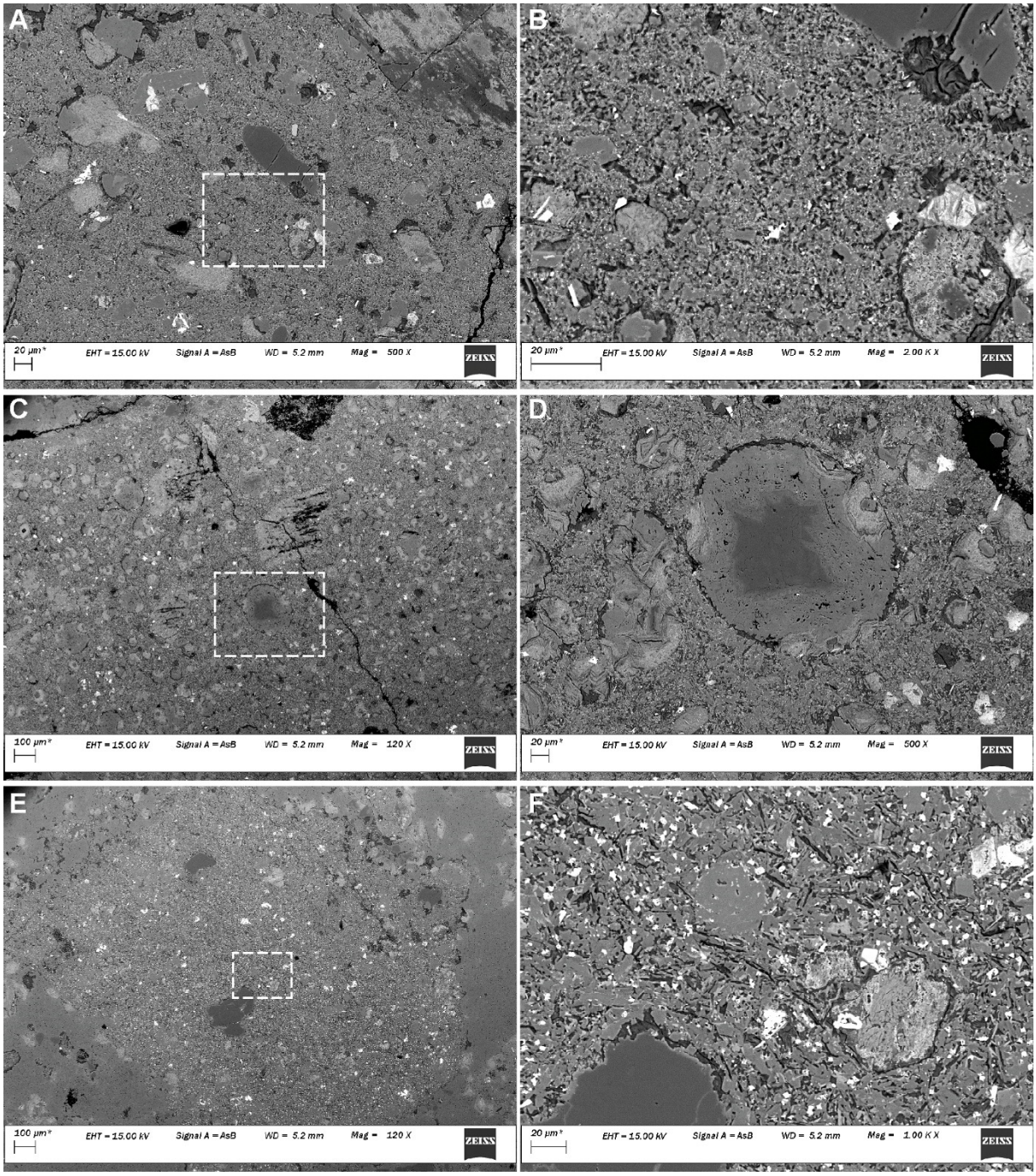

Figure 3.17: SEM electron backscatter images of a juvenile lapilli tuff sample from unit A2. **(a)** Example of a composite loaded juvenile pyroclast consisting of the common brown tachylitic groundmass. Sub-round vesicles and schist lithics are present in the pyroclast. **(b)** Zoom of box in (a) displaying a fine grained microlitic texture that represents the brown tachylite groundmass, which is the most common type of juvenile pyroclast. **(c)** A moderately vesicular juvenile lapilli pyroclast (Fig. 3.16d) with sub-round to round vesicles. **(d)** Zoom of box in (c) displaying carbonate zonation within a large and round vesicle that sits in a microlitic groundmass. **(e)** The less abundant "microlitic" type juvenile pyroclast (e.g. Fig 3.15f), observed within the juvenile lapilli tuff units, sitting in carbonate cement. **(f)** Zoom of box in (e) showing the groundmass is microlitic but coarser grained compared to (b).

3.5 Coherent lamprophyre

Coherent lamprophyre is the dominant lithofacies exposed within the LWD. It accounts for over 70 % of the exposed rock within the diatreme and forms the cliff face which outcrops along the length of the diatreme (Figs. 3.2b, 3.3). The coherent lamprophyre is characterised by being columnar jointed, and by containing common schist xenoliths, kaersutite crystals and peridotite xenoliths (Fig. 3.18e, f).

Other than the above mentioned kaersutite crystals, the lamprophyre is typically aphanitic and poorly vesicular with only rare places having moderate vesicularity (Fig. 3.18f). Schist xenoliths are a common and characteristic feature of the lamprophyre. They vary in size from a few millimetres up to 1 m, and locally show alteration that provides evidence of partial melting at their margins (Figs. 3.18c, d, 3.19a–c). Photomicrographs of schist xenoliths show quartz crystals becoming separated along pre-existing schist foliations; the separated crystals lie amongst a dark-brown glassy groundmass (Fig. 3.20f). The groundmass is isotropic with no visible cleavage or crystal boundaries.

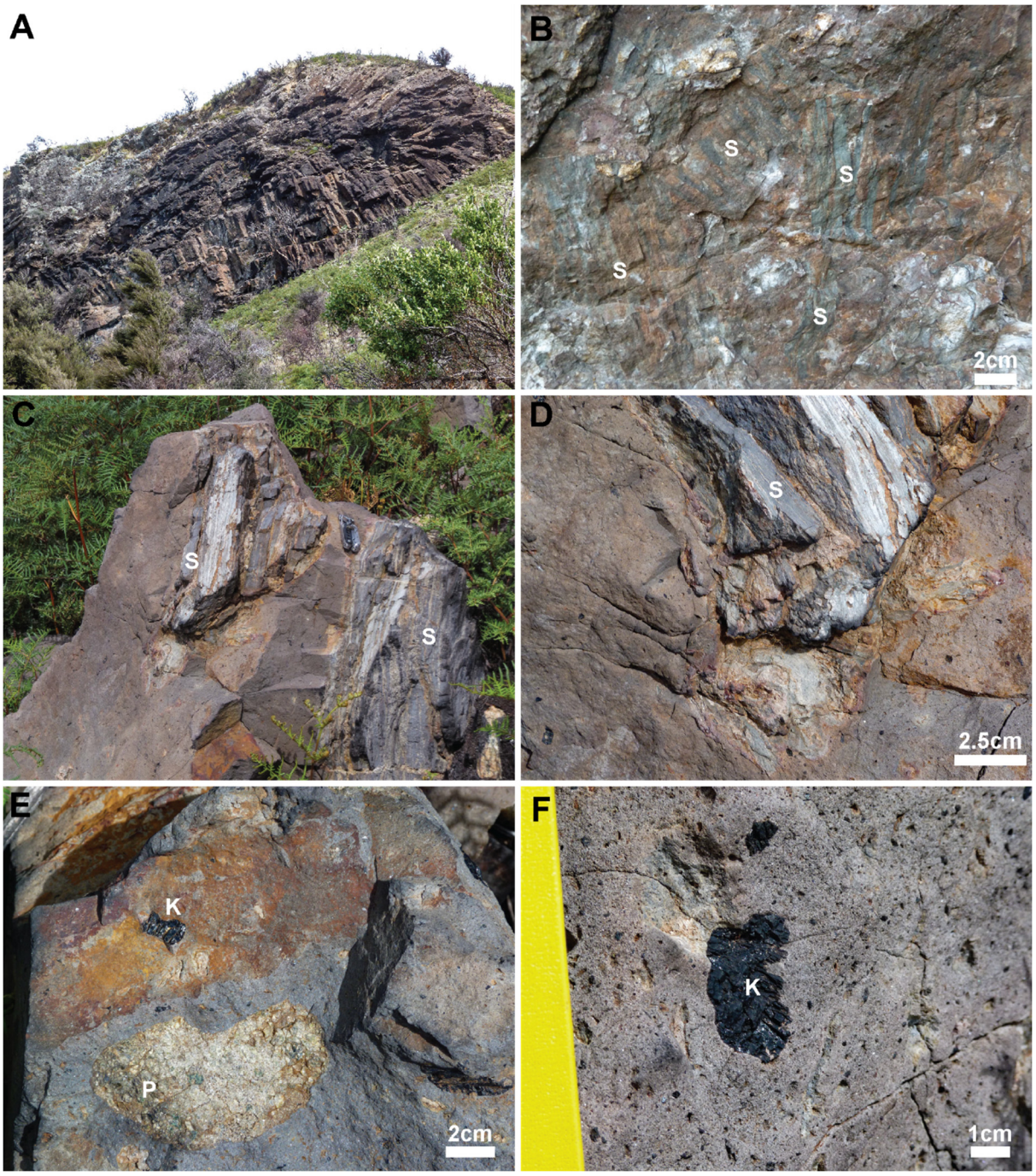

Figure 3.18: Photographs of the coherent lamprophyre. **(a)** Photo of columnar jointed coherent lamprophyre at the northern end of the diatreme with a radial column orientation. **(b)** Schist xenoliths (S) within the coherent lamprophyre; xenoliths have ill-defined borders suggesting they were partially melted and weakly welded together. **(c)** Schist xenoliths in a loose block of lamprophyre (pocket knife for scale), one of the xenoliths in **(d)** is deformed and altered around its margin suggesting the xenolith was partially melted. **(e)** Peridotite (P) and kaersutite megacrysts (K) in a broken block of lamprophyre. **(f)** Kaersutite crystal with smoothly curved shape, interpreted as a resorption texture, in a moderately vesicular lamprophyre.

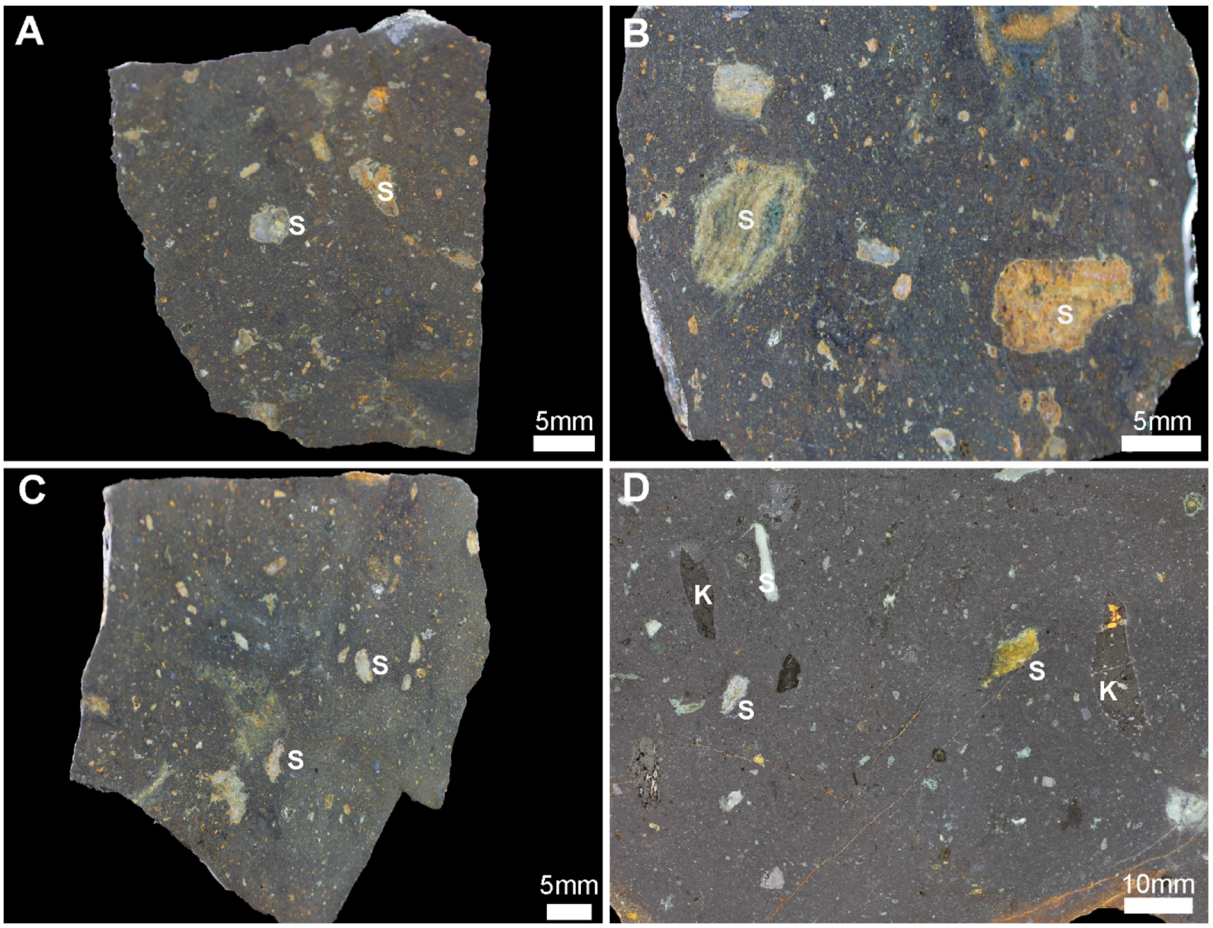

Figure 3.19: Polished slab photographs of the coherent lamprophyre. **(a, b, c)** Samples show varying amounts of schist xenolith material (S) within the lamprophyre. Some schist xenoliths display wispy textures and/or irregular margins indicating partial melting. **(d)** A relatively "fresh" sample of lamprophyre from a columnar jointed section. Schist xenoliths are still present but are less abundant and <5 mm in size. Occasional kaersutite crystals are now present (K).

The coherent lamprophyre is commonly columnar jointed. The northern (Fig. 3.21a) and southern exposures of the lamprophyre both show well developed columnar joints, bounding columns that are approximately 20–40 cm in diameter. In the northern exposure, the column axes develop a radial pattern towards the northern tip of the exposure (Fig. 3.21b) and develop a sub-horizontal and concave-up orientation towards the top of the cliff (Fig. 3.21b). Columns in the most southerly exposure are roughly horizontal.

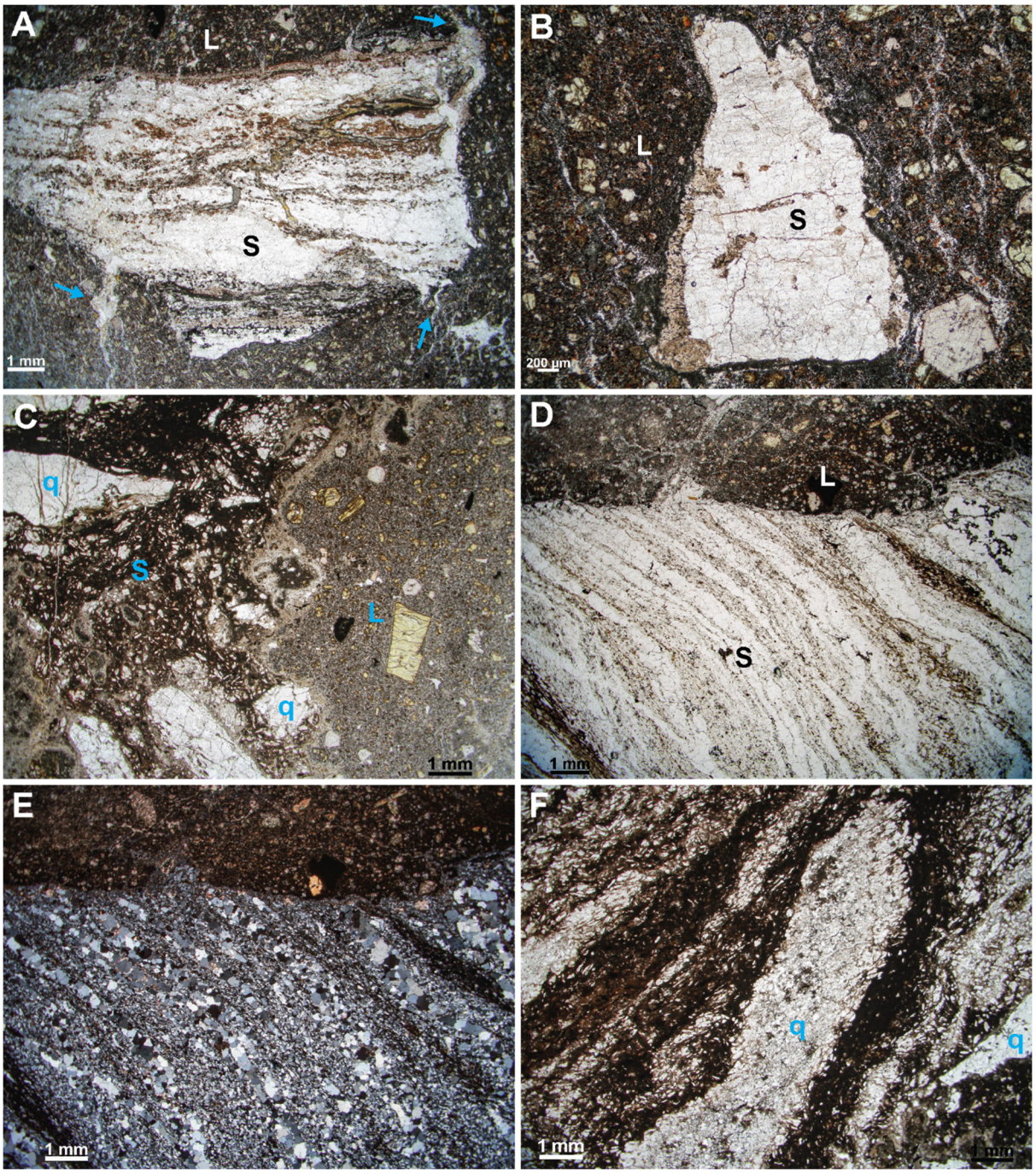

Figure 3.20: Photomicrographs of schist xenoliths within the coherent lamprophyre. **(a)** Small schist xenolith within a lamprophyric groundmass, arrows point to wispy-deformed margins of the xenolith indicating partial melting of the xenolith. **(b)** Small, predominantly quartz, schist xenolith that does not show any partial melting indicated by well-defined borders and no wispy textures. **(c)** Contact between lamprophyre and a schist xenolith, quartz is in a brown glassy groundmass. **(d)** Contact between lamprophyre and schist xenolith; quartz crystals of the schist have not separated to the extent shown in photo (c). **(e)** Crossed nicols image of (d) showing quartz grain-size variability along foliation. **(f)** Quartz in a brown glassy groundmass; quartz crystals are separated along the pre-existing schist foliation. S = schist xenolith, L = lamprophyre, q = quartz crystals.

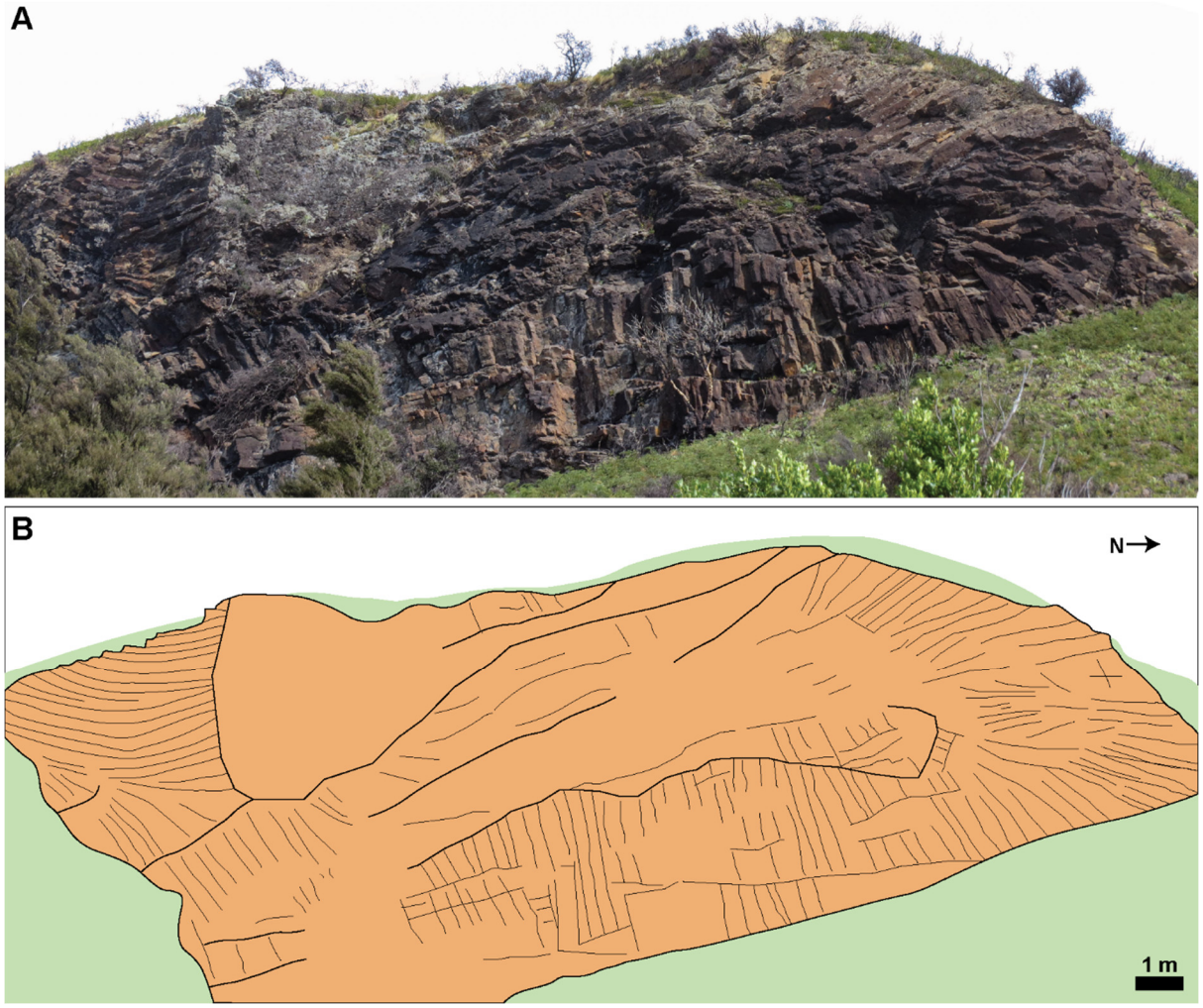

Figure 3.21: Photograph and sketch of the columnar jointing in the coherent lamprophyre. **(a)** Photo of the columnar jointed coherent lamprophyre at the northern end of the diatreme. **(b)** Sketch of the above photo highlighting the jointing geometry. A radial pattern is present at the northern tip of the lamprophyre and a curved concave-up pattern towards the top left of the outcrop. Joints typically terminate against the sub-horizontal joints running across the outcrop, and the non-jointed domain towards the upper left might represent a different lithology.

3.6 Interpretation

3.6.1 Significance of the country rock breccia and schist megablocks

The schist country-rock breccia and schist megablock deposits provide important insights into the evolution of the diatreme at Lake Wanaka. The two facies are a characteristic feature of the diatreme and represent the most voluminous clastic facies exposed in outcrop. The schist country-rock breccia is exposed along the lake shore towards the southern end of the diatreme (Figs. 3.2, 3.3, 3.6), whereas the schist megablocks are observed along the base of the coherent lamprophyre predominantly towards the northern end of the diatreme (Figs. 3.2, 3.3, 3.4).

3.6.1.1 Schist country-rock breccia

Country rock breccia deposits are characteristic of many diatremes and can form by a number of different processes (White and Ross 2011). The two main processes are; (1) syn-eruptive failure of wall rocks into the volcanic pipe (Barnett 2004; Brown et al. 2008a; Seghedi et al. 2009), either by slumping and sliding, or by rock-fall and rock avalanche of country rock (Lefebvre 2013) and (2) *in situ* brecciation of country rock near the diatreme margin to form contact breccias (Clement 1982; Lorenz and Kurszlaukis 2007) which have also been described as monobreccias (Delaney and Pollard 1981).

Interpretation of the schist country-rock breccia at the LWD needs to take into account the following observations; (1) a complete absence of juvenile material (Fig. 3.9), (2) inferred close proximity to the eastern diatreme margin (Fig. 3.2a), (3) occasional tightly packed, but not jigsaw-fit, clasts that display rare brittle fragmentation textures (Figs. 3.7, 3.9), (4) occasional blocks up to 2 m in size (Fig. 3.6), (5) a weak alignment of clasts observed in some samples (Fig. 3.7) and (6) probable situation of the deposit in the root zone or lower diatreme.

Deposition by rockslides of near-surface country rock seems unlikely given this style of deposit is often characterised by blocks of country rock up tens of metres in size that typically dip inwards towards the pipe (Brown et al. 2008b). Therefore, the best fitting mechanism for deposition of the schist country-rock breccia at the LWD is by either (1) rock fall and rock avalanche into an open space or by (2) fragmentation of the wall rock to form a contact breccia.

Creating a rock fall deposit would have required unstable and weakened country wall rock, open space for the country rock to fall into, and a trigger for the rock fall such as an explosion within the diatreme, or shaking of an unsupported wall. Space necessary for the rock fall to

accumulate into can be created by a few different mechanisms; (1) a crater or fissure that is open directly to the surface (White and Ross 2011; Lefebvre et al. 2012), (2) through magma withdrawal (Lefebvre et al. 2012), and (3) explosions that drive the volcanic debris upwards leaving behind a temporary evacuated space (Lorenz and Kurszlaukis 2007; Kurszlaukis and Lorenz 2008; Ross et al. 2008a, b; Seghedi et al. 2009; Ross et al. 2013).

Rock fall onto the crater floor can form by wall rock becoming unstable at higher levels within the diatreme structure and collapsing under gravity. The rock fall will typically deposit onto a pile of pre-existing pyroclastic debris. This scenario is not favoured, as falling onto the open crater floor increases the probability that the country rock breccia would become resedimented by explosions due to its deposition site being located in a dynamic environment. Incorporation of other types of pyroclastic material, such as juvenile pyroclasts, might be expected in deposits formed on the open crater floor. The schist country rock breccia along the lakeshore of the diatreme shows no evidence that it is situated on top of or in close proximity to any other type of pyroclastic deposit, nor does it contain any juvenile or other type of pyroclastic material. Also, whilst the current depth of exposure within the Lake Wanaka diatreme is poorly constrained, the lithofacies observed in this study suggest the schist country-rock breccia outcrop is within the root zone, or the lower diatreme. This is supported by the lack of bedded deposits, poorly mixed and poorly sorted lapilli tuff deposits, large rafts of country rock, and a general dominance of country rock material over fragmental juvenile facies. For the country rock breccia to have been deposited from a rock fall onto a crater floor situated at the root zone level, the crater floor must have been deeply excavated whilst the space above remained relatively unfilled. Alternatively, a temporary evacuated space could have been created at the root zone level through thermohydraulic explosions below the syn-eruptive crater (discussed further below). A number of workers have suggested diatremes can have deeply excavated syn- or post-eruptive pipes that can remain open for long periods of time (Kurszlaukis and Barnett 2003; Skinner and Marsh 2004; Brown et al. 2008a; Scott Smith 2008). Barnett (2008), however, argues that steep-sided pipe walls make it unlikely that a crater could remain open for long periods of time due to the unstable wall rock. At the Lake Wanaka diatreme, the open space need only be available for a brief period of time, long enough for a rock fall event.

The space required for a rock fall deposit can also be formed by thermohydraulic explosions below the syn-eruptive crater that drives the overlying pile of pyroclastic debris upwards, leaving behind a temporarily evacuated volume (Barnett 2004; Lorenz and Kurszlaukis 2007; Ross et al. 2008a; Seghedi et al. 2009). Whilst the space is created, unstable wall-rock can collapse (e.g. a rock fall) into the evacuated volume to form a country rock breccia. If this mechanism was occurring at the root zone level within the LWD, it could readily explain the occurrence of the schist country-rock breccias.

Magma withdrawal is a process that can remove the dynamic support of the surrounding wall rock, causing a collapse of the wall rock into the cavity left behind. The schist country-rock breccia is not confined to a narrow dike-like structure (Lefebvre et al. 2012), and therefore this scenario is unlikely.

Clement (1982) defined contact breccias as breccias consisting entirely of one type of clast derived from the same rock that the breccias are in contact with, and they are equivalent to the monobreccias described by Delaney and Pollard (1981). Contact breccias often display a progression from unbrecciated country rock towards increasingly fragmented rock of the same lithology, indicating that the breccias formed *in situ* (Lorenz and Kurszlaukis 2007). Clasts in contact breccias are typically angular to sub-angular in shape, exhibit jigsaw fit textures, with clast sizes ranging from 2 m down to microscopic size, but predominantly 10-20 cm in diameter (Lorenz and Kurszlaukis 2007). Brecciation of the country rock, the formative process for contact breccias, can occur via a number of mechanisms; thermohydraulic explosions (Lorenz 2003; Lorenz and Kurszlaukis 2007), hydraulic fracturing (Brown et al. 2007), under-pressures within the evolving pipe created by differences between lithostatic pressure and the in-conduit pressure of the erupting mixtures (Sparks et al. 2006) and brecciation by pore pressure build-up (Delaney and Pollard 1981). If these mechanisms break up the *in situ* country rock, they produce jigsaw fit textures in the breccia. Contact breccias also display a fabric of aligned clasts that typically dip towards the volcanic pipe. This fabric represents a weak form of bedding, and suggests formation of the contact breccia must have been followed by a gravity induced collapse of the rock mass into an open space (Barnett 2004). This effectively represents a rock-fall deposit, and thus the term contact breccia in this study is only used to describe the former style of deposit, that is, an *in situ* breccia near the margin of the diatreme with jigsaw fit textures.

The schist country-rock breccia outcrop at the LWD has extensive surficial alteration, and it runs sub-parallel to the margin of the diatreme, so it is difficult to assess whether there is a change in brecciation style and orientation moving westwards, away from the inferred diatreme margin. No change, however, is apparent that might suggest a contact breccia. Other factors that suggest the schist country-rock breccia is not an *in situ* contact breccia include; the absence of jigsaw fit textures, a weak alignment of clasts in some samples (Fig. 3.7a–c), and the occurrence of large >1 m sized blocks amongst much smaller sized clasts. Whilst the schist clasts are somewhat tightly packed, they are clearly not jigsaw fit, with most clasts typically randomly orientated. The weak alignment of clasts observed in some samples would not have occurred *in situ*, rather, it would have required movement of the clasts to achieve this alignment. All of these factors suggest the schist clasts have been transported to some degree, and therefore the schist country-rock breccia cannot be an *in situ* contact breccia.

The schist country-rock breccia on the lake shore is interpreted to represent a rock fall deposit sourced from the collapse of weakened and unstable wall rock at a higher level than the breccia deposition site. The rock fall likely occurred into a temporary space created by thermohydraulic explosions below the syn-eruptive crater at the root zone level. A rock fall can account for the randomly orientated clasts and the minor alignment of clasts seen in some samples. A range in clast sizes up to a couple of metres would also be expected for a rock fall that was sourced from an unstable vent wall. Subsequent vibrations and shaking created by activity throughout the diatreme may have contributed to some clasts becoming more tightly packed, and led to minor brittle fragmentation at the clast margins. The remaining void space between clasts was infilled by carbonate post-eruption.

3.6.1.2 Schist country-rock megablocks and megablock breccia

Large rafts and blocks of country rock metres in size are a feature of many diatremes (Brown et al. 2008a; Seghedi et al. 2009). Rock slides that mobilise country rock from the crater margin are a common process for deposition of large >10 m sized blocks into a diatreme. Blocks of country rock deposited by rock slides will share similar orientations typically dipping inwards towards the pipe. They can also display localised soft sediment deformation indicating that the country rock was poorly consolidated at the time of collapse into the conduit (Brown et al. 2008a). The random orientation of the large schist blocks in the megablock breccia at the LWD (Fig. 3.5) does not suggest that the megablocks were deposited into the diatreme conduit

from a rock slide. Schist megablocks also occur as single blocks protruding from the coherent lamprophyre (Fig. 3.4), and these also do not show any preferential orientation that might suggest a rock sliding style mechanism for deposition.

Single megablocks that protrude from the coherent lamprophyre have their weight fully supported by the surrounding lamprophyre. This suggests that the large megablocks were at least partially enveloped by the magma as it intruded into the diatreme. No "tails" of schist material connecting to the schist megablock were observed that might suggest the block settled through the lamprophyre magma, nor were any chilled margins observed other than in direct contact with the schist. Where the megablocks occur in a debris pile or a breccia (e.g. Fig 3.5), coherent lamprophyre is present in the space between the blocks. This feature can be explained by a low-viscosity magma (e.g. lamprophyre) intruding into the void space between the schist megablocks. No large megablocks are observed protruding from the coherent lamprophyre more than 2–3 m above the base of the cliff face. This suggests that the megablocks originally accumulated at a particular level within the diatreme, such as on a ledge.

The large schist megablocks are interpreted to have been dislodged from the conduit walls at higher levels within the diatreme and fallen into the open vent. The large size of the megablocks suggests they were "slabbed" off the vent wall, and fell onto a ledge within the diatreme. Later emplacement of the coherent lamprophyre may have partially to completely enveloped the megablocks, and intruded into void space between blocks that deposited as a breccia or debris pile.

3.6.2 Deposition of lapilli tuff and tuff breccia

Three lapilli tuff and tuff breccia units outcrop in close proximity to one another towards the southern end of the diatreme (Figs 3.2b, 3.3). The units are situated slightly westwards of the coherent lamprophyre, and represent the most central deposit that can be observed within the LWD structure (Fig. 3.2b). These deposits represent a dynamic volcanic history, displaying evidence of varying fragmentation styles, welding of clasts and recycling of pyroclastic material. The lapilli tuff and tuff breccia deposits represent only a small exposed portion in the context of the whole diatreme, yet they contain important information about how the diatreme developed, as discussed below.

3.6.2.1 Evidence for spatter deposits

The term welding in this section is used as a non-genetic term to describe the sticking together or merging along contacts between primary juvenile pyroclasts, composite pyroclasts, and within composite-loaded pyroclasts; it does not imply specifically compaction welding from the overburden pressure of a still-hot deposit (Sumner et al. 2005). Units A1 and A2 are juvenile-pyroclast-rich lapilli tuff and tuff breccia deposits. Only unit A2 displays evidence of welding between juvenile and composite loaded pyroclasts (Fig. 3.14), but both units are inferred to be spatter deposits as discussed below.

Spatter is defined as the accumulation of originally hot and fluid pyroclasts that agglutinate on landing. A spatter deposit represents a preserved accumulation of juvenile pyroclasts where the clast margins are either wholly or partially retained (Sumner et al. 2005). Sumner et al. (2005) categorise five types of spatter pyroclasts which range from solidified pyroclasts to fluid lava. These types are; (1) clasts that are solid and brittle upon time of landing (e.g. normal scoria), (2) clasts with brittle rims but molten cores, (3) clasts that agglutinate on landing and contain molten interiors, (4) very fluid clasts that splash on landing and merge to form clastogenic lavas and (5) clasts formed by the recycling of scoria in a fire fountain, which as a consequence have a fluid rim but a solid interior. In this study, where welding is noted, I have inferred agglutination between primary juvenile and/or composite loaded pyroclasts.

The majority of lamprophyre pyroclasts within unit A2 are likely to represent type 2 pyroclasts, with rarer pyroclasts of type 3 (Fig. 3.14), whilst unit A1 is predominantly composed of type 2 pyroclasts. The abundance of composite loaded pyroclasts containing dispersed schist lithics (Fig. 3.22) may have affected the fluidity of those spatter pyroclasts as they were deposited. A large proportion of non-deformable lithics have been suggested to inhibit the development of compaction fabrics in spatter accumulations (Brown et al. 2008b), and entrained country rock fragments are also a heat sink, cooling the composite pyroclast (e.g. Rosseel et al., 2006). Therefore, it is likely that a large proportion of the composite loaded pyroclasts in units A1 and A2 had cooled to below the glass transition temperature by the time they landed (type 2 pyroclasts). The high amount of composite loaded pyroclasts and country rock lithics may have also inhibited agglutination. Weak welding in unit A2 indicates that some pyroclasts were above the glass transition temperature, and overall, the whole unit was emplaced very close to the glass transition temperature for the lamprophyre composition pyroclasts.

The rare schist country-rock lithics that occur scattered throughout the unit A2 deposit (e.g. not dispersed within composite loaded pyroclasts) represent a minor amount of country rock debris that fell into the conduit during spatter accumulation (Fig. 3.10d). Unit A1 however, has a slightly larger proportion of free schist lithics, suggesting higher input of country-rock fall-back during spatter deposition (Figs. 3.10a, 3.13c).

3.6.2.2 Fragmentation and deposition of spatter

Spatter deposits are a common product of Hawaiian style basaltic fire-fountain deposits (Stovall et al. 2011), paroxysmal Stromboli eruptions (Andronico and Pistolesi 2010), fissure eruptions (e.g. Laki; Thordarson and Self 1993), hornitos (Rader and Geist 2015), littoral cones (Mattox and Mangan 1997), rootless cones (Hamilton et al. 2010), as well as in kimberlites (Brown et al. 2008b) and hundreds of metres below surface in fissures (Lefebvre et al. 2012).

Hawaiian fire-fountains can form various deposits such as clastogenic lavas, agglutinated spatter and non-welded pyroclasts such as bombs, scoria, and ash. Detailed studies of Hawaiian fire-fountain deposits (Stovall et al. 2011) suggest highly vesiculated magmas are a requirement for this style of deposit, with exsolution of gases driving the fragmentation. Paroxysmal eruptions on the volcanic island of Stromboli during 2009 created two discrete spatter deposits. Andronico and Pistolesi (2010) suggest the earlier eruption was triggered by the ascent of a small volume of low-porphyritic and gas-rich magma, which destabilised the shallow plumbing system of the volcano and began mixing with the highly-porphyritic and degassed magma reservoir. This led to the ejection of intermediate composition juvenile fragments with a wide range of densities that accumulated as spatter deposits atypical of those from Stromboli style eruptions. Thordarson and Self (1993) showed spatter deposits can accumulate from basaltic fissure eruptions as documented in the 1783–1785 Laki volcano in Iceland. They interpreted a change in fragmentation style that initially produced scoria and tuff cones due to hydromagmatic interactions and then later Hawaiian style spatter deposits once the groundwater supply was exhausted. Spatter deposits at Laki have also accumulated from the eruption of rootless cones (Hamilton et al. 2010). Rootless cones at Laki were formed from lava-water interactions in lava tubes, lava channels and sheet lava lobes. Small hornito-style spatter rich accumulations were suggested to form from lava flowing over water-bearing substrates. Littoral lava fountains and bubble bursts can occur when a lava tube fractures, allowing sea water to rush in and mix with the lava to create vapour explosions (Mattox and

Mangan 1997). These fragmentation processes will often produce welded spatter deposits. Mattox and Mangan (1997) suggest bubble bursts result from lower and unsteady rates of water infiltration, creating more sporadic explosions. The continuous eruption of lava fountains in comparison, suggests a constant and accessible source of water. Lefebvre et al. (2012) suggested pyroclastic spatter deposits had infilled planar cavities some 150 m below the paleosurface at the Castle Buttes Trading Post volcanic complex. The deposits contained juvenile pyroclasts that were coarse grained, poorly vesicular and fluidal, along with high amounts of lithic content shed from the unstable conduit walls. They suggested that fragmentation was driven by water welling out of fractured and jointed wall rock that interacted with the hot magma.

Juvenile and composite pyroclasts within unit A2 at the LWD are typically incipiently vesicular (5-20% vesicles) with only occasional examples (Fig. 3.16d) of moderately vesicular (40-60% vesicles) pyroclasts present (Houghton and Wilson 1989). Therefore, it is unlikely the magma that supplied the juvenile and composite loaded pyroclasts in unit A2 and the other lapilli tuff units had sufficient volatile content to generate a Hawaiian style fire-fountain eruption. Low vesicularity in the pyroclasts suggest the magma was already degassed by the time it fragmented to form spatter, or that the magma contained a low volatile content to begin with (Houghton and Wilson 1989). Fragmentation driven by the introduction of a secondary low-porphyritic and gas-rich magma into the existing magma reservoir, as suggested by Andronico and Pistolesi (2010), is supported by the presence of the second type of "microlitic" textured juvenile pyroclast in the lapilli tuff deposits at the LWD (e.g. Figs. 3.15f, 3.16c). Andronico and Pistolesi (2010) report a range in densities for the Stromboli juvenile spatter fragments, but the LWD juvenile and composite loaded pyroclasts are predominantly incipiently vesicular, so it is unlikely they were generated by a paroxysmal explosion(s). Generation of spatter from a rootless cone such as a hornito is also not supported. There is no evidence of a flowing lava; the coherent lamprophyre within the LWD is interpreted as an intrusion that was emplaced after the juvenile rich lapilli tuffs had been deposited. Whilst a magma–water generated fragmentation process is presented below, a rootless cone typically requires the flow of lava over, or into a water saturated material.

Spatter generation was most likely triggered by ground water infiltrating into the magma at depth through fractures and joints in the country rock. Vapour explosions such as bubble

bursts or lava fountains as demonstrated by Mattox and Mangan (1997) may have fragmented the magma. At the same time, unstable debris shed from the wall-rock became incorporated into the spatter deposit, and this whole process could have occurred at depths over 100 m below the paleosurface (Lefebvre et al. 2012). It is suggested that syn-eruptive degassing occurred during magma ascent within the LWD, and that external fluids interacted at depth with the lamprophyre magma. This played an important role in controlling the moment of magma fragmentation and in propelling the ejection of magma-mixture that created the spatter deposits (Mundula et al. 2013).

3.6.2.3 Recycling and remobilisation of juvenile and composite pyroclasts within the diatreme

Composite pyroclasts are ubiquitous in many maar-diatreme deposits, both within the diatreme conduit (e.g. Clement 1982; McClintock and White 2006; Ross and White 2006; Gernon et al. 2012; Lefebvre et al. 2013) and the surface maar ejecta ring deposits (e.g. Lorenz and Zimanowski 1984; Valentine and Groves 1996; Lorenz et al. 2002; Rosseel et al. 2006; Sottili et al. 2010). These clasts provide important evidence about site(s) of fragmentation and/or the recycling of pyroclasts during a maar-diatreme eruption.

Composite loaded pyroclasts can have several lithic fragments and/or pyroclasts dispersed within the primary juvenile material (Rosseel et al. 2006; White and Houghton 2006). Composite loaded pyroclasts have a number of proposed mechanisms for formation within diatremes. (1) Agglutination of primary ductile juvenile material together with country rock lithics or pre-existing pyroclasts (Rosseel et al. 2006). (2) Intrusion of magma into unconsolidated country-rock debris which mingles with the debris to form a peperite. Subsequent explosions can fragment and eject the peperite to form juvenile lapilli and bombs loaded with country rock fragments (White and McClintock 2001; Lorenz et al. 2002). (3) Incorporation of country rock debris from the collapse of conduit walls into fluidal pyroclasts (Valentine and Groves 1996; Doubik and Hill 1999). (4) Collision of dispersed wall-rock and fragmented magma at an explosion site where they weld together to form a larger clasts (Lorenz and Zimanowski 1984).

At the LWD, all of the lapilli tuff and tuff breccia deposits show evidence of single- and/or multi-stage hot-state recycling of country rock lithics and pyroclastic material. Composite loaded clasts containing only dispersed schist lithics are abundant (Fig. 3.22), with over 50 % of all pyroclasts within the lapilli tuff deposits consisting of this type of clast (e.g. Figs 3.13, 3.14, 3.15a–c). Composite loaded pyroclasts containing dispersed pyroclasts ± schist lithics are much less common (e.g. Fig. 3.15d). All three units also contain occasional juvenile pyroclasts that are distinct from the typical dark brown tachylitic pyroclasts that are predominant in the lapilli tuffs. This second type of juvenile clast has a microlitic groundmass and is rarely vesicular (Figs. 3.15f, 3.17e, f); it is also the recycled juvenile pyroclast within the composite loaded pyroclast in Figure 3.15d. The rare examples of composite loaded pyroclasts that contain pyroclasts within them represent recapitulated pyroclasts (Rosseel et al. 2006). This suggests an earlier formed juvenile pyroclast was captured within a fluidal magma and was subsequently fragmented with the older juvenile pyroclast within it, and "reborn" as a composite loaded pyroclast (Lefebvre 2013). The modest proportion of such fragments suggest that some multi-stage recycling occurred in the LWD (e.g. Fig. 3.22c). Single-stage recycling of lithics within the LWD was a common process. The abundance of composite loaded pyroclasts that contain only schist lithics (>50 %) within the lapilli tuff suggests the fragmentation site(s) was in close proximity to wall-rock material. This is most readily explained by schist wall-rock shedding into the magma and then fragmenting (Fig. 3.22b). Whilst the composite loaded pyroclasts were falling back into the conduit after ejection, small amounts of schist wall-rock material continued to shed into the pipe. This accounts for the various sized schist lithics that occur freely within the lapilli tuff and tuff breccia deposits.

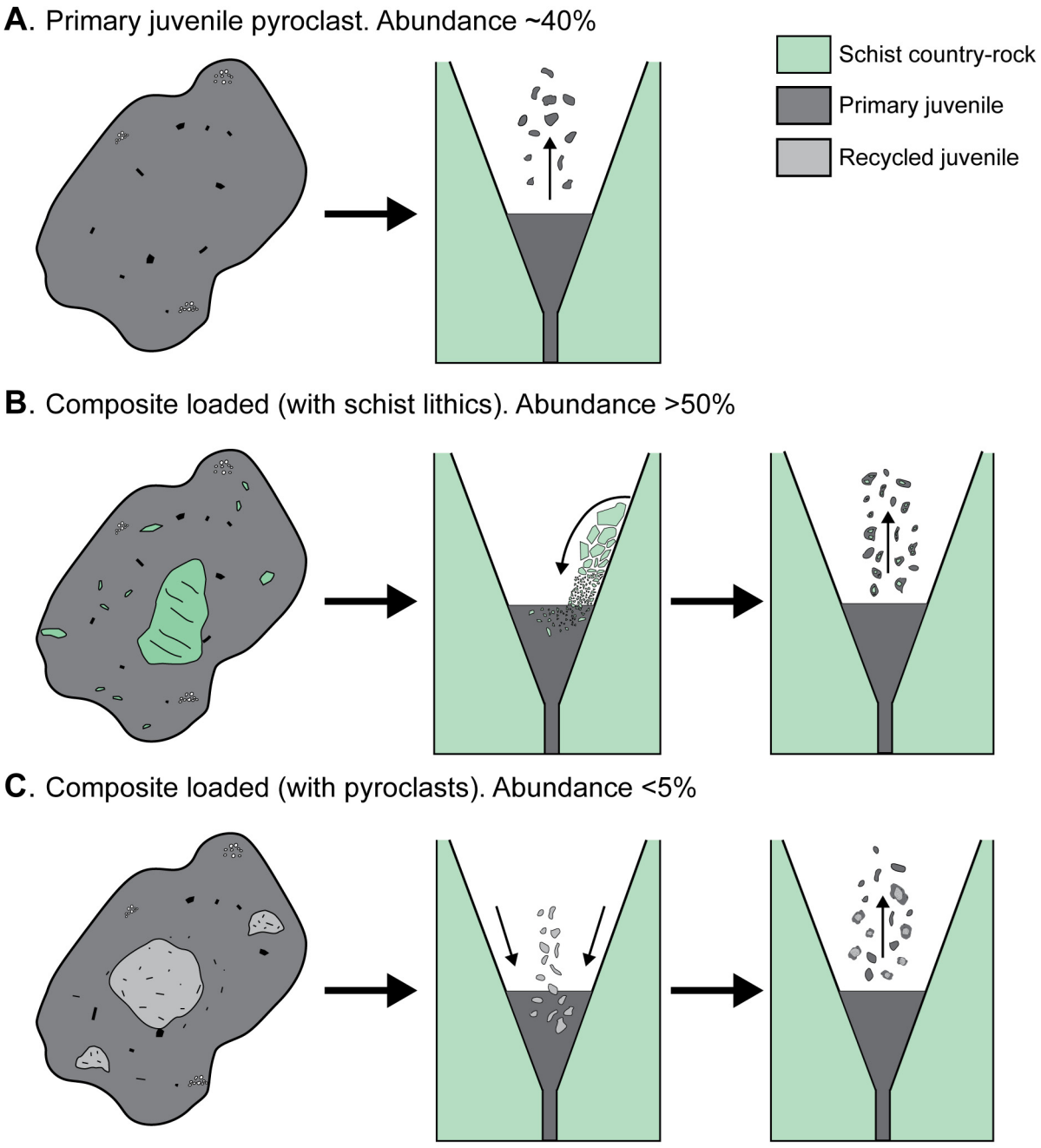

Figure 3.22: Examples of the juvenile and composite pyroclast types that occur throughout the lapilli tuff and tuff breccia deposit at the LWD. The approximate abundance of each pyroclast type is also shown, and to the right of each clast type, a diagram suggests the likely mechanism in which the pyroclast was formed. **(a)** Primary juvenile pyroclast created by fragmentation of the magma. **(b)** Composite loaded pyroclast containing various sizes of schist lithics. This type of composite pyroclast likely formed from wall rock that shed into the magma and was subsequently fragmented. **(c)** Composite loaded pyroclast containing recycled pyroclast fragments (± schist lithics). The recycled (older) pyroclasts fell into the magma from a higher level within the diatreme, somewhere above the fragmentation site, and were subsequently ejected. Note: each process demonstrated in (a), (b), and (c) would have likely been contemporaneous.

3.6.2.4 Evidence for debris jets within the diatreme

Unit A3 (Figs. 3.10g, h, 3.11, 3.12) is distinguished from units A1 and A2 based on the units higher proportion of schist country-rock lithics. This higher country rock component may indicate either a change in explosion site location (Ross and White 2006), incorporation of wall rock material during gravitational collapse into the active vent (Brown et al. 2009), or accumulation of wall rock and resedimented pyroclastic debris from different depths above (Lefebvre 2013). Unit A3 has a sub-vertical planar contact with the juvenile rich lapilli tuff unit A1 (Fig. 3.12c), where a clear transition to a country rock rich composition is observed. Debris jets have been documented to create near vertical contacts with the surrounding deposits within diatremes (Ross and White 2006; White and Ross 2011). They are transient conduits that open in response to the upwards expansion of a mixture of volcaniclastic debris, steam, and magmatic gases following an explosive magma-water interaction (Ross and White 2006). If unit A3 was emplaced via a debris jet, the explosion site must have been near the walls or floor of the vent to incorporate a large amount of country rock material and only a small juvenile component (Ross and White 2006). Large, metre sized blocks of schist country-rock sitting in unit A3 (Fig. 3.12a) were probably deposited from wall rock dislodged at a higher level within the diatreme that fell onto the crater floor. It is also possible the deposit was subsequently re-worked by one or more debris jets, which can remain completely subterranean or can propagate to the surface (Ross and White 2006).

3.6.3 Emplacement of the coherent lamprophyre

The coherent lamprophyre forms the most conspicuous outcrop within the diatreme, accounting for over 70 % of the exposed rock. This is likely controlled by the lamprophyre being more resistant to weathering compared to the other clastic facies, in particular the lapilli tuffs. An interpretive cross section (Fig. 3.23) suggests that the pyroclastic and country-rock breccia facies are the dominant infill below the eroded surface of the diatreme. Although it has a significant proportion of schist xenoliths, no evidence was found to suggest that the coherent lamprophyre is a highly welded spatter deposit or a clastogenic lava. Compared to the schist lithic-bearing composite loaded pyroclasts from the lapilli tuff, the schist xenoliths in the coherent lamprophyre are less abundant, but typically larger (e.g. commonly >10 cm in diameter). Contacts observed between the coherent lamprophyre and the lapilli tuff deposit

(Figs. 3.11, 3.12) suggest the lamprophyre has partially enveloped the deposit, typically with steep contacts that are interpreted to continue over the top of the outcrop (Fig. 3.11).

Columnar jointing occurs worldwide in a variety of rocks, but especially in coherent basaltic igneous formations (Hetényi et al. 2012). Column orientations are generally agreed to form perpendicular to the cooling isotherm, but in more complex cases the orientation can be controlled by surfaces of equal tensile stress (Spry 1962). The columnar joints themselves are formed by a decrease in volume that creates tensional stresses within the body, and within a lava body this is typically due to thermal contraction (Hetényi et al. 2012). Columnar jointed basalts commonly show two types of jointing style; (1) a colonnade style which exhibits regular columns with planar geometries, and (2) an entablature style which exhibits less regular columns typically with curved and more complex geometries. When the geological setting constrains the geometry of the emplaced lava body (e.g. a lava lake), it exerts a strong control on characteristic column stoutness. For bodies with unconfined geometries (such as a lava flow), chemistry of the lava plays a larger role, resulting in stouter columns in felsic lavas and narrower columns in mafic lavas (Hetényi et al. 2012).

The columnar joints within the coherent lamprophyre at the LWD generally display a colonnade style. Most of the lamprophyre outcrop displays simple vertical column orientations that begin to show more complexity at the northern end of the diatreme (Fig. 3.21). Here, the columns are still a colonnade style, but they have developed a radial fan-like geometry at the point of the exposure and concave-up shapes towards the top of the exposure. Assuming the column orientations in this section of the lamprophyre exposure have formed perpendicular to the cooling surface (Spry 1962), the northern section likely represents a different cooling pattern compared to the central part of the lamprophyre body. The radial joint pattern at the northern end suggests this was the edge lamprophyre, and it was exposed to colder country rock in close proximity the conduit wall. Other column geometries, such as the sub-horizontal concave-up columns (Fig. 3.21) may have developed from asymmetrical contacts between the surface of the lamprophyre and the overlying pyroclastic material.

The columnar jointed coherent lamprophyre within the LWD is interpreted to represent a late stage sill. Non-explosive, effusive, late stage intrusions of magma into maar-diatremes and other small volcanoes have been documented in other South Island Cenozoic volcanoes, as well as in many places globally (Németh 2001; Lorenz and Haneke 2004; Hoernle et al. 2006).

Quiet intrusion of dikes, sill and plugs may suggest the groundwater supply required for explosive eruptions has been exhausted (Lorenz and Haneke 2004) and/or that the magma has sufficiently degassed (Houghton and Wilson 1989). Intrusions of magma into water can also occur non-explosively (e.g. pillow lavas), however, the LWD lamprophyre sill is interpreted to have been a dry intrusion. This is supported by the generally simple colonnade joint geometries, whereas more complex entablature style might be expected if there was water involved with the cooling of the sill (Hetényi et al. 2012). Also, none of the lamprophyre displays any strongly chilled rinds that might be expected in a wet intrusion (Kawachi and Pringle 1988).

The majority of vents in the Waipiata Volcanic Field expose dominantly coherent mafic rock preserved in the form of plugs, necks, lava lakes, lava flows and dikes (Németh 2001; Németh and White 2003). These types of vents and vent complexes were classified as type 1 vents, and inferred to contain only minimal amounts of pyroclastic material in comparison to the predominantly coherent-rock composition (Németh 2001; Németh and White 2003). The LWD is not analogous to this type 1 vent style from the Waipiata Volcanic Field for the following reasons. (1) It has a deeper inferred erosional level than those of the type 1 WVF vents, yet it still contains lapilli tuff and tuff breccia deposits along with open cavity country-rock rock fall deposits. (2) A large amount of lapilli tuff and other pyroclastic deposits sitting above the lamprophyre sill have likely been eroded, and a large amount likely still exists below the current level of outcrop (Fig. 3.23).

3.7 Maar-diatreme emplacement

During initial stages of the eruption, the feeder dike intruded into the Haast Schist country rock. Thermohydraulic explosions fractured and weakened the surrounding country rock, and a maar ejecta ring likely formed. The feeder dike continued to progressively excavate downwards, lowering the syn-eruptive crater floor. Water-magma interactions created thermohydraulic explosions within the root zone that created temporary evacuated volumes. Weakened wall rock was able to fall into the space created by these explosions, creating voluminous country-rock breccias at the root zone level. Water-magma interactions at depth also led to vapour explosions which fragmented the lamprophyre magma to form spatter deposits, predominantly on the crater floor. At the same time, country rock debris was also falling into the vent, some of the debris fell onto the crater floor and other debris accumulated

on ledges close to the vent wall. The spatter deposit involved single and multi-stage recycling of pre-existing lithic and pyroclastic material. Debris jets partially resedimented some of the juvenile rich spatter deposits, incorporating more schist country rock material. The diatreme had exhausted most of the ground water supply as a large lamprophyre sill intruded into the diatreme. The lamprophyre sill initially intruded into a pile of schist country rock fragments (rock fall deposit), incorporating them into the lamprophyre as xenoliths. Weakened wall rock was also incorporated into the lamprophyre as it ascended. Late stage carbonate fluids percolated through any remaining pore space in the lapilli tuffs and country rock breccias, cementing the clasts in place.

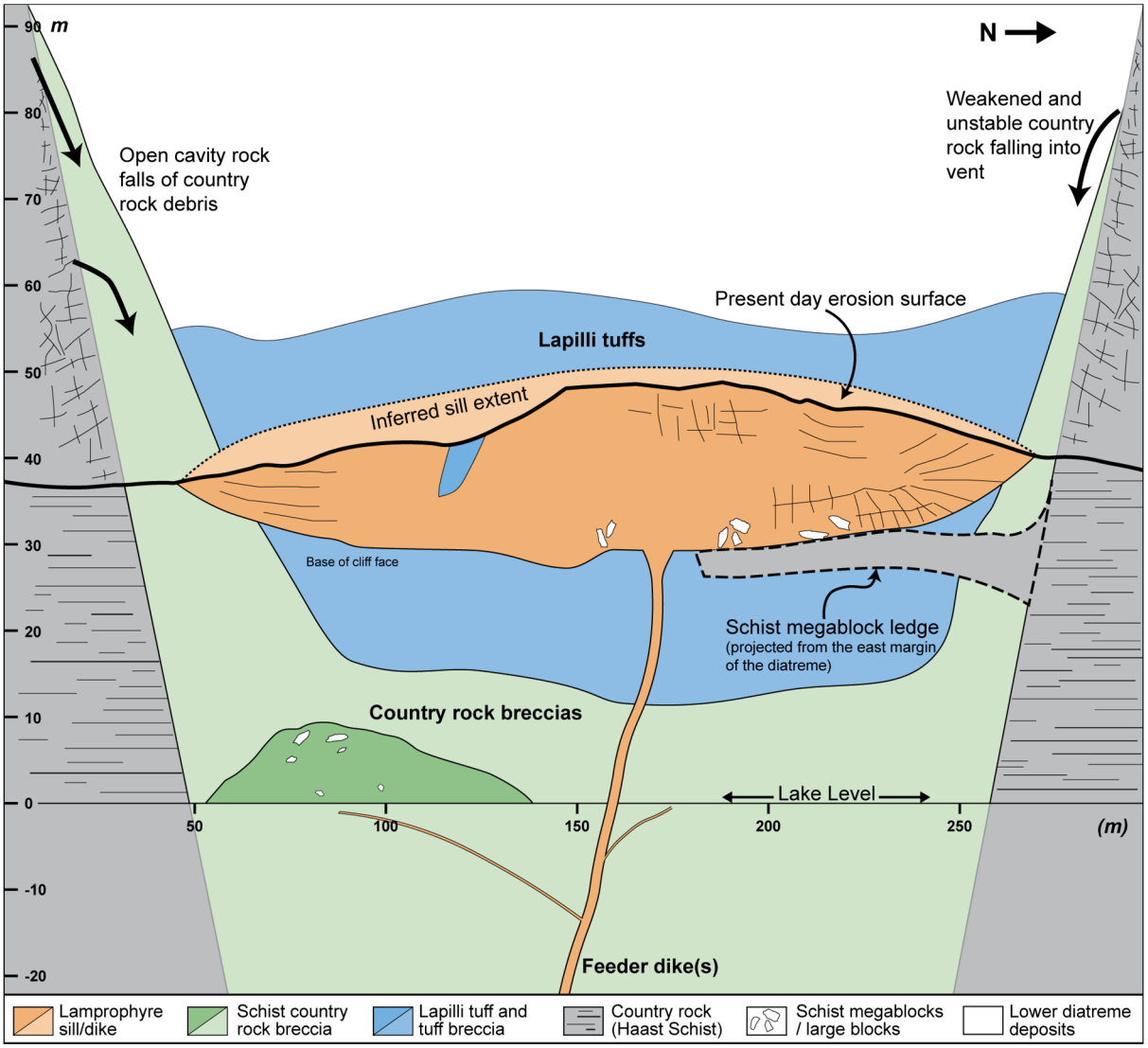

Figure 3.23: Interpretive N–S cross-section of the Lake Wanaka diatreme based on Figure 3.3. The section is extended vertically 40 m above the erosion level and 20 m below the lake level. Schist country-rock breccias are inferred to be the dominant diatreme infill (pale green). Other features shown include the wall-rock falling into the vent, the ledge where the schist megablocks accumulated, and the inferred sill outline (scale the same as Fig. 3.3).

3.8 Conclusions

The eroded Lake Wanaka diatreme offers valuable insights into the development of a lamprophyric, country-rock rich diatreme within the Alpine Dike Swarm. The current erosional level of the diatreme is likely at least 300 to 500 m below the paleosurface, rather than representing the original eruptive surface as suggested by previous workers. The deposits within the Lake Wanaka diatreme are characterised by widespread open cavity rock fall accumulation and explosive juvenile rich lapilli tuffs. The existence of both these styles of deposit suggests a dynamic environment was evolving within the root zone or the lower diatreme. A summary of the main lithofacies and their emplacement mechanisms is summarised below.

- Schist country-rock breccias were created by rock fall sourced from weakened and unstable wall rock. The rock fall deposited into a temporary evacuated space created by thermohydraulic explosions below the syn-eruptive crater that was situated near the root zone.
- The large metre sized schist megablocks protruding from the coherent lamprophyre were slabbed off the vent wall at a higher level within the diatreme. The megablocks fell onto a ledge at a particular level within the diatreme structure. A late stage lamprophyre intrusion subsequently enveloped the megablocks and also filled the void space between multiple blocks.
- Two of the lapilli tuff and tuff breccia units were formed by accumulation as spatter from a lamprophyre magma. The magma was fragmented by bubble bursts and/or lava fountains that were driven by water welling through the fractured country rock at depth and interacting with the magma to cause vapour explosions. The third tuff breccia unit was deposited by resedimentation of pre-existing spatter and country rock through debris jets, or it was deposited from a debris jet that had an explosion site close to the wall rock.
- Composite loaded pyroclasts are ubiquitous throughout the lapilli tuff deposit. They were formed from wall rock schist lithics shedding into the lamprophyre magma before it was fragmented and accumulated as spatter. There is evidence for single- and multi-stage recycling within the lapilli tuff deposit.

- The coherent lamprophyre, the most conspicuous rock within the eroded diatreme, is interpreted to have intruded as a late stage sill. Simple vertical, radial, and sub-horizontal column orientations throughout the lamprophyre exposure suggest the sill was a dry intrusion.

Chapter 4

Paleomagnetic Determination of Emplacement Temperatures

4.1 Introduction

Progressive thermal demagnetisation (PTD) is an underutilised paleomagnetic method for determining the emplacement temperatures of rocks formed from explosive volcanic eruptions (Ort et al. 2015). It is well known that volcanic rocks of various compositions and eruptive styles are capable of recording the geomagnetic field via thermoremanent magnetisation (TRM). Aramaki and Akimoto (1957) were the first workers to apply this concept in the field to determine the emplacement temperatures of a number of pyroclastic deposits in Japan. This study made the assumption that any natural remanent magnetisation (NRM) in the rock was a TRM, and only allowed them to conclude whether the rocks were emplaced hot or at ambient temperatures. Since this pioneering study, the technique of progressive thermal demagnetisation has been developed (Hoblitt and Kellogg 1979) to allow accurate emplacement temperature estimates, and it is here utilised to investigate the thermal evolution of the Lake Wanaka diatreme.

The principle behind the paleomagnetic method for determination of emplacement temperatures is succinctly explained by Paterson et al. (2009) and Bardot and McClelland (2000), and is summarised in the following. During a pyroclastic eruption, explosive activity can fragment the volcanic conduit creating a deposit consisting of juvenile pyroclasts and accidental lithics. The clasts will have a pre-existing magnetisation prior to the pyroclastic eruption. If the clasts become incorporated into a pyroclastic density current that is above ambient temperature, they will become heated and then cool down to ambient temperatures after deposition. The heating will partially or completely reset the magnetisation of the clasts, and the new magnetisation will be aligned to the ambient geomagnetic field at the time of eruption. This is because magnetic grains within the clast are warmed above their blocking temperature and therefore relax. There will be two magnetic components in the clasts; (1) the

original high temperature (high-*T*) component which will have a random orientation due to movement of clasts during the eruption and (2), a low temperature (low-*T*) component, which will have a consistent orientation aligned to the geomagnetic field at the time of emplacement. Progressive thermal demagnetisation can be used to isolate these two magnetic components and estimate the emplacement temperature of the deposit. Temperatures inferred from progressive thermal demagnetisation of a pyroclastic deposit should represent the temperature of the whole deposit after it had accumulated but before extensive cooling began, and this temperature may not coincide with each clasts emplacement temperature, which may have been greater (Bardot and McClelland 2000; Cioni et al. 2004).

In this study, progressive thermal demagnetisation was used to determine emplacement temperatures of rock at two sites within the Lake Wanaka diatreme; (a) the juvenile-rich lamprophyric lapilli tuff and tuff breccia, and (b) a schist xenolith taken from the coherent lamprophyre at a site further north of the lapilli tuff deposit (Fig. 4.12).

4.2 Methods

A total of 39 samples from two sites were analysed via progressive thermal demagnetisation at the Otago Paleomagnetic Research Facility (OPRF). Juvenile pyroclast and matrix samples from the lapilli tuff (unit A1) were taken from a large 25 cm × 15 cm block of the deposit collected in the field. The block was cut using a core saw into 3 cm thick slabs, and orientation lines were drawn on all surfaces to ensure each slab had the same orientation from when it was cut. Clasts of juvenile lamprophyre were manually cut out of the slabs to a size of 2 cm × 2 cm with the orientation lines still preserved. Once the juvenile clasts were separated from the slabs, any remaining matrix or other material still attached to the clast was ground off. The matrix samples were taken from the same slabs used for the clasts, and the same process was followed for their collection.

Schist xenolith samples were taken from a 15 cm × 8 cm block collected in the field. A similar process was also followed, where the block was slabbed and then had orientation lines drawn on each surface. As the whole schist xenolith was homogenous, samples were simply cut into 2 cm × 2 cm cubes. Visibly oxidised or weathered surfaces were ground off.

Samples were not orientated in the field, so no correlations with the geomagnetic field at the time of TRM acquisition can be made. Therefore all subsamples are oriented with respect to the block from which they were collected.

Magnetic moment measurements were made using a 2G Enterprises DC 760–3.5, pass-through superconducting rock magnetometer housed in a magnetically shielded room. Samples analysed were approximately 2 × 2 × 2 cm cubes (8 cm^3) with an orientation line drawn on each. Samples were demagnetised using an ASC TD48-SC triple shielded demagnetising oven at ~25 °C increments and subsequently measured in the magnetometer after cooling. The magnetic components were analysed and isolated using principal component analysis, PCA (Kirschvink 1980), within the PuffinPlot software (Lurcock and Wilson 2012). Only component directions defined with a maximum angular deviation (MAD) less than 15° were used to estimate deposit temperatures.

Thermomagnetic curves were generated for representative samples at the OPRF using an AGICO MFK-1CS Kappabridge. Crushed samples (0.25 cm^3) were heated to temperatures of 700 °C in air.

Thirty-five samples were subjected to IRM and hysteresis experiments which were also made at the OPRF utilising the Princeton Measurements Corporation Vibrating Sample Magnetometer (VSM, MicroMag 2900). Hysteresis analyses were performed with field increments of 8 mT to a maximum field strength of 1.0 T for clast and matrix samples and 1.4 T for the schist xenolith samples. IRM analyses were performed at field increments of 10 mT to a maximum field strength of 350 mT for clast and matrix samples and 500 mT for the schist xenolith samples.

To aid the reader, Table 4.1 lists a number of commonly used abbreviations and units within this study and their corresponding meaning.

Table 4.1: Definitions of common paleomagnetic acronyms and units used in this study. Definitions summarised from Butler (1992).

Term	Abbreviation	Definition
CRM	Chemical remanent magnetisation	Remanence created by chemical alteration or precipitation of ferromagnetic minerals
TRM	Thermoremanent magnetisation	Remanence acquired through cooling from above the Curie point in the presence of a magnetic field
VRM	Viscous remanent magnetisation	Remanence gradually acquired during long term exposure to weak magnetic fields
IRM	Isothermal remanent magnetisation	Remanence acquired by short-term exposure to a strong magnetising field
MAD	Maximum angular deviation	Measure of the precision with which the best fit line is determined
PCA	Principal component analysis	The direction of the best-fit line through a set of scattered observations
PTD	Progressive thermal demagnetisation	Method used to determine the unblocking temperature of a sample through progressive heating
T	Tesla	Unit of measure for magnetic field strength
Am^2	Ampere metre^2	Unit of measure for magnetic moment
S.I.	Magnetic susceptibility	Magnetic susceptibility has no unit of measure

4.3 Magnetic mineralogy results

4.3.1 Thermomagnetic curves

Thermomagnetic curves were analysed to determine the Curie / Néel temperatures for selected representative samples of clasts and matrix taken from the juvenile lapilli tuff, and the schist xenolith. Magnetite and hematite have Curie points of 580 °C and 675 °C respectively (Dunlop and Özdemir 2001; O'reilly 2012), and these are shown on the curves in Figure 4.1.

Thermomagnetic analysis for the juvenile clast sample indicates a Curie temperature of 580 °C (Fig. 4.1a). The sample gradually increases in magnetic susceptibility until 400 °C and has a sharp drop off between 510 and 580 °C, however the susceptibility does not reach 0 S.I. until

670 °C. The cooling curve was not reversible, and shows a higher susceptibility than the heating curve from 300 to 20 °C.

The matrix sample also has a Curie temperature of 580 °C (Fig 4.1b). It has a gradual increase in susceptibility to 460 °C and rapidly drops between 520 °C and 580 °C until it reaches 0 S.I. at 600 °C. The cooling curve is non-reversible and it has a significantly higher magnetic susceptibility than the heating curve from 450 °C to 20 °C.

Analysis of the schist xenolith indicates a Curie temperature of 630 °C (Fig. 4.1c). Magnetic susceptibility increases to a peak at 480 °C, with a subsequent rapid decrease until 620 °C and becoming non-magnetic at 660 °C. The schist sample has a very similar cooling curve compared to the heating curve, and the susceptibility is slightly lower during the extent of cooling.

4.3.2 Isothermal remanent magnetisation

Thirty-five samples in total were selected for isothermal remanent magnetisation analyses (IRM). All samples were subjected to a saturation magnetisation of 1 T. Clast and matrix samples had a final field strength of 350 mT whereas schist xenolith samples had a final field strength of 500 mT (Table 4.2). Pilot samples analysed prior to the main analysis showed saturation below these fields. Juvenile clast samples (n = 13) had a coercivity of remanence (Hcr) ranging from 27 to 37 mT with a mean of 34 mT. Matrix samples (n = 12) are consistent with the clasts, with a Hcr range of 32 to 39 mT also with a mean of 34 mT. Schist samples (n = 10) had higher values with a range of 49 to 55 mT and a mean of 53 mT (Fig. 4.2, Table 4.2). Clast samples had a remanence range (Mr) of 204.5 to 440.4 mAm^2/kg and a mean of 278.0 mAm^2/kg. The Mr for matrix samples was slightly lower, with a range of 108.9 to 235.2 mAm^2/kg and a mean of 170.9 mAm^2/kg. Remanence of the schist samples was significantly lower, with a range of 8.2 to 21.1 mAm^2/kg and a mean of 15.0 mAm^2/kg. Juvenile clasts and matrix samples typically saturated below fields of 250 mT whereas schist xenolith samples typically saturated at fields between 350 and 400 mT. Results from the IRM analyses are summarised in Table 4.2.

Table 4.2: List of results from IRM analyses on 35 samples, including juvenile clast, matrix and schist xenolith. Hsat is the saturating field, Hcr is coercivity of remanence and Mr is the remanence normalised by mass, saturating field is the strength of field which accomplishes saturation of magnetic remanence.

Type	Sample ID	Final Field (mT)	Hsat (T)	Hcr (mT)	Mr (mAm^2/kg)	Saturating field (mT)
clast	clast1_01	350	1.0	35.6	314.6	200
clast	clast2_01	350	1.0	34.3	255.5	200
clast	clast3_01	350	1.0	33.1	204.5	200
clast	clast3_02	350	1.0	31.6	296.3	200
clast	clast3_03	350	1.0	32.9	328.0	200
clast	clast4_01	350	1.0	34.1	296.5	250
clast	clast4_02	350	1.0	31.8	215.2	250
clast	clast5_01	350	1.0	36.3	298.0	200
clast	clast5_02	350	1.0	34.7	208.9	200
clast	clast6_01	350	1.0	36.6	241.1	200
clast	clast6_02	350	1.0	35.9	270.0	250
clast	clast7_01	350	1.0	27.3	440.4	250
clast	clast7_02	350	1.0	33.7	244.4	200
matrix	matrix1_01	350	1.0	34.4	186.4	150
matrix	matrix1_02	350	1.0	38.6	181.0	350
matrix	matrix1_03	350	1.0	34.1	202.5	300
matrix	matrix2_01	350	1.0	36.6	199.6	250
matrix	matrix2_02	350	1.0	34.9	151.4	200
matrix	matrix2_03	350	1.0	34.2	132.9	200
matrix	matrix3_01	350	1.0	34.9	142.0	250
matrix	matrix3_02	350	1.0	31.8	227.8	250
matrix	matrix3_03	350	1.0	36.2	235.2	300
matrix	matrix4_01	350	1.0	32.8	153.5	200
matrix	matrix4_02	350	1.0	32.5	108.9	250
matrix	matrix4_03	350	1.0	31.5	129.8	200
schist	schist1	500	1.0	54.5	18.9	350
schist	schist2	500	1.0	54.2	21.1	350
schist	schist3	500	1.0	49.2	16.0	450
schist	schist4	500	1.0	54.7	8.2	350
schist	schist5	500	1.0	53.7	8.9	350
schist	schist6	500	1.0	53.1	17.0	350
schist	schist7	500	1.0	51.8	20.4	300
schist	schist8	500	1.0	52.3	13.2	350
schist	schist9	500	1.0	50.4	11.7	300
schist	schist10	500	1.0	52.4	14.5	300

4.3.3 Magnetic hysteresis curves

The same samples from the IRM analyses were subjected to magnetic hysteresis analysis. Loops used field increments of 8 mT and a maximum field of 1 T for clast and matrix samples and 1.4 T for the schist xenolith samples. Hysteresis loops for the clast and matrix samples are very similar with thin curves and saturation in low fields (Fig. 4.3a, b). Clast samples had a saturation range (Ms) of 1.0 to 3.2 Am^2/kg with a mean of 1.9 Am^2/kg. Matrix samples had an Ms range of 0.6 to 1.3 Am^2/kg with a mean of 0.9 Am^2/kg. Hysteresis loops for the schist samples (Fig. 4.3c) show slightly wider curves with higher saturation fields. Schist xenolith samples had a significantly lower Ms range compared to clast and matrix samples of 31.4 to 85.7 mAm^2/kg and a mean of 60.4 mAm^2/kg. None of the analysed specimens exhibit wasp-waisted curve shapes (Roberts et al. 1995).

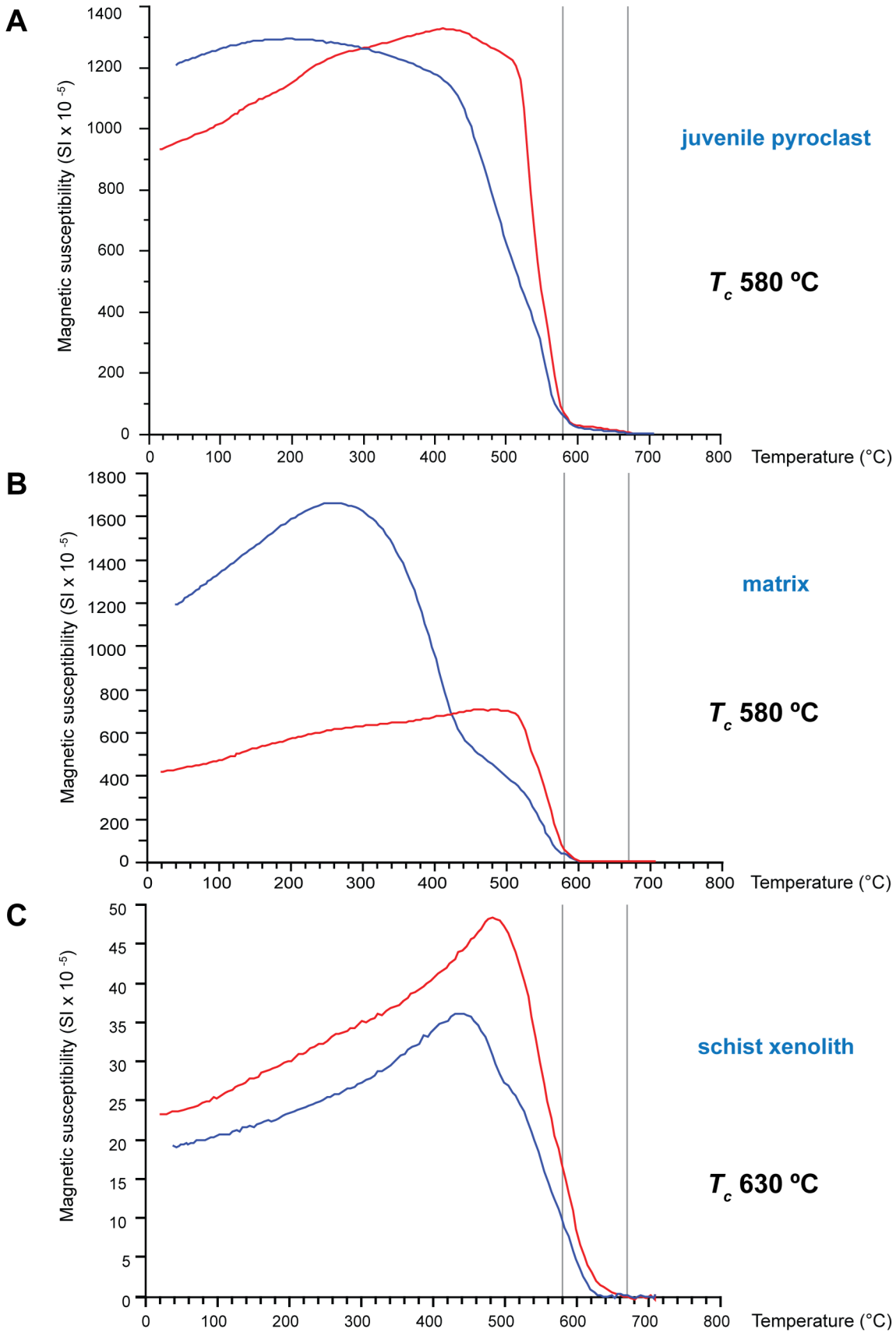

Figure 4.1: Thermomagnetic curves of representative samples. **(a)** Juvenile pyroclast, **(b)** matrix, **(c)** schist xenolith. Heating = red, cooling = blue, grey lines represent Curie temperatures for magnetite and hematite respectively.

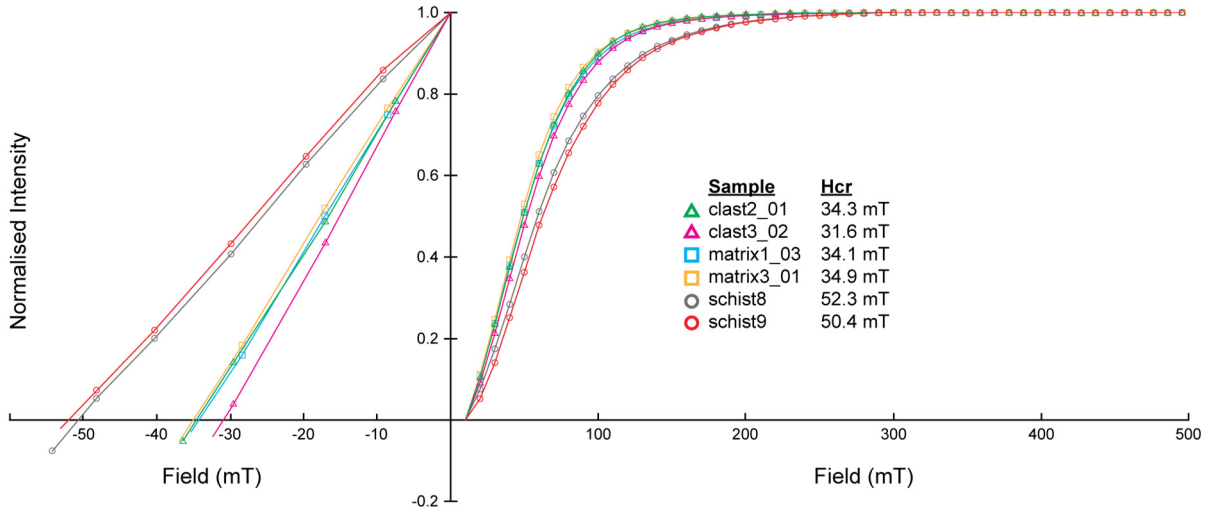

Figure 4.2: IRM curves for representative samples from the lamprophyric juvenile lapilli tuff (clasts and matrix) and the schist xenolith. Hcr is the coercivity of remanence.

4.3.4 Day type plot

The Day plot (Fig. 4.4) shows that all samples plot in the field of PSD behaviour for magnetite and titanomagnetites (Dunlop 2002a, b). All the schist samples cluster together, towards the SD-MD theoretical curve for magnetite with 40 % of the soft component (SP or MD) in mixtures with SD grains. Samples from the matrix and clast plot in a linear fashion, with the matrix samples containing 50 to 60 % of the soft component and the clast samples with 60 to 75 % of the soft component. Both populations plot closer to the SD-MD magnetite curve.

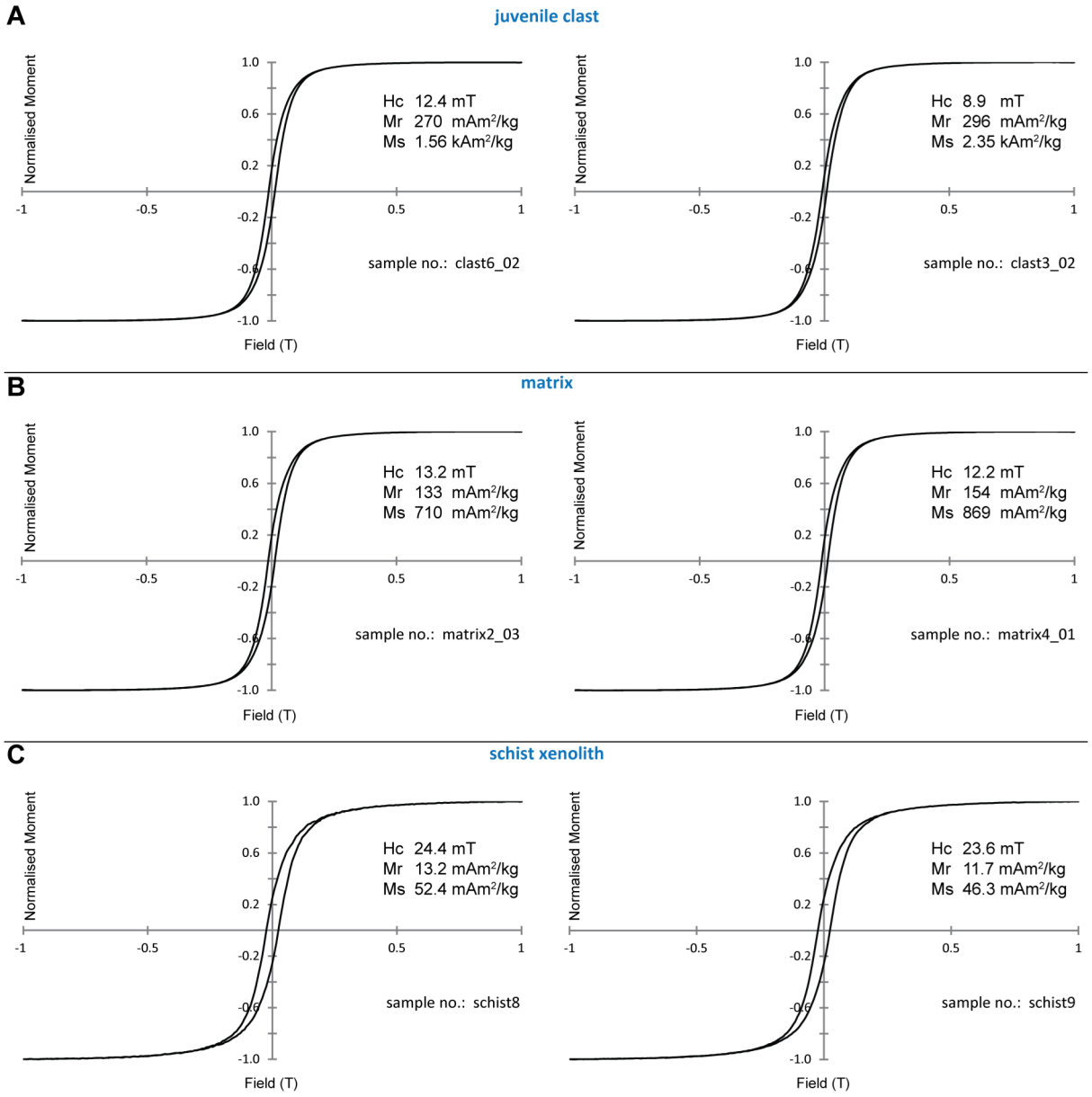

Figure 4.3: Magnetic hysteresis loops for representative samples; **(a)** juvenile clast, **(b)** matrix and **(c)** schist xenolith. Hc = coercivity, Mr = remanence, Ms = saturation.

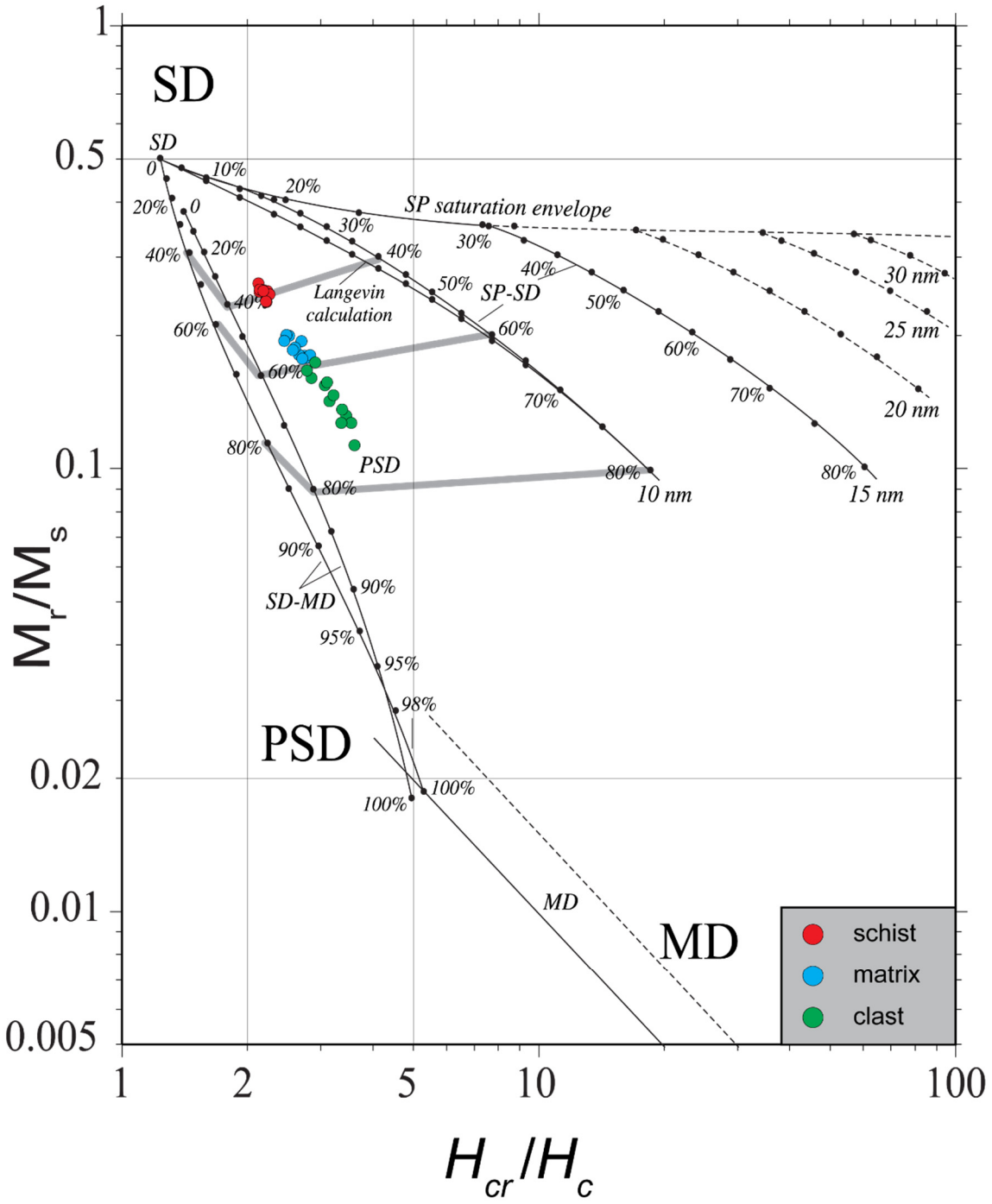

Figure 4.4: Day type plot after Dunlop (2002a, 2002b). Samples from juvenile clast, matrix and schist xenolith. SD is magnetic single domain field, PSD is magnetic pseudo-single domain field and MD is magnetic multidomain field, SP is superparamagnetic. Numbers along curves are volume fractions of the soft component (SP or MD) in mixtures with SD grains.

4.3.5 Discussion of magnetic mineralogy

Magnetite or Ti-poor titanomagnetite is interpreted as the dominant magnetic mineral in both the clast and matrix samples from the juvenile lapilli tuff. Both sample suites have very similar magnetic characteristics. The thermomagnetic curve (Fig. 4.1a) for the juvenile clast sample displays an abrupt decrease in magnetic susceptibility between 510 °C and 580 °C indicating that magnetite is the dominant magnetic mineral. The clast sample does not completely reach 0 S.I. until 680 °C and this weak persistence in magnetic susceptibility after the magnetite Curie point (580 °C) is explained by the thermal alteration of magnetite to hematite (Trindade et al. 2001). The moderate increase in susceptibility during heating, and a higher susceptibility in the cooling curve from 300 °C to 20 °C indicates the thermal alteration of some minor Fe-bearing minerals into magnetite (Dunlop and Özdemir 2001)

The matrix sample displays an abrupt reduction in susceptibility between 520 °C and 580 °C, again indicating magnetite or low-Ti bearing titanomagnetite is the dominant magnetic mineral. The sample becomes non-magnetic at 600 °C indicating hematisation of magnetite during heating was minor to non-existent. The cooling curve of the matrix sample displays a significant increase in magnetic susceptibility from 440 °C to 20 °C. Iron bearing carbonates have been demonstrated to oxidise to magnetite or maghemite during heating (Ellwood et al. 1986; Ellwood et al. 1989). The matrix in the lapilli tuff deposit contains Fe-bearing ankerite cement, and therefore the thermal alteration of the ankerite to magnetite or maghemite is probably the cause of the large increase in magnetic susceptibility displayed during cooling of the sample.

Thermomagnetic analysis of the schist xenolith sample (Fig. 4.1c) shows significant decrease in magnetic susceptibility between 490 °C and 620 °C. This range could indicate the presence of magnetite but also maghemite which has a range of reported Curie temperatures from 590 °C to 675 °C (Dunlop and Özdemir 2001). If maghemite is the dominant remanence carrying mineral, thermomagnetic curves will typically show maghemite inversion to magnetite or hematite during the heating phase (Bardot and McClelland 2000; Paterson et al. 2009). No inversion is observed in Figure 4.1c and therefore maghemite is not inferred to be present. The heating curve has a steep increase in magnetic susceptibility from 20 °C to 480 °C which might be explained by the thermal alteration of Fe-bearing sulphide minerals such as pyrite into

magnetite (Roberts and Turner 1993; Roberts 1995). However, the very similar cooling curve suggests that little to no thermal alteration affected the magnetic mineralogy during heating.

Table 4.3: Maximum remanent coercivities (Tesla) and Curie temperatures for common ferromagnetic minerals, after Lowrie (1990) and Dunlop and Özdemir (2001).

Ferromagnetic mineral	Maximum coercivity (T)	Curie temperature (°C)
Magnetite	0.3	580
Maghemite	0.3	~590–675
Titanomagnetite (x=0.3)	0.2	350
Titanomagnetite (x=0.6)	0.1	150
Pyrrhotite	0.5 - 1	325
Hematite	1.5 – 5	675
Goethite	>5	80–120

IRM analyses of the juvenile clasts do not show any indication of high coercivity minerals such as pyrrhotite or hematite, with IRM being acquired at field strengths of 200 mT. This supports that the minor presence of hematite suggested by the thermomagnetic curves in Figure 4.1a was due to thermal alteration of magnetite during heating. Magnetite and maghemite both have maximum coercivities of 300 mT, with titanomagnetites 200 mT or lower depending on Ti content (Lowrie 1990). This suggests the magnetic mineralogy of the clast samples is primarily low-Ti titanomagnetites. The matrix samples showed more variation in field strength saturation, but the majority of samples saturated below 300 mT, indicating the presence of magnetite. Again, there is no evidence of higher coercivity minerals such as hematite or pyrrhotite (Table 4.3).

The schist xenolith samples saturate in fields typically between 300 mT and 400 mT. This might indicate the presence of a slightly higher coercivity mineral such as pyrrhotite which saturates at fields of 500 mT to 1 T (Table 4.3). However, the thermomagnetic curve (Fig. 4.1c) shows no indication of a Curie point at 325 °C, the Curie temperature of pyrrhotite. Magnetite and maghemite also have similar saturation field strengths of 300 mT, again making it difficult to distinguish between the magnetic minerals in the schist.

Hysteresis loops for all samples do not show any evidence of wasp-waisted curves, which suggests individual samples have similar magnetic grain sizes and are dominated by one type of magnetic mineral with similar coercivities (Roberts et al. 1995).

Finally, the dominant magnetic domain state of all the minerals in pseudo-single domain, with the schist samples having a higher proportion of SD to MD grains, and the matrix and clast samples having a more even mixture of the two.

4.4 Paleomagnetic behaviour

Selected data from the progressive thermal demagnetisation analyses are displayed in Figures 4.5 and 4.6. For each heating step, the magnetic moment direction is plotted on an orthogonal Zijderveld diagram (Dunlop 1979). These diagrams allow the immediate resolution of a multi-component magnetisation of a given sample.

Site A: Juvenile rich lapilli tuff and tuff breccia

Thermal demagnetisation data for the juvenile clast samples indicate two antipodal magnetic components. A low temperature component is observed between 20 °C and 327 °C and a high temperature component is observed between 349 °C and 725 °C for 10/13 samples measured (Fig. 4.5). The break point for the two components is between 327 and 349 °C (Fig. 4.5c). Only 5/13 samples had completely demagnetised by 725 °C. Thermal demagnetisation of the matrix also shows two antipodal magnetic components. Seven out of 14 samples have a low temperature component between 20 °C and 284 °C and a high temperature component between 309 °C and 716 °C. Six out of 14 samples have a low temperature component between 20 °C and 309 °C and a high temperature component between 335 °C and 716 °C. The break point between the two components is estimated to be between 295 °C and 325 °C (Fig. 4.5c). Only 1/14 samples had completely demagnetised by 716 °C.

Site B: Schist xenolith

Thermal demagnetisation of the schist xenolith samples indicates only one magnetic component is present. The Zijderveld diagram (Fig. 4.6b) shows a single component for which the direction does not change throughout thermal demagnetisation. The intensity plot typically displays a flat trend before it starts to rapidly demagnetise towards origin from 400-500 °C. Six out of the 11 samples measured were completely demagnetised by 716 °C.

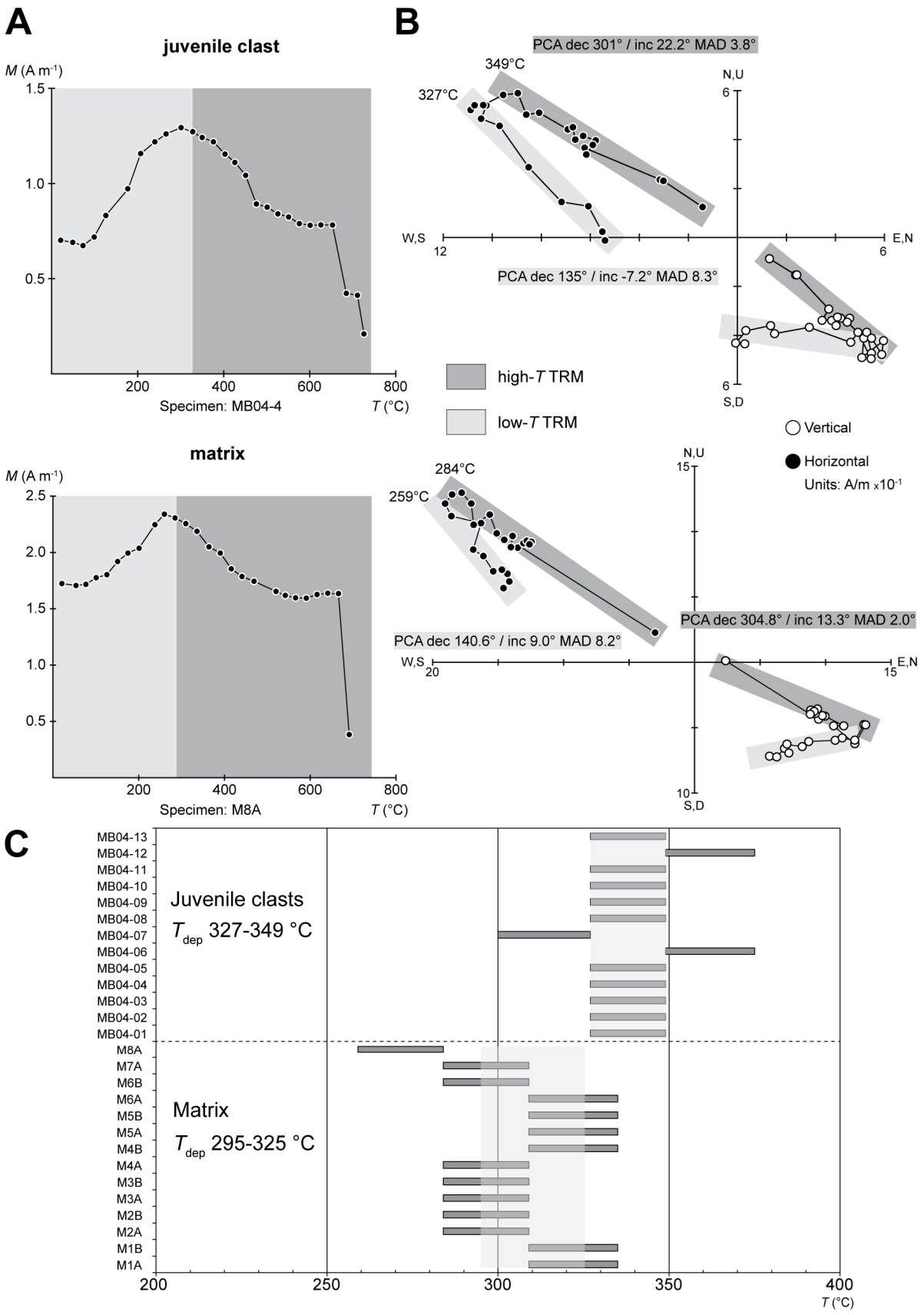

Figure 4.5: Progressive thermal demagnetisation diagrams for the juvenile-rich lapilli tuff sample. **(a)** Demagnetisation intensity plot for juvenile clast (top) and matrix (bottom) specimens. **(b)** Corresponding Zijderveld

plot for the same specimens. **(c)** Estimate of the site deposition temperatures (T_{dep}) by overlapping of the unblocking ranges for all of the measured juvenile clast samples (top) and matrix samples (bottom).

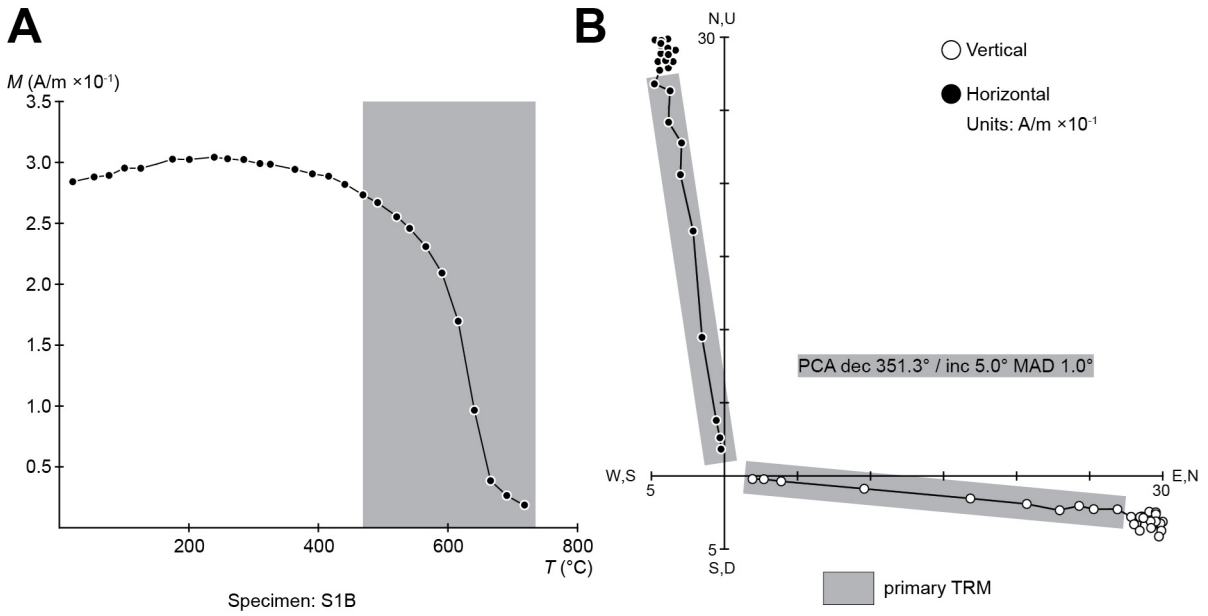

Figure 4.6: Progressive thermal demagnetisation diagrams for the schist xenolith. **(a)** Demagnetisation intensity plot for a schist xenolith specimen. **(b)** Corresponding Zijderveld plot for the same schist xenolith specimen.

4.4.1 Magnetic component directions

Site A: Juvenile rich lapilli tuff and tuff breccia

The high-*T* component directions are tightly clustered for both the juvenile clast and matrix samples; clast samples have an α_{95} of 3.2 (Fig. 4.8a) and the matrix with an α_{95} of 1.1 (Fig. 4.8b). The clasts have a mean PCA direction of dec 301.3° / inc 12.8°, and the matrix dec 306.0° / inc 13.0°.

Low-*T* magnetic component directions for both matrix and juvenile clasts also show good agreement with each other, plotting in similar directions with a high 95 % confidence. Juvenile clast samples have an α_{95} of 5.3 (Fig. 4.8a) and the matrix samples plot with an α_{95} of 4.0 (Fig. 4.8b) Clast samples have a mean PCA direction of dec 140.5° / inc 3.4° and matrix samples have a mean PCA direction of dec 138.0° / inc 2.1°. Figure 4.8c shows 95 % confidence ellipses and mean directions for each component showing the strong correlation between the two sample sets. When the low-*T* component directions are reversed by 180° (Fig 4.7) they plot

close to the high-*T* component directions, indicating the two magnetic components are antipodal.

Site B: Schist xenolith

Schist xenolith samples indicate only one primary component. Each of the eleven samples from the schist xenolith plot tightly together with an α_{95} of 1.7 (Fig. 4.8d). The mean PCA direction for the primary magnetic component is dec 350.7° / inc 4.8°.

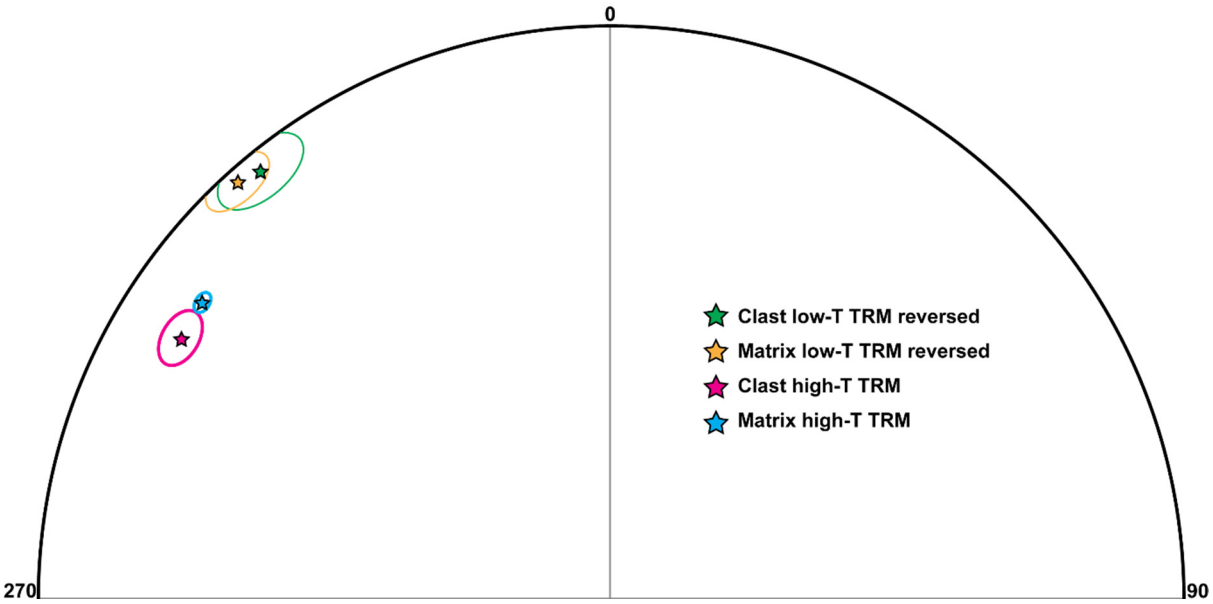

Figure 4.7: Equal area projection of the mean high-*T* component directions, and mean low-*T* component directions for the juvenile clast and matrix samples. The low-*T* component directions for both sample suites were reversed by 180°. Stars represent the mean direction, ellipses are the α_{95} confidence ellipse.

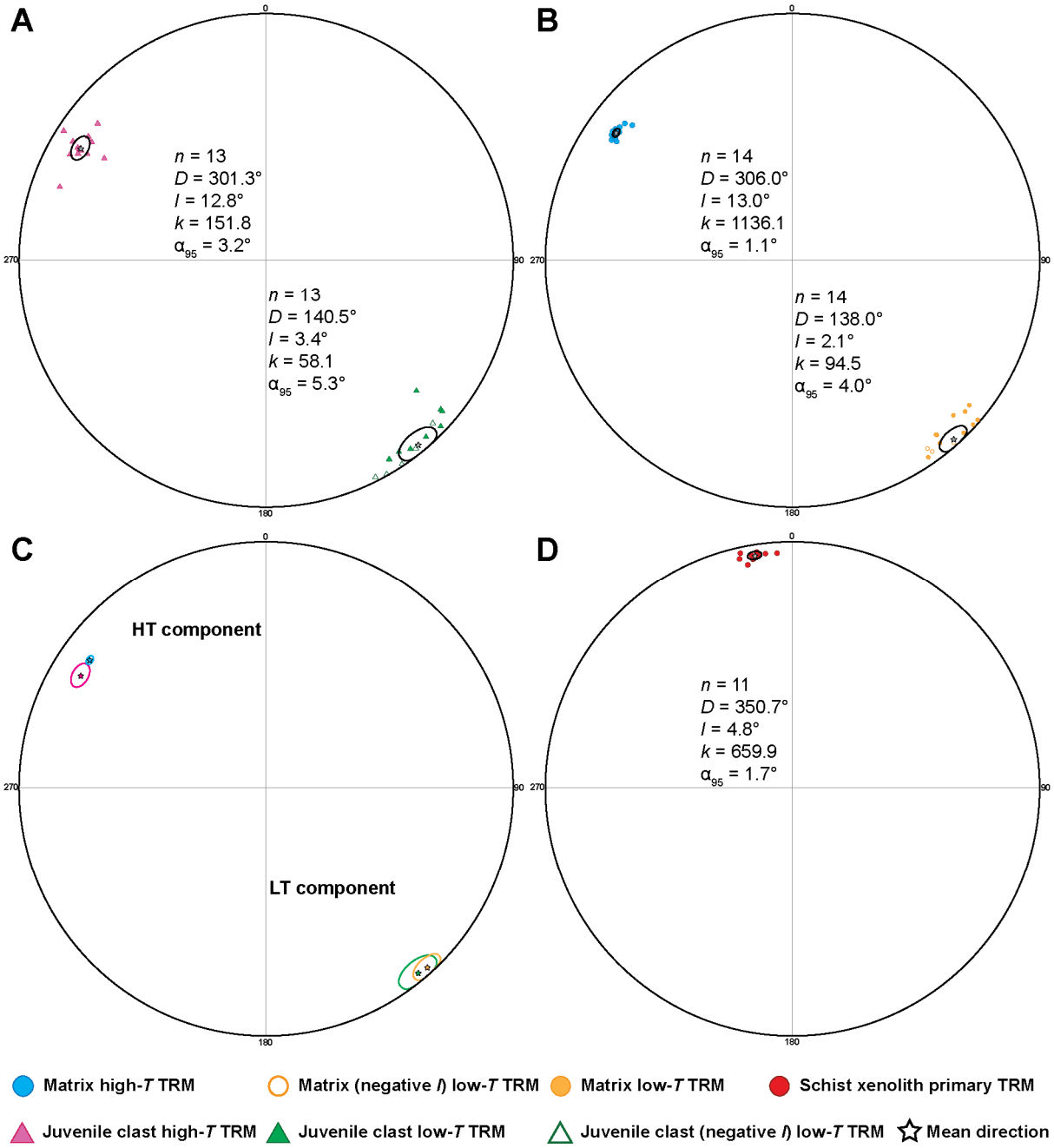

Figure 4.8: Equal area projections of high-*T* and low-*T* component directions for juvenile clast, matrix and schist xenolith specimens. **(a)** Juvenile clast specimens from the lapilli tuff sample (site A). **(b)** Matrix specimens from the lapilli tuff sample (site A). **(c)** Combined mean directions for both juvenile clast and matrix samples for comparison. **(d)** Equal area projection of the primary magnetic component for the schist xenolith specimens (site B). The 95% confidence ellipse and mean (star) are shown on each projection. Fisher distribution statistics shown: *n* is the number of specimens, *D* is the declination, *I* is the inclination, *k* is the precision parameter, α_{95} is the 95% confidence limit.

4.4.2 Discussion

A primary assumption of the paleomagnetic method for estimating emplacement temperatures is that the remanence acquired at the time of deposition is of a thermal origin (i.e. a TRM) (Bardot and McClelland 2000; Paterson et al. 2009). Viscous remanent magnetisation (VRM) occurs where the magnetisation of a rock "relaxes" and aligns to the ambient geomagnetic field when exposed to it for a long period of time. This period is typically from when the rock of a deposit has cooled to when the samples are collected (Paterson et al. 2009). Figure 4.9 can be used to estimate the minimum emplacement temperature for a given age of a deposit, below which may be unreliable due to the effect of VRM. For the 26 Ma deposit of the LWD, temperatures above 200 °C for magnetite and 320 °C for hematite bearing rocks, can be assumed to be of a thermal origin.

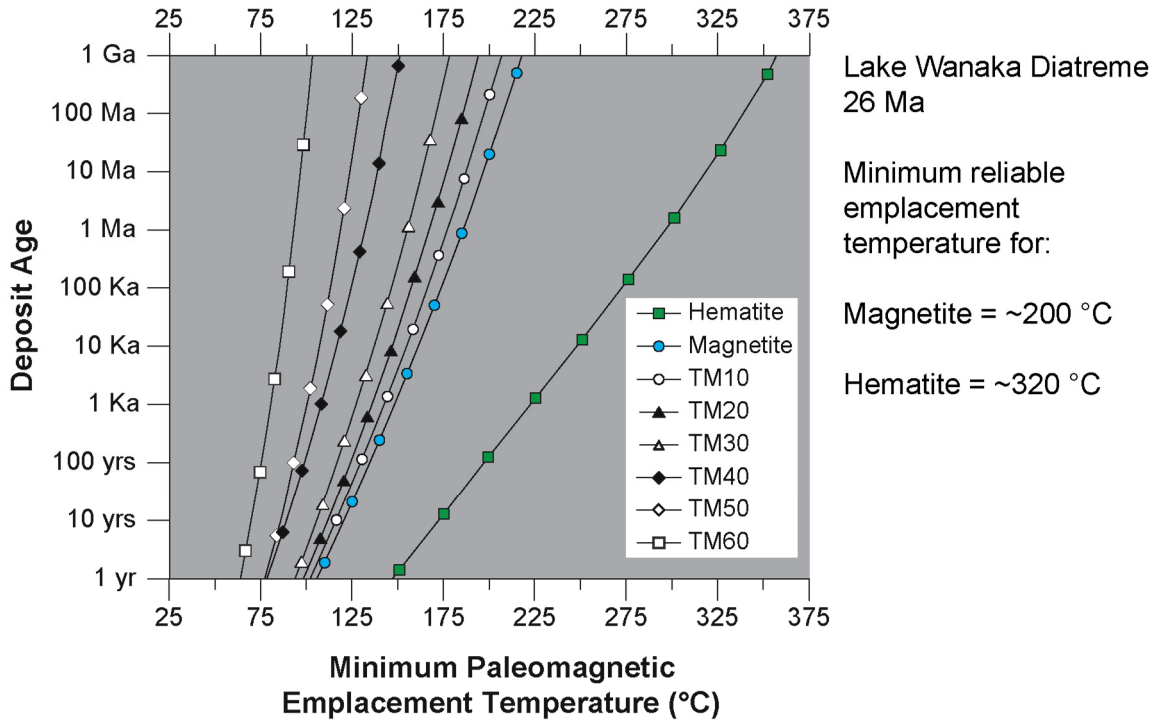

Figure 4.9: Deposit age plotted versus minimum paleomagnetic emplacement temperature as predicted by viscous magnetisation (VRM) theory for hematite, magnetite and part of the titanomagnetite series (TM10–TM60). The deposit age from the LWD suggests temperatures above ~200 °C for magnetite bearing rocks can be interpreted as TRM. Modified from Pullaiah et al. (1975); Paterson et al. (2009).

The data presented in section 4.3 suggests that magnetite or a low-Ti bearing titanomagnetite is the dominant remanence carrier for the clast and matrix samples of the juvenile lapilli tuff.

It is therefore concluded, that the two magnetic components exhibited in these samples do not equate to a VRM. Samples from the schist xenolith show a less complex single magnetic component. Section 4.3 concluded the magnetic mineralogy is predominantly magnetite, and therefore the single component is also unlikely to represent a VRM.

Another factor that needs to be addressed when interpreting paleomagnetic data from rocks is chemical remanent magnetisation (CRM). A CRM may occur where the existing minerals in a rock are altered to a ferromagnetic mineral or where new ferromagnetic minerals are precipitated from solution. Whilst CRM acquisition is predominantly encountered in sedimentary rocks (Butler 1992) there are examples of CRM acquisition in volcanic pyroclastic terranes (Bardot and McClelland 2000; McClelland et al. 2004; Paterson et al. 2009; Nakaoka and Suzuki-Kamata 2014). CRM can affect the blocking temperatures in a sample, potentially obscuring the emplacement temperature and creating a false TRM component. McClelland et al. (2004) proposed the use of thermomagnetic curves (Fig. 4.1) to detect the presence of a CRM. Curie temperatures that coincide with the maximum unblocking temperature or emplacement temperature could be considered to represent a CRM. Thermomagnetic curves for the juvenile clast and matrix samples do not show any indication of Curie temperature around the estimated low-*T* TRM of 300 °C to 350 °C. As has previously been discussed, alteration during heating is suggested as to why the samples do not become completely non-magnetic at the 580 °C Curie temperature for magnetite.

The schist xenolith samples only have one component and thus the Curie temperature coincides with temperature estimate of being greater than or equal to Curie temperature of the xenolith. Paterson et al. (2009) suggests maghemite is a common CRM carrying mineral, but should be evident by maghemite inversion to hematite and magnetite on the thermomagnetic curve. Data presented in section 4.3 suggests maghemite may make up a portion of the magnetic mineralogy in the schist xenolith along with magnetite. Therefore if a CRM is present in the schist xenolith it has completely obscured any pre-existing primary component all the way to 630 °C. The lack of a noticeable maghemite inversion in Figure 4.1c indicates the remanence in the schist xenolith is unlikely to be due to a CRM.

In conclusion, the components presented in section 4.4 for the juvenile lapilli tuff and schist xenolith are interpreted to be of a thermal origin (TRM) acquired during volcanic processes.

4.5 Interpretation of thermoremanent magnetisation

Interpreting the two TRM components in the juvenile lapilli tuff sample within a volcanological context presents a challenging proposition. As discussed in section 4.1, the high-*T* TRM component directions of a pyroclastic deposit should be randomly orientated. This is due to the clasts in the deposit having acquired a magnetisation at some stage prior to eruption, and then becoming mixed up in the pyroclastic deposit post-eruption. The results presented in section 4.4.1; however, show that the high-*T* component directions for both the juvenile clasts and matrix are tightly clustered (Fig. 4.8), suggesting the whole rock was affected by the thermal event responsible for the magnetisation. This presents two possible scenarios for the acquirement of the high-*T* TRM component in the studied samples; (1) the juvenile lapilli tuff was deposited hot, above the Curie temperature for magnetite (>580 °C) and cooled below the Curie point only after the deposit had stabilised, or (2) the whole deposit was reheated after deposition by an external heat source above 580 °C, and this reset any previous TRM component the juvenile clasts or matrix may have acquired.

In Chapter 3, samples from the juvenile lapilli tuff were shown to exhibit weak welding or agglutination textures between some of the juvenile clasts (Fig. 3.14). Recognition of welding textures in rocks of some kimberlites has been suggested to indicate high emplacement temperatures of the deposits (Brown et al. 2008b; Seghedi et al. 2009). These textures are not restricted to kimberlites, with diatremes from the Hopi Buttes Volcanic Field also containing welded deposits (Lefebvre 2013). Welding has important thermal implications for the juvenile lapilli tuff deposits at the LWD, as agglutination between juvenile clasts can only take place above the glass transition temperature (Giordano et al. 2005; Sumner et al. 2005). Above this temperature, glass particles will deform viscously allowing welding, below this temperature however, particles will behave in an elastic manner when under stress, thus making welding impossible (Giordano et al. 2005). Basalt has a glass transition range of 500 °C to 739 °C which is dependent on cooling rate and H_2O content of the melt (Giordano et al. 2005). No experimental data exists for the glass transition temperature of lamprophyric melts and accordingly basalt represents the closest comparison in terms of SiO_2 wt% content. Therefore, at least some of the juvenile clasts from the LWD lapilli tuffs were emplaced at minimum range of 500 °C to 739 °C, which could account for the required emplacement temperature of >580 °C as suggested by the paleomagnetic results. The majority of juvenile clasts within the lapilli

tuff deposit at the LWD; however, do not exhibit welding textures. Previous workers have suggested that large amounts of non-deformable lithics in some deposits, such as schist country-rock, inhibit the development of compaction deformation fabrics (Brown et al. 2008b). The most likely explanation though, is that the juvenile clasts were simply below the required glass transition temperature. A lack of welding in the majority of the juvenile clasts does not suggest the clasts were cool upon emplacement, it only suggests the clasts were not above the minimum glass transition temperature to agglutinate. The whole deposit must have been hot enough to be emplaced above the Curie point of magnetite at 580 °C, and the clasts that exhibit welding textures were emplaced at even higher temperatures. The tight clustering of the high-*T* TRM directions also indicates that once the juvenile rich deposit was formed, it must have been stable by the time the deposit cooled below the Curie temperature.

Scenario 2 requires the presence of a hot body of magma to heat the lapilli tuff and tuff breccia deposit above a minimum temperature of 580 °C. The simplest explanation to achieve this would be through heating from a nearby coherent lamprophyre that intruded close to the deposit. A coherent lamprophyre is in fact located in close proximity to the lapilli tuff deposit (Fig. 3.11), however, this same lamprophyre is inferred to be responsible for the low-*T* TRM component. It is not possible for the one coherent lamprophyre in outcrop to be responsible for two heating pulses that would be required to explain both the high-*T* and low-*T* TRM components. Therefore, the hot deposition in scenario 1 is the preferred explanation for the high-*T* TRM component in the lapilli tuffs.

Results presented in section 4.4 show that the low-*T* TRM component for juvenile clasts ranged from 327 °C to 349 °C, whereas the matrix samples had a slightly lower range of 295 °C to 325 °C (Fig. 4.5). The component directions for both juvenile clasts and matrix cluster tightly, indicating the whole deposit was heated in place to these temperatures. In a pyroclastic density current, these temperatures would typically be interpreted as the emplacement temperature of the deposit (Bardot and McClelland 2000; Paterson et al. 2009). In this study though, the high-*T* TRM component is interpreted as the emplacement temperature of the lapilli tuff, and therefore the low-*T* TRM component must be a later reheating event.

A coherent lamprophyre in outcrop near the lapilli tuff and tuff breccia deposit (Fig. 3.11) is suggested as the source of the later reheating event required for the low-*T* TRM component. In Chapter 3, it was inferred that the characteristic columnar jointed lamprophyric sill of the

LWD intruded late, post-dating the other pyroclastic lithofacies in the diatreme. Mafic magmas are commonly very hot, with Esperança and Holloway (1987) determining that lamprophyre magmas can be brought to near surface conditions at temperatures of 1000 to 1200 °C. Therefore, if the deposit could be exposed to these temperatures for a long enough time period, the necessary temperatures suggested by the low-*T* TRM component could be easily reached. The lamprophyric sill is located within 5 m of the lapilli tuff outcrop, and it is possible that part of the lamprophyre was closer than this at the time of emplacement but has subsequently been eroded. Limited research exists that has focused on quantitatively determining heat transfer from a lava or magma into a surrounding package of rocks. Baker et al. (2015) employed experimentally calibrated pollen darkening to measure the temperature profile around a thin basaltic sill that intruded into wet lake sediments. They recorded a temperature of 304 °C within 1 cm of the contact, and dropping to 250 °C at 1 m from the contact. McClelland (1981) investigated the thermal affect Tertiary basalt dikes had on Silurian-Devonian andesite and basaltic-andesite lavas in Scotland. Assuming the 6.2 m wide dike intruded at 1150 °C and heat was conducted, a temperature of ~700 °C near the contact, and ~75 °C at 4.3 m away from the contact was determined. For a 1.2 m wide dike, the temperature was ~700 °C near the contact and ~150 °C 1.2 m away from the contact. Delaney and Pollard (1982) suggest in a conductive system, temperatures at the contact between the dike and wall rock can remain well below that of the initial uncooled magma for much of the duration of heat transfer.

The exposed lamprophyre sill at the LWD is within 5 m of the lapilli tuff outcrop. Baker et al. (2015) suggests that heat transport into the sediments they studied was convective hydrothermal rather than conductive. There is evidence to suggest the juvenile-rich lapilli tuffs in the LWD were clastic, poorly consolidated, and contained open void space at the time of lamprophyre sill intrusion. The carbonate cement that infilled the pore space in the lapilli tuff shows a transition from precipitation of ankerite to late-stage calcite dominant (Chapter 5, Fig. 5.7). Also, the stable isotope analyses on carbon and oxygen show no magmatic input (Figs. 5.2, 5.3), and suggests the carbonate was derived from groundwater percolating through the country rock. The lack of magmatic input in the carbonate cement suggests it did not infill void space in the lapilli tuff until after the eruption had ceased. Peperitic margins on the lamprophyre might also be expected if the sill intruded into a wet, poorly consolidated pile of

pyroclastic material (White et al. 2000; Skilling et al. 2002). Therefore, the lapilli tuffs are interpreted to have been predominantly dry at the time of lamprophyre sill intrusion and there may have been significant empty pore space between the juvenile clasts of the lapilli tuff deposit. Heat transfer was likely to be convective, with hot or air or volcanic gases transferring heat from the sill into the deposit through the open voids. The lapilli tuffs were likely heated to 295 °C to 347 °C as suggested by the paleomagnetic data through a combination of convection and minor conduction. Other factors such as dike width (Barker et al. 1998) and continued magma flux (Petcovic and Dufek 2005) can significantly affect heat flow into the surrounding host rock. The large volume of coherent lamprophyre in the LWD indicates a period of sustained magma intrusion that would aid in the heating of the lapilli tuff deposit.

A 2D model was created to simulate a lamprophyre sill intruding into the lapilli tuff using the software *KWare Heat 3D* Wohletz (2008) (Fig. 4.10). A 20 m wide lamprophyre sill at 1100 °C was chosen to intrude the juvenile rich lapilli tuff, heating it via convection. The lapilli tuffs were modelled with a specific heat capacity of 840 J/kg K, a density of 2800 kg/m^3, and a porosity of 25 %. Depth of emplacement for the sill was 340 m below surface, with a thermal gradient of 0.02 °C/m. The model shows at age = 1.23 yrs., the sill heats the lapilli tuff to ~230 °C at 5 m away from the contact, before rapidly decreasing to around 35 °C at 10 m from the sill contact. This basic model agrees with some of the discussed research above, particularly the findings that the temperature of the host rock rapidly decreases only a few metres away from the contact of the hot intrusion. This model suggests, if the lapilli tuffs at the LWD were within 5 m of the lamprophyre sill contact, the temperatures estimated by the progressive thermal demagnetisation were attainable.

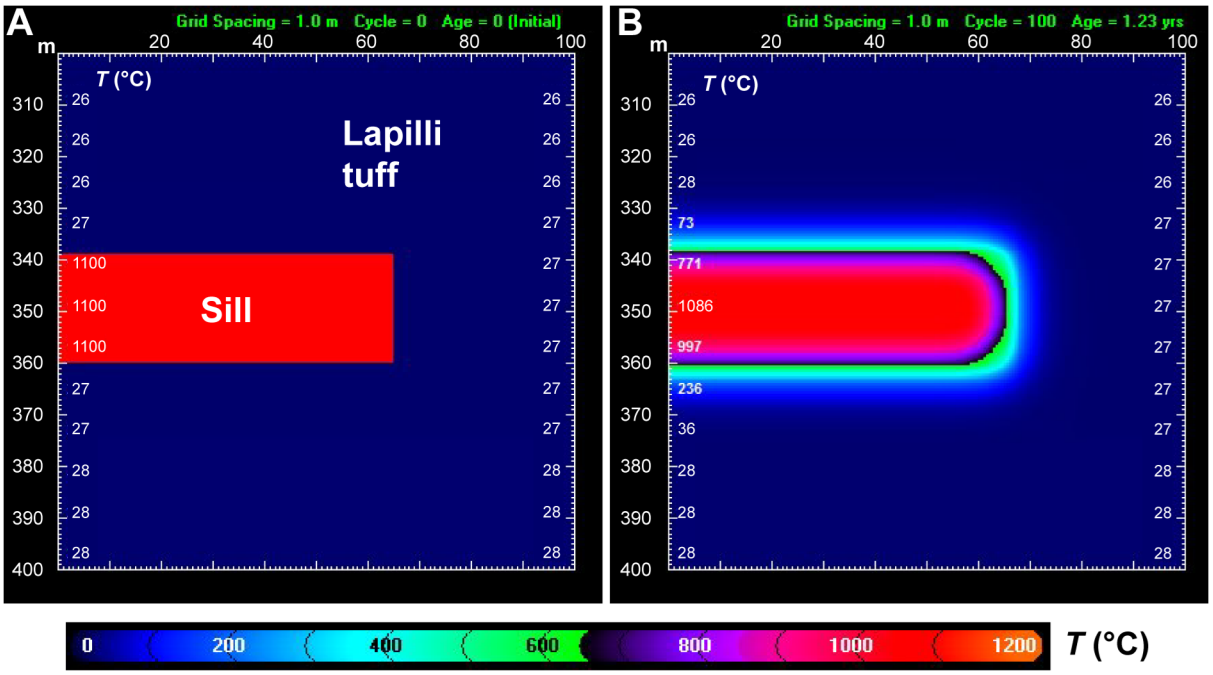

Figure 4.10: Heat 3D model for a 20 m wide lamprophyre sill intruding into the lapilli tuff deposit at the Lake Wanaka diatreme, software by Wohletz (2008). **(a)** Sill intrusion at age = 0 (initial), lamprophyre sill is 1100 °C. **(b)** Heat transfer via convection at age = 1.23 yrs, temperature is displayed on the inside of the Y-axis, and the heat colours correspond to the bar at the bottom of the figure. Deposit depth is shown on the outside of the Y-axis, and deposit length is shown on top of the X-axis.

Schist xenoliths are a defining characteristic of the lamprophyre sill at the LWD. The size of the xenoliths is quite variable, typically ranging from less than 1 cm to 50 cm. In this study, only a xenolith in the 10–20 cm size range was investigated, and the related findings should be interpreted with respect to this size of xenolith. Progressive thermal demagnetisation data suggests that the xenolith was heated above Curie temperature throughout, in this case at least 630 °C. Tight clustering of the magnetic directions across all of the samples (Fig. 4.8d) suggest the xenolith was completely heated through. To support these findings, x-ray diffraction (XRD) analyses were performed on a number of schist xenolith samples, which are presented in more detail in Chapter 5. Mineralogy determined from the XRD analyses show the schist xenolith contains sanidine, a high temperature potassium feldspar. Sanidine is the namesake of the sanidinite metamorphic facies, which is the highest temperature, lowest pressure metamorphic facies (Grapes 2010). Sanidine shows a continuous solid solution between Na- and K feldspars at temperatures above 650 °C (Prevec et al. 2008; Grapes 2010).

Hercynite, an aluminium spinel, was also revealed by the XRD analysis. This mineral is common in high temperature metamorphic environments, and requires temperatures of >800 °C (Montel et al. 1986; Bayhan et al. 2006). The presence of both these minerals, sanidine and hercynite, are important as it suggests the schist xenolith was heated to at least 650 °C. Country-rock xenoliths are known to be common in diatremes world-wide, and their study through paleomagnetic methods could provide new insights into the thermal evolution of the magmas or pyroclastic jets that entrained them.

A number of techniques in addition to paleomagnetism have been used to assess the thermal conditions of kimberlites in Canada and southern Africa. Stasiuk et al. (1999) used dispersed organic matter (DOM) inclusions to determine the thermal conditions within a diamondiferous Cretaceous kimberlite in Canada. They concluded DOM within the kimberlite crater facies (i.e. within the uppermost part of the diatreme structure) were thermally unaltered. DOM inclusions from hypabyssal dikes and brecciated hypabyssal kimberlite exhibited significant thermal alteration. Emplacement temperature estimates within this zone ranged from 200 °C to 650 °C. Pell et al. (2015) used colour alteration indices for conodonts from carbonate xenoliths in a number of pipes within the Chidliak kimberlite field in Canada. They determined emplacement temperatures for the conduit filling kimberlite deposits of 225 °C to > 925 °C over a heating timeframe of 10–20,000 hrs. Conodont samples suggesting a temperature of 700 °C and higher were inferred to indicate highly welded or clastogenic kimberlites. The reported range of temperatures from both these studies agree with the temperatures presented from the LWD here. The inference of welding in the deposits with higher emplacement temperatures also supports the suggestion that the juvenile-rich lapilli tuffs at the LWD show localised welding textures.

A number of other studies have also focused on obtaining thermal information from within kimberlites utilising other geochemical methods. Fedortchouk and Canil (2004) used olivine-ilmenite pairs to estimate an emplacement temperature of kimberlite magmas to be 1070 °C - 1130 °C. Stripp et al. (2006) inferred temperatures of <370 °C in pyroclastic rocks within a South African kimberlite from the stability of post emplacement hydrothermal alteration assemblages. Buse et al. (2010) also found similar temperatures of 250 °C to 400 °C for hydrothermal alteration assemblages within basalt xenoliths from a southern African kimberlite. Skinner and Marsh (2004) have inferred cooler temperatures of less than 250 °C

within the diatreme facies kimberlite rock. They suggest the presence of unaltered country rock xenoliths and "inter-clast groundmass" serpentine indicates the kimberlite magma must have rapidly cooled to <250 °C once it breached the surface.

Studies employing the paleomagnetic method of estimating emplacement temperatures have commonly focussed on pyroclastic density currents from stratovolcanoes and more-silicic volcanoes (McClelland et al. 2004; Paterson et al. 2009; Nakaoka and Suzuki-Kamata 2014; Sulpizio et al. 2014; Zanella et al. 2014). Only a few studies utilising the paleomagnetic method have been applied to diatreme deposits. These studies have only focussed on kimberlites, and the current study is the only one the author is aware of that has applied the technique to a non-kimberlite diatreme. One of the earliest documented studies was on four South African kimberlite pipes by McFadden (1977). This study used samples from wall rock close to the pipe and accidental lithics to infer an emplacement temperature of about 300 °C. The most recent and in depth study was by Fontana et al. (2011) who employed similar techniques to those used in the current study. They suggest the pipe-filling pyroclastic rocks of a southern African kimberlite were emplaced at temperatures above 570 °C, above the Curie point of the measured clasts. This finding is very similar to the results presented in this study for the juvenile-rich lapilli tuffs. Gernon et al. (2009) in an earlier study from the same kimberlite deposit, determined pyroclastic flow deposits were emplaced at temperatures of 200 °C to 440 °C. This study also utilised thermoremanent magnetisation, measuring basalt clasts from pyroclastic flow deposits along with geochemical support from serpentine-diopside assemblages. They concluded kimberlite eruptions can produce hot pyroclastic flows capable of travelling kilometres away from their source. Workers have also argued that low-temperature pyroclastic deposits can also form in diatremes due to water-magma interaction during phreatomagmatic eruptions (Brown et al. 2008a; Kurszlaukis and Lorenz 2008). Some diatremes might experience a transition from cold to hot emplacement temperatures that is mirrored by a change in eruption style from phreatomagmatic to magmatic (van Straaten et al. 2013).

These various studies have utilised a combination of paleomagnetic techniques and other methods to help constrain some of the thermal characteristics of diatremes. Much of the literature pertains to kimberlite eruptions; however, these should still be applicable to the current study. The range in emplacement temperatures discussed in these studies likely reflects

the variability of diatreme deposits that are controlled by eruption style, location and timing. The >580 °C temperature for the emplacement of the juvenile-rich lapilli tuff in the LWD is in agreement with the higher end temperatures reported in the discussed studies. This high temperature appears to fall within expected ranges for a juvenile-rich deposit that shows characteristics of welding and is situated within the lower diatreme structure.

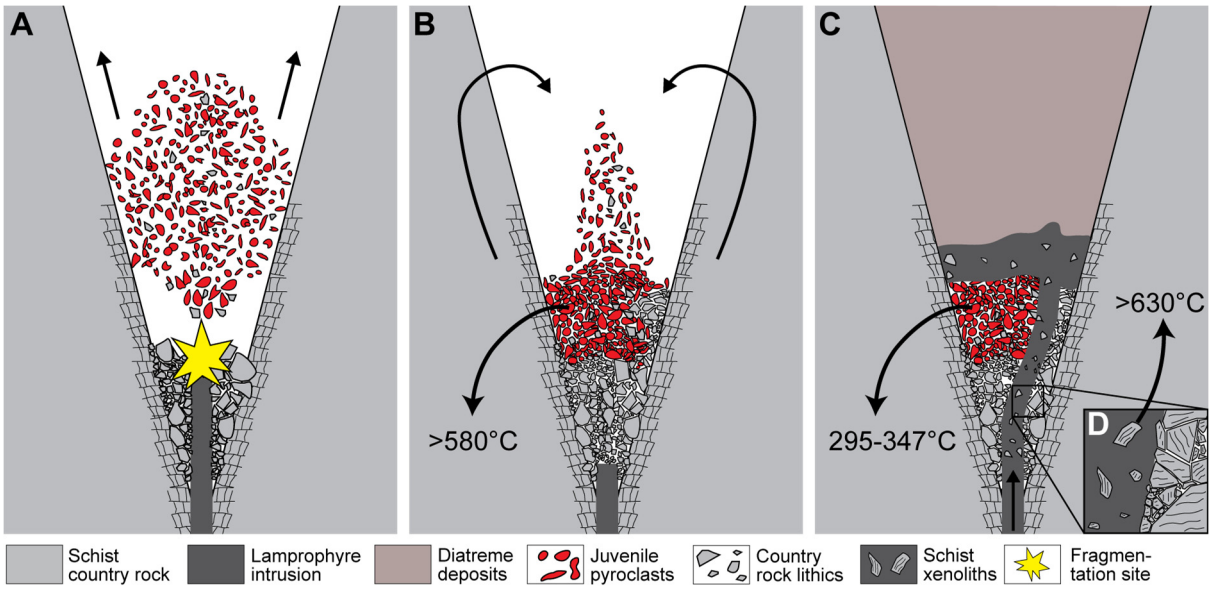

Figure 4.11: Idealised cross-section of the thermal evolution of the Lake Wanaka diatreme, no scale is implied. **(a)** Initial explosion and fragmentation the lamprophyre magma. The fragments are dominated by juvenile pyroclasts with occasional country rock lithics incorporated from the fragmentation site and unstable wall-rock. **(b)** A juvenile-rich lapilli tuff accumulates (as spatter) and minor agglutination occurs between juvenile clasts. The deposit is emplaced at a minimum temperature of 580 °C before it stabilises and cools to ambient temperatures. **(c)** A late stage lamprophyre sill intrudes into a poorly consolidated pile of country rock resulting in the entrainment of a number of schist xenoliths. The xenoliths are heated to a minimum of 630 °C. The lamprophyre sill ascends through the lower diatreme in close proximity to the juvenile-rich lapilli tuffs which are reheated to 295–349 °C. **(d)** Zoom of the schist country rock becoming entrained into the lamprophyre intrusion.

The following paragraph will summarise the thermal evolution of different stages within the LWD with respect to deposits described in Chapter 3. Figure 4.12 shows the sample locations and a summary of thermal events is illustrated in Figure 4.11.

1. Lamprophyre magma near the syn-eruptive crater was fragmented by vapour explosions due to water-magma interactions at depth.

2. The fragmented juvenile pyroclasts deposited whilst still hot, at a minimum temperature of 580 °C, while some of the pyroclasts must have been at higher temperatures due to observed localised agglutination between juvenile pyroclasts.
3. The juvenile-rich lapilli tuff stabilised and cooled below the magnetite Curie point. The pyroclasts were only poorly to moderately consolidated, with void space still present between the clasts.
4. A lamprophyre sill intruded in close proximity to the juvenile-rich lapilli tuff during the waning stages of the LWD eruption. Heat from the sill convected hot air and volcanic gases to warm the lapilli tuff deposit to ~350 °C.
5. Schist lithics from the wall-rock were entrained into the lamprophyre as xenoliths and were heated to >630 °C. As the sill and lapilli tuff cooled, carbonate fluids percolated through the rock cementing the clasts.

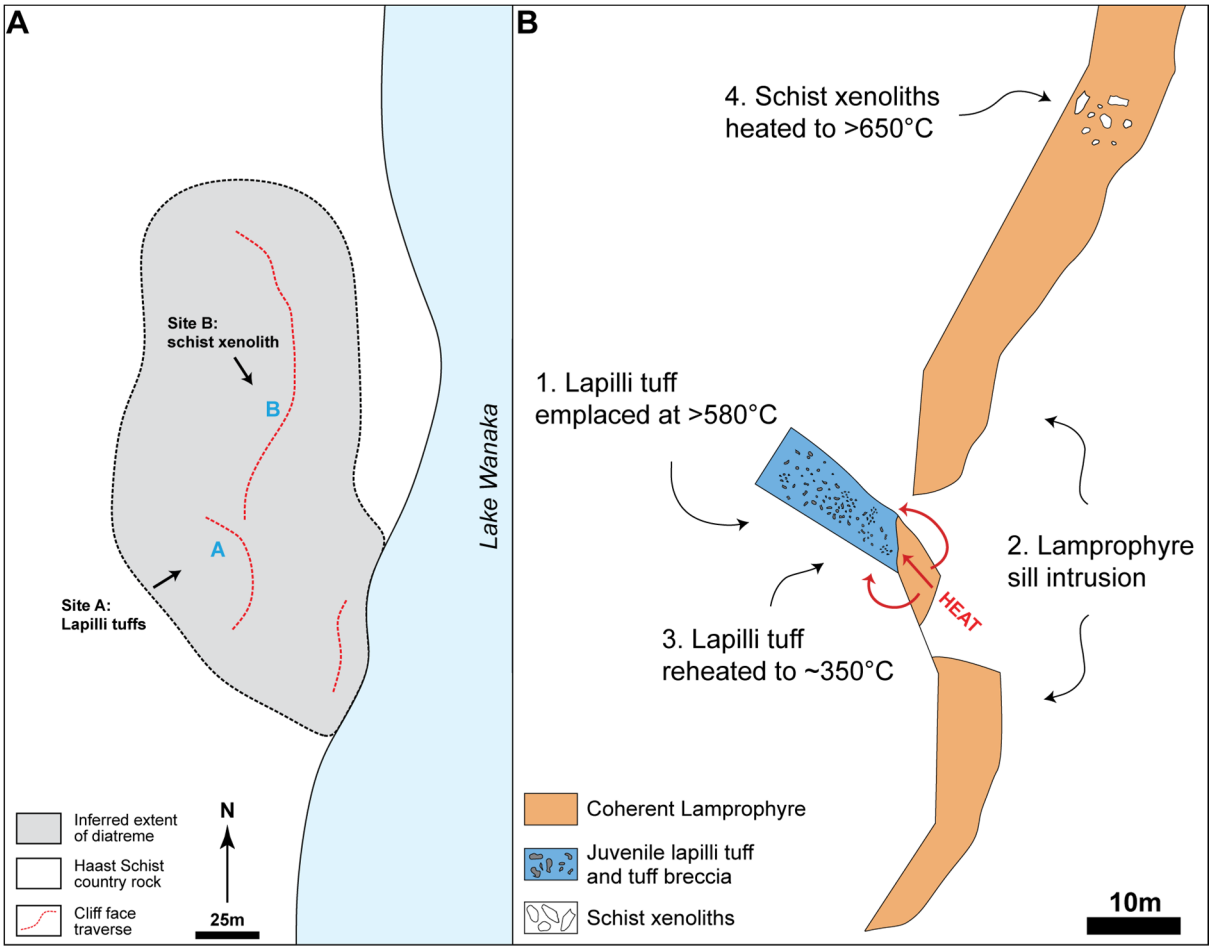

Figure 4.12: Map of the sample site locations and the deposit temperature ranges determined from this study. **(a)** Plan view map of the inferred extent of the Lake Wanaka diatreme, sample location sites are shown. **(b)** Plan view geology map of the cliff face outcrop projected onto the surface, the thermal stages for each deposit are shown.

4.6 Conclusions

Analysis of rock magnetic properties through progressive thermal demagnetisation reveals the following.

- Lapilli tuff clasts were emplaced at temperatures above 580 °C and later reheated to 327-349 °C.
- Lapilli tuff matrix samples were also emplaced above 580 °C and later reheated to 295-325 °C.
- Schist xenolith in the coherent lamprophyre was heated to a minimum of 630 °C.

The consistent high temperatures attained by the different rocks sampled indicates high temperatures in the diatreme soon after lapilli tuff deposition, and additional heating during subsequent intrusion of a nearby sill. These high temperatures are consistent with ranges reported in other studies of kimberlite composition diatremes. The present day exposure of the Lake Wanaka diatreme represents a very hot stage in the diatremes evolution. Cooler pyroclastic deposits created by phreatomagmatic explosions may have existed, but have since been eroded. The paleomagnetic method for estimation of emplacement temperatures has been shown that it can be applied to diatreme deposits, but it is limited by the Curie point of magnetite in accurately estimating deposits emplaced above this temperature.

Chapter 5

Geochemistry

5.1 Introduction

This chapter is primarily focussed on the geochemistry of the carbonate cement in both the juvenile-rich lapilli tuff and the schist country-rock breccia deposits. Stable isotope analyses for carbon and oxygen were performed to determine the source of the fluids that formed the cement in the lapilli tuffs. Before the analyses, it was expected the carbonate cement would have a mantle signature. Intrusives with carbonatitic composition are common throughout the Alpine Dike Swarm (Cooper 1986; Cooper and Paterson 2008), and isotopic studies on carbonate in breccias and veins from the nearby Mt. Alta diatreme have indicated mixing between mantle derived carbon and meteoric water as the source (Wellnitz 2015). It was inferred the carbonate cement at the LWD precipitated from an aqueous solution that contained dissolved mantle derived CO_2 (Keller 1981; Hubberten et al. 1988; Woolley and Church 2005).

Carbonate cement from both the lapilli tuff and country rock breccias were analysed by x-ray diffraction (XRD) to determine their mineralogy. The mineralogy of some schist xenoliths that were entrained within the coherent lamprophyre were also of interest to determine any mineralogical support for the heating suggested by the paleomagnetic data. The sample chosen (Fig. 3.20c, f) shows quartz separation along foliation fabrics and a glassy brown groundmass, both evidence of partial melting. These textures are different from those of typical schist fragments observed within the diatreme.

5.2 Methodology

X-ray diffraction measurements were performed on sample powders using a PANalytical X'Pert-Pro MPD PW3040/60 XRD with a Rapid RTMS X'Celerator Detector system at the University of Otago. The scans were collected in the 2θ range (3°–80°) with 0.008° step for 2 h, with X'Pert Data Collector version 2.0e software.

Samples for carbon and oxygen isotope analyses were prepared by using a fine dremel drill bit to grind out carbonate-rich material from the lapilli tuff and schist country-rock breccia, which was subsequently ground into a fine powder. Care was taken in sample selection to avoid late-stage calcite, but some fine veinlets of calcite may have been present in analysed specimens. Each sample was split so that it was measured twice, sample-A and sample-B (Table 5.1). The country rock breccia carbonate analysis was not reported because the sample produced insufficient CO_2 yield. Carbon and oxygen isotopes were analysed at the University of Otago department of Chemistry. Samples were analysed using the phosphoric acid and spectrographic analysis technique (Craig 1957; Walters et al. 1972). 200µg of carbonate was reacted at 23°C with 104% phosphoric acid for 24 hours on the first batch, and 15 hours for the second batch. The evolved gas was measured with a Finigan GasBench spectrometer.

Cathodoluminescence microscopy was done with a petrographic TECHNOSYN 8200 Mk II Cold Cathode Luminescence system on two thin section samples to characterise the cement, at the Department of Geology, University of Otago.

5.3 Results

5.3.1 Schist xenolith results

XRD analysis shows the presence of sanidine feldspar and hercynite spinel, along with quartz, and albite (Fig. 5.1). Quartz shows a clear peak at ~27° 2θ position, with sanidine also showing clear peaks at ~28° 2θ position. Hercynite also shows a distinct peak at ~37° 2θ position but with lower counts. The minerals listed here are considered the major mineral assemblage of the sample, with minor minerals becoming less certain due to noise and therefore they are not reported here.

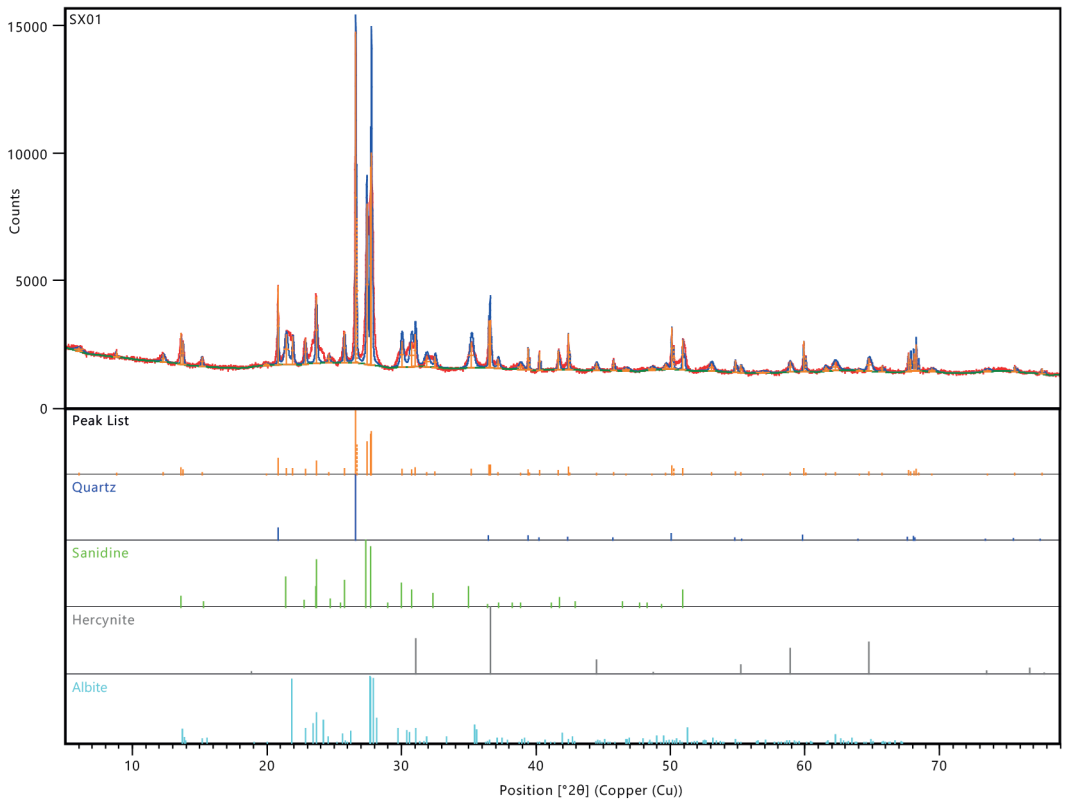

Figure 5.1: XRD data plot for a schist xenolith sample (Fig. 3.20c, f), with a peak list of the major minerals present shown below the red total count graph. Sanidine and hercynite are high-T low-P minerals.

5.3.2 Carbonate geochemistry results

Carbon isotopes had a range of -2.09 to -0.62 $\delta^{13}C_{VPDB}$ ‰ with the unit A1 lapilli tuff samples at the lighter end of the range (Table 5.1). Oxygen isotopes had a very tight range of 14.96 to 15.63 $\delta^{18}O_{VSMOW}$ ‰. Carbon isotopes plot within the freshwater and marine carbonate reservoir field (Fig. 5.2a) and oxygen isotopes plot in the sedimentary and metamorphic rock reservoir ranges (Fig. 5.2b) according to Hoefs (2013).

Table 5.1: Values for C and O stable isotopes sampled from the juvenile-rich lapilli tuff and tuff breccia deposit.

Sample ID	Cb species	$\delta^{13}C_{VPDB}$, ‰	$\delta^{18}O_{VSMOW}$, ‰	Unit
S1-A	Ankerite	-0.84	15.31	Unit A2
S1-B	Ankerite	-0.73	15.38	Unit A2
MB04-A	Ankerite	-2.07	14.99	Unit A1
MB04-B	Ankerite	-2.09	14.96	Unit A1
MB05-A	Ankerite	-0.62	15.53	Unit A2
MB05-B	Ankerite	-0.65	15.63	Unit A2

Figure 5.3 shows potential processes in which originally mantle derived carbonate can be altered to within kimberlites (Giuliani et al. 2014). The LWD ankerite cement samples plot at the end of the "incorporation of sedimentary carbonates" process. Whilst there are insufficient data points to plot a clear trend, the three samples plot at the far end of process, with no points plotting near the ideal mantle carbonate box. In Figure 5.4, a number of carbon and oxygen isotope ratios are shown from carbonatites sampled from the Alpine Dike Swarm. In comparison, the LWD samples do not plot near any of the ADS samples or the suggested carbonatite groupings, though they plot just outside the Haast Schist carbonate grouping.

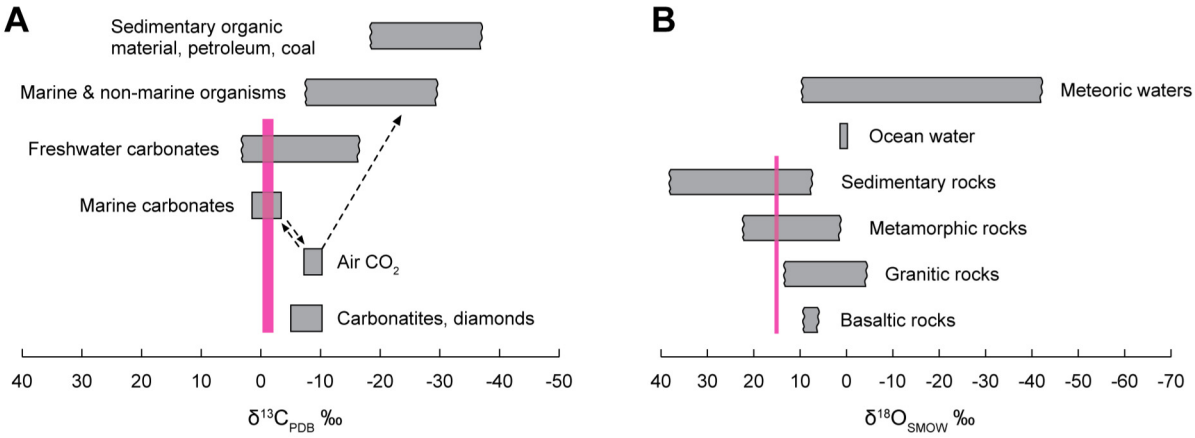

Figure 5.2: Range of **(a)** carbon isotope values and **(b)** oxygen isotope values for samples shown in Table 5.1 represented by pink bars. Carbon and oxygen reservoir values after Hoefs (2013).

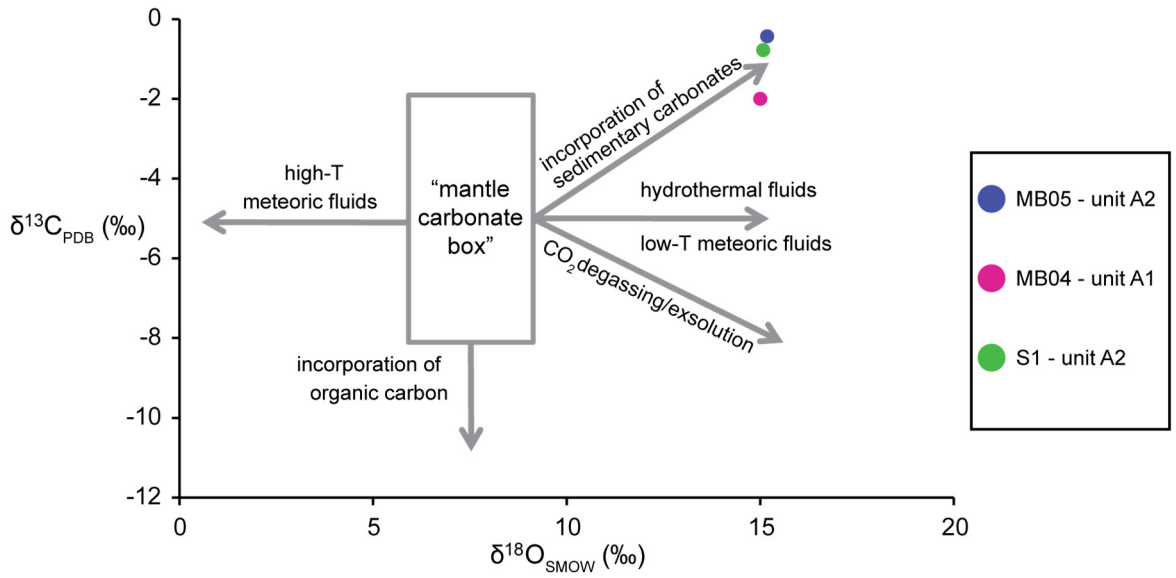

Figure 5.3: Schematic $\delta^{13}C$–$\delta^{18}O$ diagram showing expected C–O isotopic compositions of mantle carbonates and syn- and post eruptive processes capable of modifying the compositions of carbonates crystallised from mantle

derived magmas. Modified from Giuliani et al. (2014) and Demény et al. (1998). LWD samples plot within the sedimentary field and there is no trend indicating they were modified from mantle carbonate.

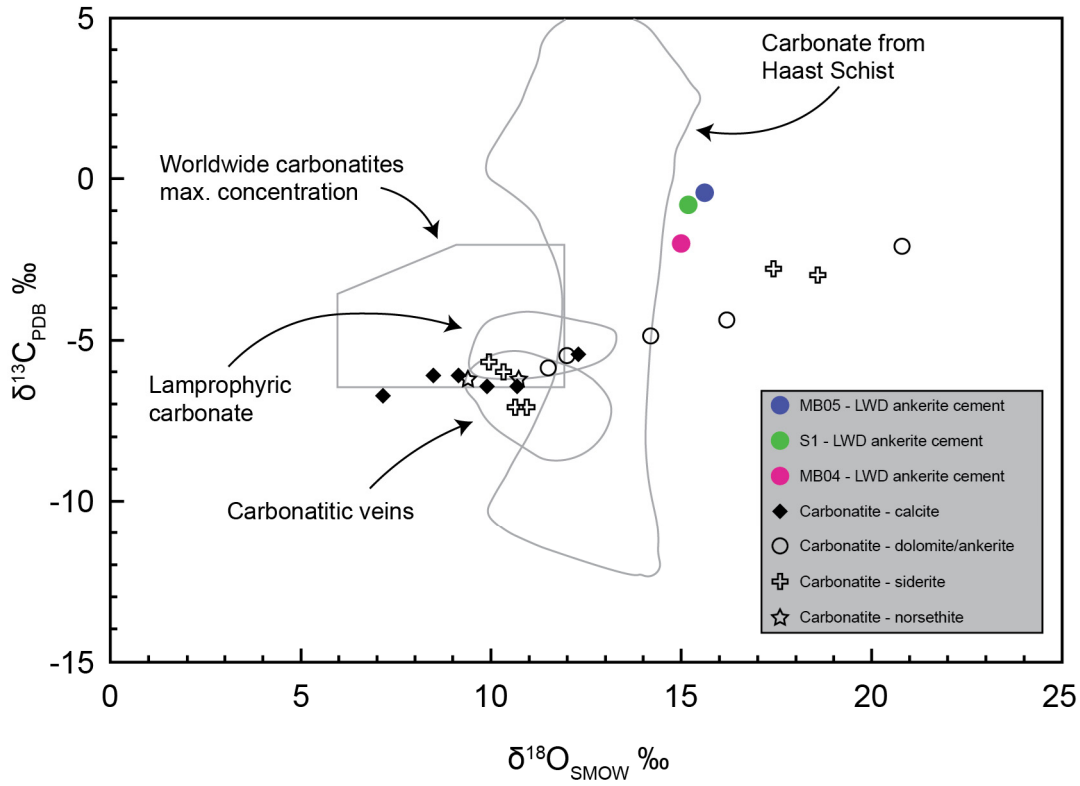

Figure 5.4: Oxygen and carbon isotope ratios for carbonatites within the Alpine Dike Swarm. Values are also outlined for carbonates from the Haast Schist country-rock, and calcite from lamprophyre and carbonatite veins. Ankerite cement carbonate samples from the LWD lapilli tuff are plotted for comparison. Modified from Cooper and Paterson (2008) and data taken from Blattner and Cooper (1974), White (1998) and Paterson (1992).

XRD measurements for both lapilli tuff carbonate cement samples (unit A1 and unit A2) have high counts at the 31° 2θ position indicating ankerite as the carbonate species (Fig. 5.5a, b). The schist country-rock breccia sample (Fig. 5.6) also has a high count at the 31° 2θ position indicating that ankerite is also the carbonate species in this deposit.

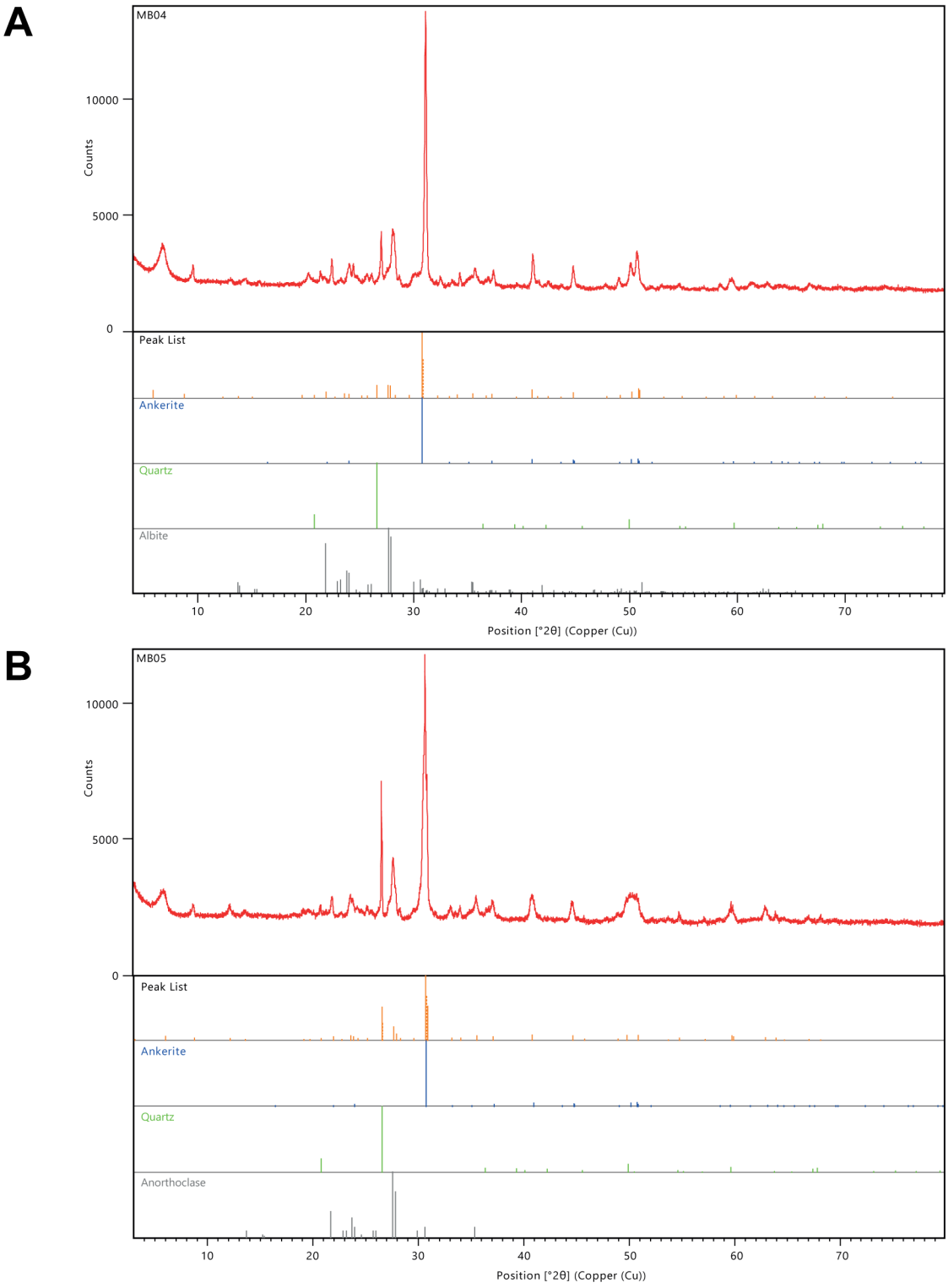

Figure 5.5: XRD data plot for carbonate cement samples from **(a)** lapilli tuff unit A1 and **(b)** lapilli tuff unit A2. Ankerite is the carbonate composition for both samples. A peak list of major minerals is shown below the red total count plot.

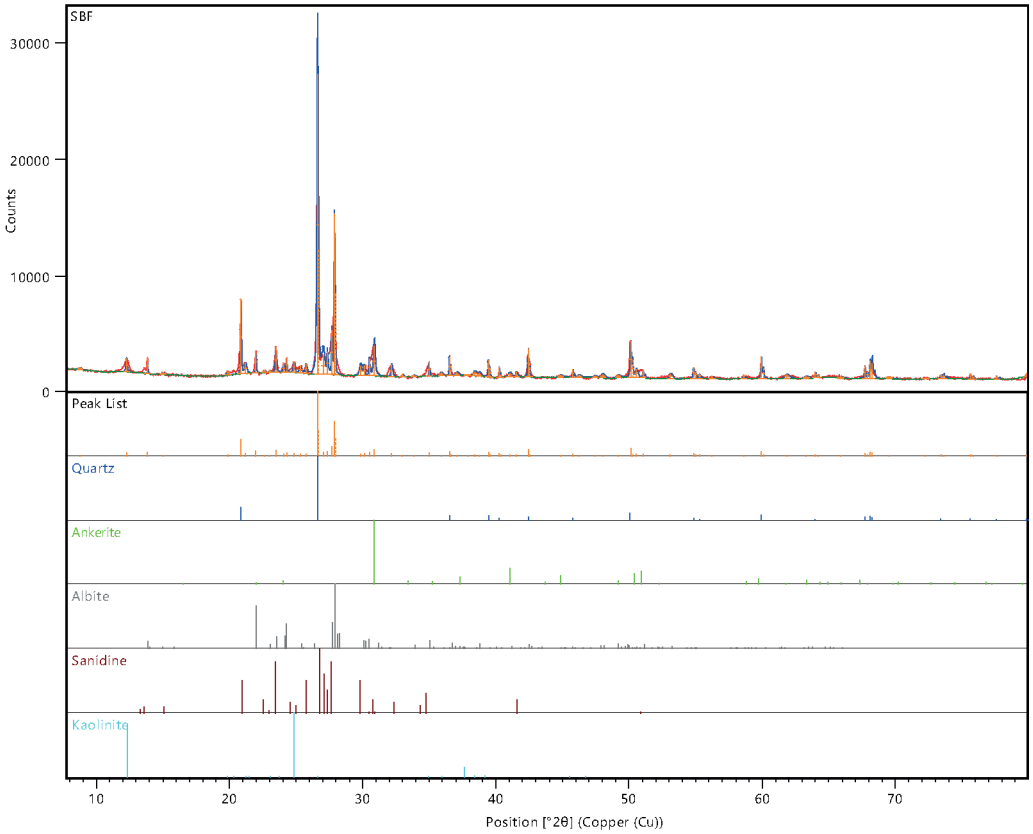

Figure 5.6: XRD data plot for the schist country-rock breccia carbonate sample. A sample without surface alteration was used for the analysis (Fig. 3.6d). The analysis shows ankerite is the carbonate composition and a peak list of other major minerals present is shown below the top peak-count plot.

Cathodoluminescence analysis of the ankerite cement from the lapilli tuff (unit A1 and unit A2) shows the presence of calcite (Fig. 5.7). Calcite sits in the core of the cement, and is also present along joints in the ankerite (Fig. 5.7d). Both samples show minor calcite occurring in vesicles and dispersed schist fragments within the juvenile pyroclasts (Fig. 5.7b, d).

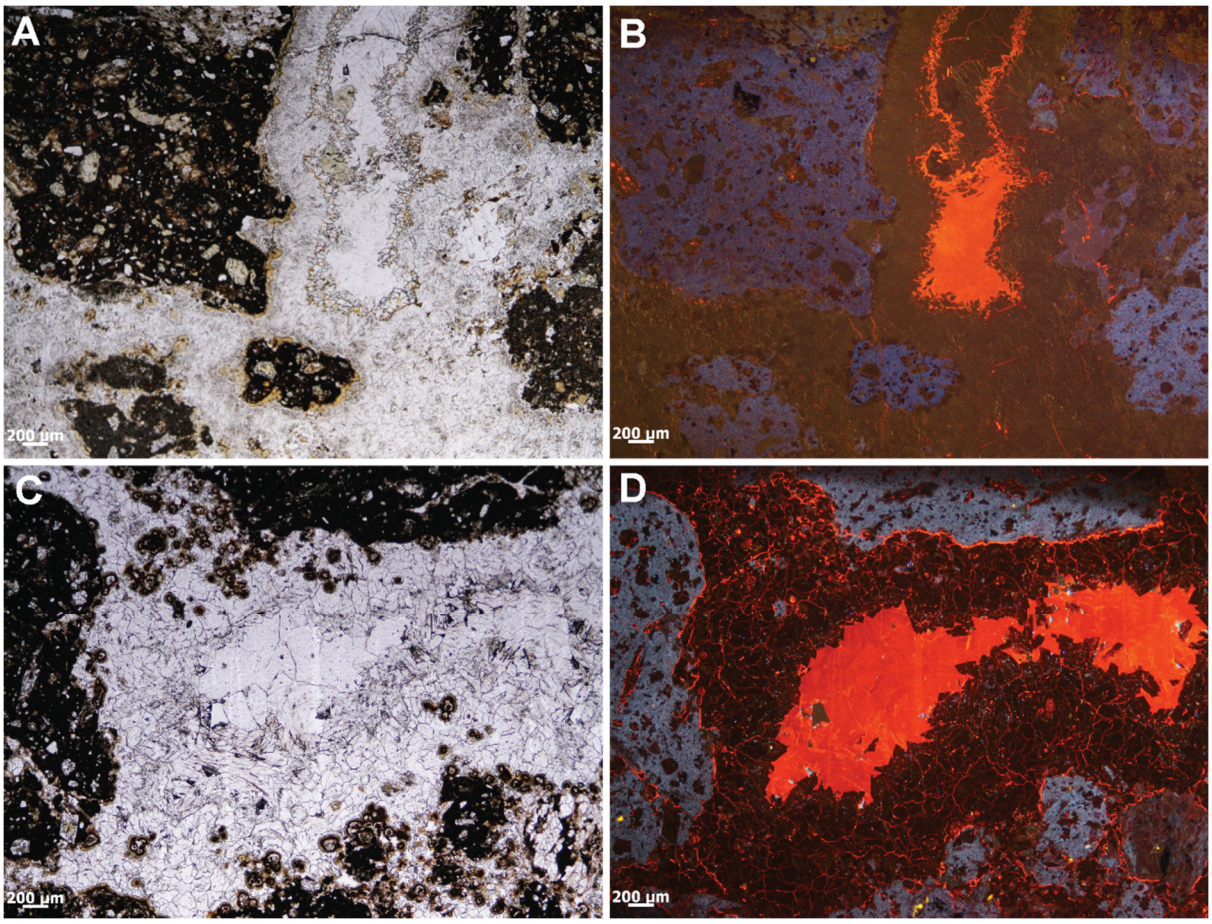

Figure 5.7: Cathodoluminescence (CL) images of carbonate cement in the lapilli tuffs with their corresponding plane polarised light (PPL) photomicrographs to the left. **(a)** PPL photomicrograph of carbonate cement in the unit A2 juvenile lapilli tuff. **(b)** CL image of (a) with the orange indicating the occurrence of calcite. Calcite predominantly occurs in the core of the carbonate cement with minor occurrences in the juvenile clasts. **(c)** PPL photomicrograph of the carbonate cement in the unit A1 juvenile lapilli tuff. **(d)** CL image of (c) with the orange indicating the occurrence of calcite. Calcite occurs in the cement along fractures and within the core of the cement. A minor amount is also replacing minerals in the juvenile clasts.

5.4 Discussion

5.4.1 Schist xenolith geochemistry

The presence of sanidine in the schist xenolith is important because it has clear implications for the thermal state attained by the rock. Sanidine shows a continuous solid solution between Na- and K feldspars at temperatures above 650 °C (Prevec et al. 2008; Grapes 2010). Sanidine is inferred to occur predominantly in the dark brown groundmass observed under thin section (Fig. 3.20f). The aluminium spinel, hercynite, was also present in the XRD analysis. This mineral

is common in high temperature metamorphic environments, and requires temperatures of >800 °C (Montel et al. 1986; Bayhan et al. 2006).

5.4.2 Carbonate geochemistry

The source(s) of volatiles in diatremes, in particular CO_2 and H_2O, is contentious due to the debate that surrounds the magmatic vs phreatomagmatic eruption style for this type of volcano. Carbon and oxygen stable isotope analyses for carbonate within diatremes is a useful technique for determining the source of these volatiles. In a comprehensive review of carbonate in kimberlites worldwide, Giuliani et al. (2014) found the majority of results for $\delta^{13}C$ fell in a range of -2 to -8 $\delta^{13}C_{VPDB}$ ‰, which is considered to be representative of mantle carbon. However, only a small number of oxygen isotope results fell within 6–9 $\delta^{18}O_{VSMOW}$ ‰ which is the representative range for mantle carbonate. Several processes are capable of modifying the original mantle composition, including interaction with late-stage magmatic fluids, meteoric waters, hydrothermal fluids, and incorporation of sedimentary material (Fig. 5.3). Giuliani et al. (2014) also found carbonates in kimberlite breccias typically have higher $\delta^{18}O$ values than carbonates in massive and hypabyssal kimberlites, which suggests significant interaction with hydrous fluids in the brecciated parts of the kimberlite pipe. Results for carbonate cement in the LWD presented in section 5.3.2 show the $\delta^{13}C$ and $\delta^{18}O$ values do not fall within expected ranges for a mantle carbonate source. However, as Giuliani et al. (2014) suggest, the isotopic signature of mantle derived carbonate in diatremes and kimberlites can be modified, and therefore it is possible the LWD carbonate cements precipitated from a modified mantle-sourced carbonate fluid.

Carbonatite intrusions from the Alpine Dike Swarm (Fig. 5.4) typically plot within a range of $\delta^{13}C$ -5 to -7 ‰ (Blattner and Cooper 1974), and carbonates from lamprophyre dikes have a range of $\delta^{13}C$ -4 to -6 ‰ (White 1998). Also, recently analysed carbonate samples from veins and breccias within the Mt. Alta diatreme have a range of $\delta^{13}C$ -2.5 to -4.5 ‰ (all samples relative to VPDB) and an oxygen isotopic range (all samples relative to VSMOW) of $\delta^{18}O$ ~7 to 12 ‰ (Wellnitz 2015). All these results are distinct from the LWD isotopic values, which suggests a magmatic source for carbonate in the lapilli tuffs is unlikely. Oxygen isotopes for the LWD carbonate cement suggest the oxygen reservoir was from metamorphic or sedimentary rock, and the carbon isotope values suggest the carbon was sourced from a freshwater or marine carbonate reservoir (Hoefs 2013). This suggests that groundwater

percolating through the Haast Schist country rock was the source for the carbonate in the lapilli tuff cement at the LWD. However, the availability of carbon in the Haast Schist is very low, and also the quartzofeldspathic protolith contains extremely low amounts of calc-silicate and marble rock that could sufficiently explain the high $\delta^{18}O$ values that the LWD carbonate samples have (Cooper and Paterson 2008). Figure 5.4 shows the carbonate samples from the LWD plot close to the Haast Schist carbonate field of Blattner and Cooper (1974). In these samples, they suggest the uniformity in $\delta^{18}O$ values but variability in $\delta^{13}C$, indicates a H_2O source for the $\delta^{18}O$ but a mixed source for the $\delta^{13}C$ such as atmospheric CO_2 or metamorphic fluids (Templeton et al. 1998).

The stable isotope values of the carbonate cement from the LWD lapilli tuffs is comparable to typical values for the Haast Schist carbonates. There is insufficient evidence to suggest they were modified from a magmatic source. The fluids were likely derived from mixing of meteoric and/or metamorphic fluids with atmospheric CO_2, and were precipitated post-eruption. The carbonate species from the juvenile-rich lapilli tuffs is predominantly ankerite with cathodoluminescence microscopy suggesting calcite is present in the later-precipitated "cores" of cement. Ankerite alteration elsewhere in the Haast Schist has been suggested to occur at temperatures of around 250 °C (Craw et al. 1991) and possibly persist at 150 °C (Craw 1989).

5.5 Conclusion

- Albite was thermally altered to sanidine in the schist xenolith suggesting it was heated to >650 °C. Hercynite spinel which is also present in the xenolith suggests heating to >800 °C. These temperature ranges are in agreement with the temperature of the lamprophyre which was likely >1000 °C.
- Carbonate cement in the juvenile-rich lapilli tuff and schist country-rock breccia is primarily ankerite, with small amounts of late-stage calcite also occurring in the cement of the lapilli tuff.
- Carbon and oxygen stable isotope analyses indicate the carbonate has a non-magmatic origin and can be correlated to typical Haast Schist isotopic ranges. The carbonate was likely sourced from mixing of meteoric water and/or metamorphic fluids with atmospheric CO_2.
- The ankerite formed post-eruption at temperatures <250 °C.

Chapter 6

Synthesis and Conclusion

The Lake Wanaka diatreme, situated within the Alpine Dike Swarm, NW Otago, is an example of an eroded Cenozoic diatreme. In this study, I used a combination of field-focused and analytical laboratory techniques to document and emphasise the different lithofacies within the diatreme and their volcanic evolution.

One of the original aims of this study was to determine the volcano-structural depth of the current exposure of the eroded diatreme. During fieldwork, I documented a number of features within the Lake Wanaka diatreme that indicate the current level of erosion represents the root zone or lower diatreme. These features include, voluminous monomict country-rock breccias, unbedded and poorly mixed lapilli tuffs, and large blocks of country rock that occur within these two facies along with the coherent lamprophyre. Whilst these features cannot give an exact paleodepth of the deposit, the Lake Wanaka diatreme is inferred to have been eroded by least 300 to 500 m. Figure 6.1 shows an idealised schematic of a diatreme with the suggested level that the Lake Wanaka diatreme represents.

Another focus of this study was to characterise the different pyroclastic deposits and related facies, and determine what they indicate about the eruptive evolution of the diatreme. The schist country-rock breccias were likely deposited into an open cavity created by thermohydraulic explosions. These explosions took place below the syn-eruptive crater near the root zone level of the diatreme. Consequent shaking and vibrations from explosive volcanic activity helped the breccia become more tightly packed in places and caused brittle fragmentation at clast contacts. Large metre-plus sized blocks of schist were slabbed off the weakened and unstable vent wall and became incorporated into the lapilli tuffs and country rock breccias, as well as becoming enveloped by the late stage lamprophyre sill. The juvenile-rich lapilli tuff and tuff breccias predominantly accumulated from spatter. Abundant wall-rock lithics that were shed into the magma prior to and during the eruption, led to abundant composite loaded pyroclasts throughout the lapilli tuffs. Fragmentation of the lamprophyre magma was initiated by ground water welling into the magma at depth through fractured

country rock. Vapour explosions resulted from the magma-water interaction and created bubble bursts and/or more intensive lava fountains. The columnar jointed coherent lamprophyre that is prominently exposed, intruded late as a sill. The lapilli tuffs were cemented by a post-eruptive carbonate fluid derived from mixing of meteoric water, and atmosphere CO_2.

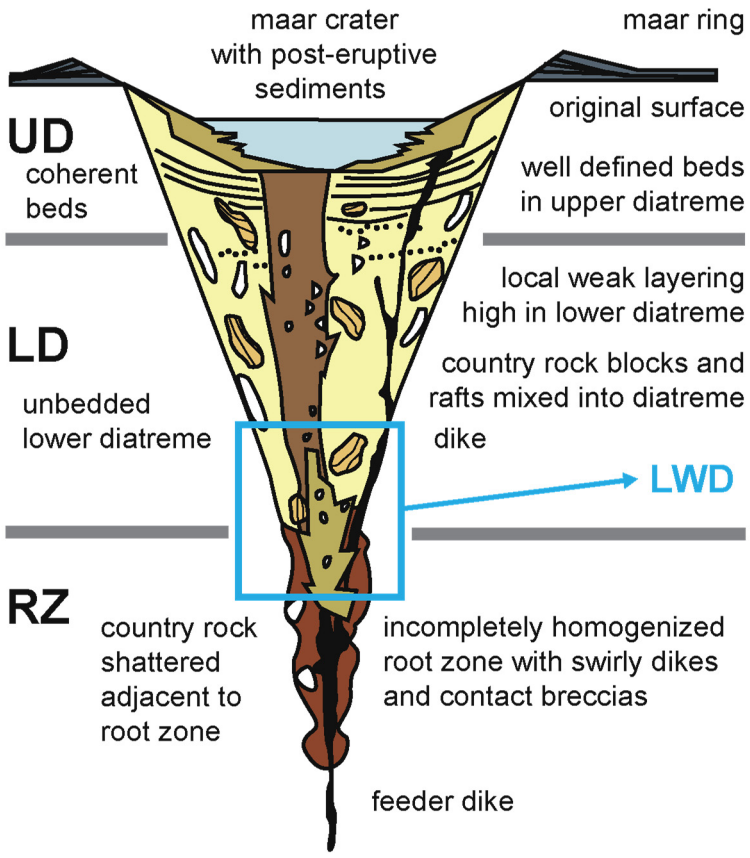

Figure 6.1: Schematic diagram of an idealised diatreme showing typical deposits and features of the upper diatreme (UD), lower diatreme (LD) and root zone (RZ). The blue box indicates the volcano-structural level that the present day Lake Wanaka diatreme may represent (no scale implied), modified from White and Ross (2011).

These deposits indicate the Lake Wanaka diatreme was initially dominated by phreatomagmatic explosions that contributed to much of the diatreme fill, and during the later stages of the eruption, non-explosive effusive intrusions were dominant.

Determining the thermal history of some of the deposits within the Lake Wanaka diatreme was also an aim of this study. Paleomagnetic analyses indicate high temperatures in the diatreme soon after lapilli tuff deposition (>580 °C), and additional heating during subsequent intrusion by a nearby sill (295–347 °C). Schist xenoliths within the lamprophyre sill were also heated to

high temperatures (>630 °C). This is the only paleomagnetic study investigating the emplacement temperatures of a non-kimberlite diatreme that I am aware of. The data I have presented suggests that the paleomagnetic method for determination of emplacement temperatures is a valuable technique that can be successfully applied to various styles of pyroclastic deposits.

In the Otago region, the Waipiata Volcanic Field contains remnants of small volcanoes that are most comparable to the Lake Wanaka diatreme (Table 6.1). The type 1 vents of the WVF predominantly consist of eroded lava lakes, dikes, sills and plugs. Although the extent of erosion in these vents is poorly constrained, they contain minimal pyroclastic deposits. This suggests a low explosive history for these vents and they do not appear analogous to the LWD. Type 2 vents contain significant pyroclastic infill, suggesting intense explosions during their history. Many of the deposits within the type 2 vents are bedded, and there are no reported country rock breccias within the vents. These features suggest the type 2 vents are most likely upper diatreme deposits, therefore placing them at a higher volcano-structural level compared to the diatreme in this study. The Lake Wanaka diatreme is, perhaps, best compared to the other diatremes within the Alpine Dike Swarm. Whilst they were not observed during this study, basic observations gathered from previous workers suggest the diatremes are dominated by randomly orientated schist country-rock breccias, rare lamprophyric breccias, and central coherent lamprophyres. These features are very similar to those documented at the LWD, and all the diatremes within the Alpine Dike Swarm may have been eroded down to the root zone level and evolved from similar eruptive processes.

Table 6.1: Comparison of volcanic characteristics between the Lake Wanaka diatreme within the Alpine Dike Swarm, and the Type 1 and Type 2 vents of the Waipiata Volcanic Field. Characteristics for the WVF vents summarised from Németh (2001), Németh and White (2003) and Németh (2003).

Parameter	LWD (ADS)	Type 1 vent (WVF)	Type 2 vent (WVF)
Morphology	~ 200 m, ellipsoid	300–600 m, symmetrical shapes	Up to several hundred metres, symmetrical shapes
Estimated erosion	300–500 m	Poorly constrained	Up to 275–700 m
Fragmentation style	Phreatomagmatic	Effusive, minor phreatomagmatic	Phreatomagmatic with late stage Strombolian-style
Fragmentation intensity	Moderate	Low	High

Deposition style	Open cavity rock-fall and spatter. Intrusive sills and dikes.	Intrusive and/or extrusive lavas	Base surges, minor spatter
Vent fill types	Country-rock breccias and pyroclastic material. Late stage intrusives.	Lava dominant, minor pyroclastic material	Dominated by bedded pyroclastic material, no country-rock breccias
Lithics derived from Cenozoic marine strata?	No	Yes	Yes

The results presented in this study have shown that the Lake Wanaka diatreme was produced by phreatomagmatic explosions that created a number of different styles of deposit. Some of these deposits were emplaced at high temperatures which is consistent with the thermal evolution of a number of kimberlite volcanoes. Diatremes created by phreatomagmatic explosions should also be considered to be capable of producing high temperature deposits. These findings may also be applied to other diatremes within the Alpine Dike Swarm.

References

Adams C 1981. Migration of late Cenozoic volcanism in the South Island of New Zealand and the Campbell Plateau.

Adams C, Cooper AF 1996. K-Ar age of a lamprophyre dike swarm near Lake Wanaka, west Otago, South Island, New Zealand. New Zealand Journal of Geology and Geophysics 39(1): 17-23.

Andronico D, Pistolesi M 2010. The November 2009 paroxysmal explosions at Stromboli. Journal of Volcanology and Geothermal Research 196(1): 120-125.

Aramaki S, Akimoto S-i 1957. Temperature estimation of pyroclastic deposits by natural remanent magnetism. American journal of Science 255(9): 619-627.

Baker LL, Bernard A, Rember WC, Milazzo M, Dundas C, Abramov O, Keszthelyi L 2015. Temperature profile around a basaltic sill intruded into wet sediments. Journal of Volcanology and Geothermal Research 302: 81-86.

Bardot L, McClelland E 2000. The reliability of emplacement temperature estimates using palaeomagnetic methods: a case study from Santorini, Greece. Geophysical Journal International 143: 39-51.

Barker CE, Bone Y, Lewan MD 1998. Fluid inclusion and vitrinite-reflectance geothermometry compared to heat-flow models of maximum paleotemperature next to dikes, western onshore Gippsland Basin, Australia. International Journal of Coal Geology 37(1): 73-111.

Barnett W 2004. Subsidence breccias in kimberlite pipes—an application of fractal analysis. Lithos 76(1): 299-316.

Barnett WP 2008. The rock mechanics of kimberlite volcanic pipe excavation. Journal of Volcanology and Geothermal Research 174(1): 29-39.

Bayhan H, Aydar E, Sen E, Gourgaud A 2006. Melting of crustal xenoliths within ascending basalt: Example from the Kula volcanic field, western Anatolia, Turkey. Comptes Rendus Geoscience 338(4): 237-243.

Bellamy DJ, Springett B, Hayden P, Johnson P 1990. Moa's ark: The voyage of New Zealand, Penguin Books.

Blattner P, Cooper A 1974. Carbon and oxygen isotopic composition of carbonatite dikes and metamorphic country rock of the Haast Schist terrain, New Zealand. Contributions to mineralogy and petrology 44(1): 17-27.

Brown R, Gernon T, Stiefenhofer J, Field M 2008a. Geological constraints on the eruption of the Jwaneng Centre kimberlite pipe, Botswana. Journal of Volcanology and Geothermal Research 174(1): 195-208.

Brown R, Buse B, Sparks R, Field M 2008b. On the welding of pyroclasts from very low-viscosity magmas: examples from kimberlite volcanoes. The Journal of Geology 116(4): 354-374.

Brown R, Tait M, Field M, Sparks R 2009. Geology of a complex kimberlite pipe (K2 pipe, Venetia Mine, South Africa): insights into conduit processes during explosive ultrabasic eruptions. Bulletin of Volcanology 71(1): 95-112.

Brown R, Kavanagh J, Sparks R, Tait M, Field M 2007. Mechanically disrupted and chemically weakened zones in segmented dike systems cause vent localization: Evidence from kimberlite volcanic systems. Geology 35(9): 815-818.

Buse B, Schumacher JC, Sparks RSJ, Field M 2010. Growth of bultfonteinite and hydrogarnet in metasomatized basalt xenoliths in the B/K9 kimberlite, Damtshaa, Botswana: insights into hydrothermal metamorphism in kimberlite pipes. Contributions to Mineralogy and Petrology 160(4): 533-550.

Butler RF 1992. Paleomagnetism: magnetic domains to geologic terranes, Blackwell Scientific Publications Boston.

Campbell H, Landis C 2001. New Zealand awash. New Zealand Geographic 51: 6-7.

Cas R, Landis C, Fordyce R 1989. A monogenetic, Surtla-type, Surtseyan volcano from the Eocene-Oligocene Waiareka-Deborah volcanics, Otago, New Zealand: a model. Bulletin of volcanology 51(4): 281-298.

Cioni R, Gurioli L, Lanza R, Zanella E 2004. Temperatures of the AD 79 pyroclastic density current deposits (Vesuvius, Italy). Journal of Geophysical Research: Solid Earth (1978–2012) 109(B2).

Clement CR 1982. A comparative geological study of some major kimberlite pipes in the Northern Cape and Orange Free State. Unpublished thesis.

Clough MC 1988. The Minaret EL 33378 - Report on the fieldwork carried out during December 1987 - BP Oil NZ Ltd. Mineral Report Series MR1873: 1-18.

Cole J, Lewis K 1981. Evolution of the Taupo-Hikurangi subduction system. Tectonophysics 72(1): 1-21.

Cook DH 1984. The Minaret Diatreme. Unpublished 3rd Year Report thesis, Otago University, Dunedin, New Zealand. 42 p.

Coombs DS, Cas R, Kawachi Y, Landis C, McDonough W, Reay A 1986. Cenozoic volcanism in north, east and central Otago. Royal Society of New Zealand Bulletin 23: 278-312.

Cooper A, Barreiro B, Kimbrough D, Mattinson J 1987. Lamprophyre dike intrusion and the age of the Alpine fault, New Zealand. Geology 15(10): 941-944.

Cooper AF 1986. A Carbonatitic Lamprophyre Dike Swarm from the Southern Alps, Otago and Westland. Late Cenozoic volcanism in New Zealand. Royal Society of New Zealand Bull. 23: 313-336.

Cooper AF, Paterson LA 2008. Carbonatites from a lamprophyric dyke-swarm, South Westland, New Zealand. The Canadian Mineralogist 46(4): 753-777.

Cox S 1984. Niger Peak Geology. Unpublished 3rd Year Report thesis, University of Otago, Dunedin, New Zealand. 71 p.

Craig H 1957. Isotopic standards for carbon and oxygen and correction factors for mass-spectrometric analysis of carbon dioxide. Geochimica et cosmochimica acta 12(1): 133-149.

Craw D 1989. Shallow-level, late-stage gold mineralisation in Sawyers Creek, Shotover valley, northwest Otago, New Zealand. New Zealand journal of geology and geophysics 32(3): 385-393.

Craw D 1995. Reinterpretation of the erosion profile across the southern portion of the Southern Alps, Mt Aspiring area, Otago, New Zealand. New Zealand journal of geology and geophysics 38(4): 501-507.

Craw D, Reay A, Johnstone R 1991. Hydrothermal alteration geochemistry of Nugget gold vein system, Shotover valley, northwest Otago, New Zealand. New Zealand journal of geology and geophysics 34(4): 419-427.

Delaney PT, Pollard DD 1981. Deformation of host rocks and flow of magma during growth of minette dikes and breccia-bearing intrusions near Ship Rock, New Mexico. United States Geological Survey Professional Paper 1202: 1-61.

Delaney PT, Pollard DD 1982. Solidification of basaltic magma during flow in a dike. American Journal of Science 282(6): 856-885.

Demény A, Ahijado A, Casillas R, Vennemann T 1998. Crustal contamination and fluid/rock interaction in the carbonatites of Fuerteventura (Canary Islands, Spain): a C, O, H isotope study. Lithos 44(3): 101-115.

Doubik P, Hill BE 1999. Magmatic and hydromagmatic conduit development during the 1975 Tolbachik eruption, Kamchatka, with implications for hazards assessment at Yucca Mountain, NV. Journal of Volcanology and Geothermal Research 91(1): 43-64.

Dunlop DJ 1979. On the use of Zijderveld vector diagrams in multicomponent paleomagnetic studies. Physics of the Earth and Planetary Interiors 20(1): 12-24.

Dunlop DJ 2002a. Theory and application of the Day plot (Mrs/Ms versus Hcr/Hc) 1. Theoretical curves and tests using titanomagnetite data. Journal of Geophysical Research: Solid Earth (1978–2012) 107(B3): EPM 4-1-EPM 4-22.

Dunlop DJ 2002b. Theory and application of the Day plot (Mrs/Ms versus Hcr/Hc) 2. Application to data for rocks, sediments, and soils. Journal of Geophysical Research: Solid Earth (1978–2012) 107(B3): EPM 5-1-EPM 5-15.

Dunlop DJ, Özdemir Ö 2001. Rock magnetism: fundamentals and frontiers, Cambridge university press.

Ellwood BB, Balsam W, Burkart B, Long GJ, Buhl ML 1986. Anomalous magnetic properties in rocks containing the mineral siderite: paleomagnetic implications. Journal of Geophysical Research: Solid Earth (1978–2012) 91(B12): 12779-12790.

Ellwood BB, Burkart B, Rajeshwar K, Darwin RL, Neeley RA, McCall AB, Long GJ, Buhl ML, Hickcox CW 1989. Are the iron carbonate minerals, ankerite and ferroan dolomite, like siderite, important in paleomagnetism? Journal of Geophysical Research: Solid Earth (1978–2012) 94(B6): 7321-7331.

Esperança S, Holloway JR 1987. On the origin of some mica-lamprophyres: experimental evidence from a mafic minette. Contributions to Mineralogy and Petrology 95(2): 207-216.

Fedortchouk Y, Canil D 2004. Intensive variables in kimberlite magmas, Lac de Gras, Canada and implications for diamond survival. Journal of Petrology 45(9): 1725-1745.

Fleming CA 1962. New Zealand biogeography: a paleontologist's approach, Biological Society, Victoria University.

Fontana G, Mac Niocaill C, Brown RJ, Sparks RSJ, Field M 2011. Emplacement temperatures of pyroclastic and volcaniclastic deposits in kimberlite pipes in southern Africa. Bulletin of volcanology 73(8): 1063-1083.

Gamble M 1984. The geology of Mt Alta-Triple Peak. Unpublished Hons. thesis, University of Otago, Dunedin, New Zealand.

Gernon T, Fontana G, Field M, Sparks R, Brown R, Mac Niocaill C 2009. Pyroclastic flow deposits from a kimberlite eruption: the Orapa South Crater, Botswana. Lithos 112: 566-578.

Gernon TM, Brown RJ, Tait MA, Hincks TK 2012. The origin of pelletal lapilli in explosive kimberlite eruptions. Nature communications 3: 832.

Giordano D, Nichols AR, Dingwell DB 2005. Glass transition temperatures of natural hydrous melts: a relationship with shear viscosity and implications for the welding process. Journal of Volcanology and Geothermal Research 142(1): 105-118.

Giuliani A, Phillips D, Kamenetsky VS, Fiorentini ML, Farquhar J, Kendrick MA 2014. Stable isotope (C, O, S) compositions of volatile-rich minerals in kimberlites: A review. Chemical Geology 374: 61-83.

Grapes R 2010. Pyrometamorphism, Springer Science & Business Media.

Hamilton CW, Thordarson T, Fagents SA 2010. Explosive lava–water interactions I: architecture and emplacement chronology of volcanic rootless cone groups in the 1783–1784 Laki lava flow, Iceland. Bulletin of volcanology 72(4): 449-467.

Hetényi G, Taisne B, Garel F, Médard É, Bosshard S, Mattsson HB 2012. Scales of columnar jointing in igneous rocks: field measurements and controlling factors. Bulletin of volcanology 74(2): 457-482.

Hoblitt RP, Kellogg KS 1979. Emplacement temperatures of unsorted and unstratified deposits of volcanic rock debris as determined by paleomagnetic techniques. Geological Society of America Bulletin 90(7): 633-642.

Hoefs J 2013. Stable isotope geochemistry, Springer Science & Business Media.

Hoernle K, White JDL, Bogaard PVD, Hauff F, Coombs DS, Werner R, Timm C, Garbe-Schönberg D, Reay A, Cooper AF 2006. Cenozoic intraplate volcanism on New Zealand: Upwelling induced by lithospheric removal. Earth and Planetary Science Letters 248(1-2): 350-367.

Hoskins RH 1982. Stages of the New Zealand marine Cenozoic: a synopsis, New Zealand Geological Survey, Department of Scientific and Industrial Research.

Houghton B, Wilson C 1989. A vesicularity index for pyroclastic deposits. Bulletin of volcanology 51(6): 451-462.

Hubberten H-W, Katz-Lehnert K, Keller J 1988. Carbon and oxygen isotope investigations in carbonatites and related rocks from the Kaiserstuhl, Germany. Chemical geology 70(3): 257-274.

Kamp PJ, Green PF, White SH 1989. Fission track analysis reveals character of collisional tectonics in New Zealand. Tectonics 8(2): 169-195.

Kawachi Y, Pringle IJ 1988. Multiple-rind structure in pillow lava as an indicator of shallow water. Bulletin of volcanology 50(3): 161-168.

Kear D, Mortimer N 2003. Waipa Supergroup, New Zealand: a proposal. Journal of the Royal Society of New Zealand 33(1): 149-163.

Keller J 1981. Carbonatitic volcanism in the Kaiserstuhl alkaline complex: evidence for highly fluid carbonatitic melts at the Earth's surface. Journal of Volcanology and Geothermal Research 9(4): 423-431.

King PR 1999. Cretaceous to Recent Sedimentary Patterns in New Zealand, Institute of Geological & Nuclear Sciences Limited.

King PR 2000. Tectonic reconstructions of New Zealand: 40 Ma to the Present. New Zealand Journal of Geology and Geophysics 43(4): 611-638.

Kirschvink J 1980. The least-squares line and plane and the analysis of palaeomagnetic data. Geophysical Journal International 62(3): 699-718.

Kurszlaukis S, Barnett WP 2003. Volcanological and Structural Aspects of the Venetia Kimberlite Cluster–a case study of South African kimberlite maar-diatreme volcanoes. South African Journal of Geology 106(2-3): 165-192.

Kurszlaukis S, Lorenz V 2008. Formation of "Tuffisitic Kimberlites" by phreatomagmatic processes. Journal of Volcanology and Geothermal Research 174(1): 68-80.

Landis C, Campbell H, Begg J, Mildenhall D, Paterson AM, Trewick S 2008. The Waipounamu Erosion Surface: questioning the antiquity of the New Zealand land surface and terrestrial fauna and flora. Geological Magazine 145(02): 173-197.

Lee DE, Lee WG, Mortimer N 2001. Where and why have all the flowers gone? Depletion and turnover in the New Zealand Cenozoic angiosperm flora in relation to palaeogeography and climate. Australian Journal of Botany 49(3): 341-356.

Lefebvre NS 2013. Volcanology of maar-diatreme volcanic vent complexes, Hopi Buttes Volcanic Field, Navajo Nation, Arizona, USA. Unpublished thesis, University of Otago.

Lefebvre NS, White JDL, Kjarsgaard BA 2012. Spatter-dike reveals subterranean magma diversions: Consequences for small multivent basaltic eruptions. Geology 40(5): 423-426.

Lefebvre NS, White JDL, Kjarsgaard BA 2013. Unbedded diatreme deposits reveal maar-diatreme-forming eruptive processes: Standing Rocks West, Hopi Buttes, Navajo Nation, USA. Bulletin of Volcanology 75(8).

Liu J, Scott JM, Martin CE, Pearson DG 2015. The longevity of Archean mantle residues in the convecting upper mantle and their role in young continent formation. Earth and Planetary Science Letters 424: 109-118.

Lorenz V 1973. On the formation of maars. Bulletin Volcanologique 37(2): 183-204.

Lorenz V 1975. Formation of phreatomagmatic maar-diatreme volcanoes and its relevance to kimberlite diatremes. Physics and Chemistry of the Earth 9: 17-27.

Lorenz V 1986. On the growth of maars and diatremes and its relevance to the formation of tuff rings. Bulletin of Volcanology 48(5): 265-274.

Lorenz V 2003. Maar-diatreme volcanoes, their formation, and their setting in hard-rock or soft-rock environments. Geolines 15: 72-83.

Lorenz V, Zimanowski B 1984. Fragmentation of alkali-basaltic magmas and wall-rocks by explosive volcanism. Annales Sci Uni Clermont-Fd. II 75: 15-25.

Lorenz V, Haneke J 2004. Relationship between diatremes, dykes, sills, laccoliths, intrusive-extrusive domes, lava flows, and tephra deposits with unconsolidated water-saturated sediments in the late Variscan intermontane Saar-Nahe Basin, SW Germany. Geological Society, London, Special Publications 234(1): 75-124.

Lorenz V, Kurszlaukis S 2007. Root zone processes in the phreatomagmatic pipe emplacement model and consequences for the evolution of maar–diatreme volcanoes. Journal of Volcanology and Geothermal Research 159(1): 4-32.

Lorenz V, Zimanowski B, Buettner R 2002. On the formation of deep-seated subterranean peperite-like magma–sediment mixtures. Journal of Volcanology and Geothermal Research 114(1): 107-118.

Lowrie W 1990. Identification of ferromagnetic minerals in a rock by coercivity and unblocking temperature properties. Geophysical Research Letters 17(2): 159-162.

Lurcock PC, Wilson GS 2012. PuffinPlot: A versatile, user-friendly program for paleomagnetic analysis. Geochemistry, Geophysics, Geosystems 13(6).

Martin U, White J 2001. Depositional and eruptive mechanisms of density current deposits from a submarine vent at the Otago Peninsula, New Zealand. Particulate Gravity Currents:(Special Publication 31 of the IAS)(31-32): 245.

Mattox TN, Mangan MT 1997. Littoral hydrovolcanic explosions: a case study of lava-seawater interaction at Kilauea Volcano. Journal of Volcanology and Geothermal Research 75(1-2): 1-17.

McClelland E 1981. Paleomagnetic estimates of temperatures reached in contact metamorphism. Geology 9(3): 112-116.

McClelland E, Wilson CJ, Bardot L 2004. Palaeotemperature determinations for the 1.8-ka Taupo ignimbrite, New Zealand, and implications for the emplacement history of a high-velocity pyroclastic flow. Bulletin of volcanology 66(6): 492-513.

McClintock M, White JD 2006. Large phreatomagmatic vent complex at Coombs Hills, Antarctica: wet, explosive initiation of flood basalt volcanism in the Ferrar-Karoo LIP. Bulletin of Volcanology 68(3): 215-239.

McFadden P 1977. A palaeomagnetic determination of the emplacement temperature of some South African kimberlites. Geophysical Journal International 50(3): 587-604.

Mildenhall D, Mortimer N, Bassett K, Kennedy E 2014. Oligocene paleogeography of New Zealand: maximum marine transgression. New Zealand Journal of Geology and Geophysics 57(2): 107-109.

Montel J-M, Weber C, Pichavant M 1986. Biotite-sillimanite-spinel assemblages in high-grade metamorphic rocks: occurrences, chemographic analysis and thermobarometric interest. Bulletin de minéralogie 109(5): 555-573.

Moorhouse B, White J, Scott J 2015. Cape Wanbrow: A stack of Surtseyan-style volcanoes built over millions of years in the Waiareka–Deborah volcanic field, New Zealand. Journal of Volcanology and Geothermal Research 298: 27-46.

Mortimer N 2004. New Zealand's Geological Foundations. Gondwana Research 7(1): 261-272.

Mortimer N, Cooper A 2004. U-Pb and Sm-Nd ages from the Alpine Schist, New Zealand. New Zealand Journal of Geology and Geophysics 47(1): 21-28.

Mortimer N, Rattenbury M, King P, Bland K, Barrell D, Bache F, Begg J, Campbell H, Cox S, Crampton J 2014. High-level stratigraphic scheme for New Zealand rocks. New Zealand Journal of Geology and Geophysics 57(4): 402-419.

Mundula F, Cioni R, Funedda A, Leone F 2013. Lithofacies characteristics of diatreme deposits: Examples from a basaltic volcanic field of SW Sardinia (Italy). Journal of Volcanology and Geothermal Research 255: 1-14.

Nakaoka R, Suzuki-Kamata K 2014. Rock-magnetic evidence for the low-temperature emplacement of the Habushiura pyroclastic density current, Niijima Island, Japan. Geological Society, London, Special Publications 396(1): 51-66.

Németh K 2001. Phreatomagmatic volcanism at the Waipiata volcanic field, Otago, New Zealand. Unpublished PhD thesis.

Németh K 2003. Calculation of long-term erosion in Central Otago, New Zealand, based on erosional remnants of maar/tuff rings. Z. Geomorph. N. F. 47(1): 29-49.

Németh K, White JDL 2003. Reconstructing eruption processes of a Miocene monogenetic volcanic field from vent remnants: Waipiata Volcanic Field, South Island, New Zealand. Journal of Volcanology and Geothermal Research 124(1-2): 1-21.

O'reilly W 2012. Rock and mineral magnetism, Springer Science & Business Media.

Ort MH, Porreca M, Geissman JW 2015. The use of palaeomagnetism and rock magnetism to understand volcanic processes: introduction. Geological Society, London, Special Publications 396(1): 1-11.

Paterson AL 1992. A Study of Carbonatites and Associated Fenitisation at Haast River, South Westland, New Zealand. Unpublished PhD thesis, University of Otago.

Paterson GA, Roberts AP, Mac Niocaill C, Muxworthy AR, Gurioli L, Viramonté JG, Navarro C, Weider S 2009. Paleomagnetic determination of emplacement temperatures of pyroclastic deposits: an under-utilized tool. Bulletin of Volcanology 72(3): 309-330.

Pell J, Russell JK, Zhang S 2015. Kimberlite emplacement temperatures from conodont geothermometry. Earth and Planetary Science Letters 411: 131-141.

Petcovic HL, Dufek JD 2005. Modeling magma flow and cooling in dikes: Implications for emplacement of Columbia River flood basalts. Journal of Geophysical Research: Solid Earth (1978–2012) 110(B10).

Porritt L, Cas R, Crawford B 2008. In-vent column collapse as an alternative model for massive volcaniclastic kimberlite emplacement: an example from the Fox kimberlite, Ekati

Diamond Mine, NWT, Canada. Journal of Volcanology and Geothermal Research 174(1): 90-102.

Prevec S, Kuhn B, Büttner S 2008. Tectosilicate oikocrysts in impact melt-hosted mafic xenoliths, contact sublayer of the Sudbury Igneous Complex, Canada. LPI Contributions 1423: 3009.

Pullaiah G, Irving E, Buchan K, Dunlop D 1975. Magnetization changes caused by burial and uplift. Earth and Planetary Science Letters 28(2): 133-143.

Rader E, Geist D 2015. Eruption conditions of spatter deposits. Journal of Volcanology and Geothermal Research 304: 287-293.

Roberts AP 1995. Magnetic properties of sedimentary greigite (Fe 3 S 4). Earth and Planetary Science Letters 134(3): 227-236.

Roberts AP, Turner GM 1993. Diagenetic formation of ferrimagnetic iron sulphide minerals in rapidly deposited marine sediments, South Island, New Zealand. Earth and Planetary Science Letters 115(1): 257-273.

Roberts AP, Cui Y, Verosub KL 1995. Wasp-waisted hysteresis loops: Mineral magnetic characteristics and discrimination of components in mixed magnetic systems. Journal of Geophysical Research Atmospheres(100).

Ross P-S, White JD 2006. Debris jets in continental phreatomagmatic volcanoes: a field study of their subterranean deposits in the Coombs Hills vent complex, Antarctica. Journal of Volcanology and Geothermal Research 149(1): 62-84.

Ross P-S, White JD, Zimanowski B, Büttner R 2008a. Rapid injection of particles and gas into non-fluidized granular material, and some volcanological implications. Bulletin of Volcanology 70(10): 1151-1168.

Ross P-S, White JD, Zimanowski B, Büttner R 2008b. Multiphase flow above explosion sites in debris-filled volcanic vents: insights from analogue experiments. Journal of Volcanology and Geothermal Research 178(1): 104-112.

Ross P-S, White J, Valentine G, Taddeucci J, Sonder I, Andrews R 2013. Experimental birth of a maar–diatreme volcano. Journal of Volcanology and Geothermal Research 260: 1-12.

Rosseel JB, White J, Houghton B 2006. Complex bombs of phreatomagmatic eruptions: role of agglomeration and welding in vents of the 1886 Rotomahana eruption, Tarawera, New Zealand. Journal of Geophysical Research: Solid Earth (1978–2012) 111(B12).

Scott J, Lee D, Fordyce R, Palin J 2014a. A possible late Oligocene–early Miocene rocky shoreline on Otago schist. New Zealand Journal of Geology and Geophysics 57(2): 185-194.

Scott JM, Waight TE, van der Meer QHA, Palin JM, Cooper AF, Munker C 2014b. Metasomatized ancient lithospheric mantle beneath the young Zealandia microcontinent and its role in HIMU-like intraplate magmatism. Geochemistry, Geophysics, Geosystems 15: 3477-3501.

Scott Smith BH 2008. Canadian kimberlites: geological characteristics relevant to emplacement. Journal of Volcanology and Geothermal Research 174(1): 9-19.

Seghedi I, Maicher D, Kurszlaukis S 2009. Volcanology of Tuzo pipe (Gahcho Kué cluster)—Root–diatreme processes re-interpreted. Lithos 112: 553-565.

Skilling I, White J, McPhie J 2002. Peperite: a review of magma–sediment mingling. Journal of Volcanology and Geothermal Research 114(1): 1-17.

Skinner E 2008. The emplacement of class 1 kimberlites. Journal of Volcanology and Geothermal Research 174(1): 40-48.

Skinner E, Marsh J 2004. Distinct kimberlite pipe classes with contrasting eruption processes. Lithos 76(1): 183-200.

Sottili G, Taddeucci J, Palladino D 2010. Constraints on magma–wall rock thermal interaction during explosive eruptions from textural analysis of cored bombs. Journal of Volcanology and Geothermal Research 192(1): 27-34.

Sparks R, Baker L, Brown R, Field M, Schumacher J, Stripp G, Walters A 2006. Dynamical constraints on kimberlite volcanism. Journal of Volcanology and Geothermal Research 155(1): 18-48.

Spry A 1962. The origin of columnar jointing, particularly in basalt flows. Journal of the Geological Society of Australia 8(2): 191-216.

Stasiuk L, Lockhart G, Nassichuk W, Carlson J 1999. Thermal maturity evaluation of dispersed organic matter inclusions from kimberlite pipes, Lac de Gras, Northwest Territories, Canada. International Journal of Coal Geology 40(1): 1-25.

Stipp J, McDougall I 1968. Geochronology of the Banks Peninsula volcanoes, New Zealand. New Zealand journal of geology and geophysics 11(5): 1239-1258.

Stovall WK, Houghton B, Gonnermann H, Fagents S, Swanson D 2011. Eruption dynamics of Hawaiian-style fountains: the case study of episode 1 of the Kīlauea Iki 1959 eruption. Bulletin of volcanology 73(5): 511-529.

Stripp G, Field M, Schumacher J, Sparks R, Cressey G 2006. Post-emplacement serpentinization and related hydrothermal metamorphism in a kimberlite from Venetia, South Africa. Journal of Metamorphic Geology 24(6): 515-534.

Sulpizio R, Zanella E, Macias JL, Saucedo R 2014. Deposit temperature of pyroclastic density currents emplaced during the El Chichon 1982 and Colima 1913 eruptions. Geological Society, London, Special Publications 396(1): 35-49.

Sumner J, Blake S, Matela R, Wolff J 2005. Spatter. Journal of Volcanology and Geothermal Research 142(1): 49-65.

Templeton A, Chamberlain C, Koons P, Craw D 1998. Stable isotopic evidence for mixing between metamorphic fluids and surface-derived waters during recent uplift of the Southern Alps, New Zealand. Earth and Planetary Science Letters 154(1): 73-92.

Thordarson T, Self S 1993. The Laki (Skaftár Fires) and Grímsvötn eruptions in 1783–1785. Bulletin of Volcanology 55(4): 233-263.

Timm C, Hoernle K, Werner R, Hauff F, Bogaard PVD, White J, Mortimer N, Garbe-Schönberg D 2010. Temporal and geochemical evolution of the Cenozoic intraplate volcanism of Zealandia. Earth-Science Reviews 98(1-2): 38-64.

Trindade R, Mintsa Mi Nguema T, Bouchez J 2001. Thermally enhanced mimetic fabric of magnetite in a biotite granite. Geophysical research letters 28(14): 2687-2690.

Valentine GA, Groves KR 1996. Entrainment of country rock during basaltic eruptions of the Lucero volcanic field, New Mexico. The Journal of Geology: 71-90.

van Straaten BI, Kopylova M, Murphy B 2013. Pyroclastic kimberlite deposits from the Victor Northwest pipe (Ontario, Canada): the transition from phreatomagmatic to magmatic explosivity. Canadian Journal of Earth Sciences 50(10): 1059-1068.

Walters LJ, Claypool GE, Choquette PW 1972. Reaction rates and δO 18 variation for the carbonate-phosphoric acid preparation method. Geochimica et Cosmochimica Acta 36(2): 129-140.

Waters JM, Craw D 2006. Goodbye Gondwana? New Zealand biogeography, geology, and the problem of circularity. Systematic Biology 55(2): 351-356.

Wellnitz K 2015. Study of fluids from NW Otago, New Zealand. Unpublished raw data, University of Otago.

White J, McClintock M 2001. Immense vent complex marks flood-basalt eruption in a wet, failed rift: Coombs Hills, Antarctica. Geology 29(10): 935-938.

White J, Houghton B 2006. Primary volcaniclastic rocks. Geology 34(8): 677-680.

White JD, McPhie J, Skilling I 2000. Peperite: a useful genetic term. Bulletin of Volcanology 62(1): 65-66.

White JDL, Ross P-S 2011. Maar-diatreme volcanoes: A review. Journal of Volcanology and Geothermal Research 201(1-4): 1-29.

White SR 1998. The Mid-Cenozoic Siberia Fault Zone (SFZ) in Northwest Otago, New Zealand and a Study of Greenschist Facies Metamorphism in the Haast Schist. Unpublished PhD thesis, University of Otago, Dunedin, New Zealand.

Wohletz K 2008. KWare geological software. 10th July.

Woolley A, Church A 2005. Extrusive carbonatites: a brief review. Lithos 85(1): 1-14.

Zanella E, Sulpizio R, Gurioli L, Lanza R 2014. Temperatures of the pyroclastic density currents deposits emplaced in the last 22 kyr at Somma-Vesuvius (Italy). Geological Society, London, Special Publications 396(1): 13-33.

Appendix A

Digital data

The following can be found on the attached CD – Raw data from IRM analysis – Raw data from hysteresis loops – Progressive thermal demagnetisation data – Raw XRD data for the analysed samples – Carbon and oxygen isotope results – All figures as PNG files – PDF copy of thesis